HYDROGEN FLUORIDE MODIFIED DUST FOR SELF-CLEANING APPLICATIONS

BY

JOHNNY EBAIKA ADUKWU

A Thesis Presented to the

DEANSHIP OF GRADUATE STUDIES

KING FAHD UNIVERSITY OF PETROLEUM & MINERALS

DHAHRAN, SAUDI ARABIA

In Partial Fulfillment of the

Requirements for the Degree of

MASTER OF SCIENCE

In

MECHANICAL ENGINEERING

April 2020

KING FAHD UNIVERSITY OF PETROLEUM & MINERALS

DHAHRAN- 31261, SAUDI ARABIA

DEANSHIP OF GRADUATE STUDIES

This thesis, written by **JOHNNY EBAIKA ADUKWU** under the direction of his thesis advisor and approved by his thesis committee, has been presented and accepted by the Dean of Graduate Studies, in partial fulfillment of the requirements for the degree of **MASTER OF SCIENCE IN MECHANICAL ENGINEERING.**

Zuhair Gasem — Digitally signed by Zuhair Gasem DN: cn=Zuhair Gasem, o=KFUPM, ou=Chair, ME Dept, email=zuhair@kfupm.edu.sa, c=SA Date: 2020.05.14 11:30:08 +03'00'

Dr. Zuhair M. Gasem
Department Chairman

Dr. Suliman Saleh Al-Homidan
Acting Dean of Graduate Studies

Date

Bekir Sami Yilbas

Dr. Bekir Sami Yilbas
(Advisor)

H. Qahtani

Dr. Hussain Al-Qahtani
(Member)

Abdullah Al-Sharafi — Digitally signed by Abdullah Al-Sharafi DN: cn=Abdullah Al-Sharafi, o=KFUPM, ou, email=alsharafi@kfupm.edu.sa, c=SA Date: 2020.05.13 16:51:54 +03'00'

Dr. Abdullah Al-Sharafi
(Member)

Dedication

To God Almighty and my family for their love and kindness

ACKNOWLEDGMENTS

I wish to acknowledge the following persons for their support, instruction, and guidance during my thesis work.

First, my supervisor Dr. Bekir Sami Yilbas for his fatherly supervision and for the time sacrificed to inculcate in me the spirit of hard work during my master's studies. Sir, I am very privileged to have you as my supervisor.

I also wish to express my gratitude to my committee members, Dr. Hussain Al-Qahtani and Dr. Abdullah Al-Sharafi for their wise, salient, and practical input to my thesis work.

Furthermore, I wish to express my appreciation to both Dr. Mazen Khalid and Dr. Almaz Jalilov for their practical guidance to carry out my research in the department of chemistry.

I want to also give credit to Dr. Abba Abubaker and Dr. Ghassan Abdelmajid for the time taken to go through my thesis work and for their contributions to make my thesis a success. Not forgetting my colleagues Mr. Saeed Bahatab and Mr. Mubarak Yakubu for their support while carrying out my experimental work.

I wish to also express my thanks to my grandmother, Mrs. Cecilia Adukwu for her prayers and support; to my lovely mother, Mrs. Milicent Adukwu for her blessings and encouragement; to my uncle, Engr. Victor Adukwu, for his encouragement; to my sister, Blessing Adukwu, and to all who in one way or another made this project a success.

TABLE OF CONTENTS

LIST OF TABLES

LIST OF FIGURES

LIST OF ABBREVIATIONS

ANN	:	Artificial Neural Network
AFM	:	Atomic Force Microscopy
BIPV	:	Building Integrated Photovoltaic
CCD	:	Charge coupled device
CFD	:	Computational Fluid Dynamics
CVD	:	Chemical Vapor Deposition
CAE	:	Constant Angle Energy
CSM	:	Certified Scrum Master
DE	:	Discrete Element
DP	:	Dust Particle
DPC	:	Dust Particle Crystal
DPM	:	Dried Mud Particle
EDS	:	Electrodynamic Dust Shield
EDX	:	Energy dispersive X-ray Spectroscopy

FEG	:	Field Emission Gun
FEI	:	Field Emission Intensity
FTIR	:	Fourier Transform Infra-Red Spectroscopy
GPR	:	Gaussian Process Regression
HF	:	Hydrogen Fluoride
HFDC	:	Hydrogen Fluoride Crystalized Dust
HDKR	:	Hays, Davies, Klutcher, Reindl
HFDM	:	Hydrogen Fluoride Dried Mud
HFDP	:	Hydrogen Fluoride Dust Particle
IBIC	:	Ion Beam Induced Charge
ICP	:	Inductive Coupled Plasma Spectrometry
KSA	:	Kingdom of Saudi Arabia
MST	:	Micro Scratch Tester
OSM	:	Outdoor Soiling Microscopy
DPM	:	Dried Mud Particle
PCM	:	Phase Change Material
PDMS	:	Polydimethylsiloxane

PECVD	:	Plasma-Enhanced Chemical Vapor Deposition
PFOTS	:	Perfluorooctyl
PH	:	Power of Hydrogen
PM	:	Particulate Matter
PV	:	Photovoltaic
PVD	:	Physical Vapor Deposition
SEM	:	Scanning Electron Microscopy
TEOS	:	Tetraethoxysilane
UAE	:	United Arab Emirates
UAV	:	Unmanned Aerial Vehicle
UV	:	Ultraviolet
VG	:	Vacuum Generators
XPS	:	X-ray Photoelectron Spectroscopy

SYMBOL	**:**	**DEFINITION**	**UNIT**
$\mathbf{A_c}$	:	Cleaned surface area of dust	mm^2
$\mathbf{A_o}$	:	Hamakers constant	kgm^2s^{-2}
$\mathbf{A_r}$	:	Area Ratio	dimensionless

$\mathbf{a_i}$	:	Acceleration of moving dust particle	ms^{-2}
c	:	Capillary constant	m^{-5}
$\mathbf{C_D}$	:	Drag Coefficient	dimensionless
$\mathbf{C_L}$	:	Lift Coefficient	dimensionless
$\boldsymbol{\delta}$	:	Inclination angle	degree
È	:	Electric Field Intensity	V/m
$\mathbf{F_{Adh}}$	:	Force of Adhesion	N
$\mathbf{F_{Cor}}$	:	Corrected Tangential force	nN
$\mathbf{F_D}$	:	Drag force	N
$\mathbf{F_L}$	:	Lift Force	N
$\mathbf{F_f}$	:	Friction Force	N
$\mathbf{F_g}$	:	Gravitational Force	N
g	:	Acceleration due to gravity	ms^{-2}
$\mathbf{I_o}$	:	Light Intensity	candela
$\boldsymbol{k}$	:	Atomic microscope probe tip spring constant	N/m
$\boldsymbol{k\sigma_d}$	:	Atomic microscope probe constant	N/mV
$\boldsymbol{\sigma_d}$	:	Atomic microscope probe deflection	m/V

L	:	Particle distance on glass surface	m
ΔL	:	Total removal length along for dust	m
L_d	:	Minimum incremental length for scratch test	m
m	:	Mass of particle	Kg
m_p	:	Mass of dust particle	Kg
m_{post}	:	Mass of dust after electrostatic activation	Kg
m_{pre}	:	Mass of dust before electrostatic activation	Kg
Δm	:	Mass gain by dust	Kg
η	:	Coefficient of Viscosity	$Kgm^{-1}s^{-1}$
η_a	:	Performance ratio for dust removal	dimensionless
η_{EDS}	:	Cleaning efficiency for electrodynamic dust shield	no unit
Oh	:	Ohnesorge number	dimensionless
Θ	:	Contact angle	degree
Θ_t	:	Angle of tilt	degree
Θ_e	:	Equilibrium of contact angle	degree
Θ_e^{CB}	:	Casie-Baxter equilibrium contact angle	degree
Θ_t	:	Angle of tilt	degree

$\boldsymbol{\rho}$	:	Density	Kgm^{-3}
$\boldsymbol{\rho_a}$	:	Density of air	Kgm^{-3}
$\boldsymbol{\rho_p}$	:	Density of particle	Kgm^{-3}
q	:	Charge on dust particle	Coulomb
r	:	Roughness of a particle	m
$\mathbf{r_s}$	:	Roughness parameter	m
$\mathbf{R_p}$	:	Radius of a particle	m
R	:	Radius of dust particle	m
$\mathbf{R_R}$	:	Radius of a particle with rough edges	m
S	:	Spreading Coefficient	mJ/m^2
$\boldsymbol{\tau}$	:	Transmittance of light	nm
$\boldsymbol{\Delta t}$	:	Flow time for liquid infusion into dust	s
$\mathbf{u_F}$	:	Particle influenced velocity	ms^{-1}
$\mathbf{u_i}$	:	Velocity of dust particle	ms^{-1}
$\mathbf{u_o}$	:	Threshold velocity for particle removal	ms^{-1}
$\mathbf{u_t}$	:	Tracked dust velocity from experiment	ms^{-1}
$\boldsymbol{\mu}$	:	viscosity of probe liquid	Pa.s

μ_d	:	Kinetic friction coefficient	dimensionless
μ_{dm}	:	Dust particle mobility	$Kg^{-1}sC^{-1}$
μ_f	:	Fluid viscosity	Pa.s
μ_{Fr}	:	Friction Coefficient	dimensionless
v/v	:	Volume per volume	no unit
ΔV	:	Atomic force microscope probe voltage	mV
V_n	:	Normalized velocity ratio	dimensionless
V_{Max}	:	Maximum velocity of dust particle	ms^{-1}
ύ	:	Dust Particle drift velocity	ms^{-1}
W_A	:	Work of Adhesion	J
W_{ad}	:	Average Adhesion work done to move dust	μJ
$W_{ad-\Delta L}$	:	Adhesion work done along a distance (ΔL)	μJ
γ_S	:	Surface energy of solid (dust/glass surface)	mJ/m^2
γ_{S-L}	:	Surface energy of solid liquid interface	mJ/m^2
γ_L	:	Liquid surface tension	mJ/m^2
γ_{Sa}	:	Interfacial free energy between solid and air	mJ/m^2
γ_{Sl}	:	Interfacial free energy between solid and liquid	mJ/m^2

γ_{la}	:	Interfacial surface free energy between liquid and air	mJ/m^2
γ^{LW}	:	Liftshitz-vanderwaal component of surface free energy	mJ/m^2
γ^{+}	:	Electron acceptor component of surface free energy	mJ/m^2
γ^{-}	:	Electron donor component of surface free energy	mJ/m^2
γ_s^{LW}	:	surface free energy of solid for liftshitz-vanderwaal	mJ/m^2
γ_s^{+}	:	surface free energy of solid for electron donor	mJ/m^2
γ_s^{-}	:	Surface free energy of solid for electron acceptor	mJ/m^2
γ_l^{P}	:	surface free energy of liquid for polar component	mJ/m^2
γ_l^{d}	:	surface free energy of liquid for non-polar component	mJ/m^2
Z_o	:	Particle-surface separation distance	m

ABSTRACT

Full Name : [Adukwu Johnny Ebaika]

Thesis Title : [Hydrogen Fluoride Modified Dust for Self-Cleaning Applications]

Major Field : [Mechanical Engineering]

Date of Degree : [April 2020]

Changes in climatic conditions in Middle East have resulted in continues increase in dust storms in the region. Particles from dust storms have a significant effect on solar harvesting devices through alteration of optical transmittance and thermal performance of these devices. In this study, environmental dust treatment by hydrogen fluoride is considered in line with dust removal from surfaces. Chemical constituents and physical characteristics of treated hydrogen fluoride and collected dust particles are investigated using analytical tools such as scanning electron, optical and atomic force microscope, energy dispersive spectroscopy, X-ray diffraction, inductive coupled mass spectrometry and Fourier transform infrared spectroscopy. The dust removal analysis is carried out on glass samples of hydrophilic and hydrophobic states while introducing collected and hydrogen fluoride-treated dust on sample surfaces. Experiments are conducted using the high-speed camera recording dust removal process. The effect of hydrogen fluoride on the treated dust particles are examined for self-cleaning applications; dust particles treatment with hydrogen fluoride provides one of the possible solutions for dust removal process from glass surfaces as demonstrated by mechanical tilt and avalanche methods. This can subsequently enhance the performance of solar harvesting devices when applied in the field conditions.

ملخص الرسالة

أدت التغيرات في الظروف المناخية في الشرق الأوسط إلى استمرار الزيادة في العواصف الترابية في المنطقة. الجسيمات من العواصف الترابية لها تأثير كبير على أجهزة الحصاد الشمسي من خلال تغيير النفاذية البصرية والأداء الحراري لهذه الأجهزة. في هذه الدراسة ، يتم اعتبار معالجة الغبار البيئي بواسطة فلوريد الهيدروجين بما يتماشى مع إزالة الغبار من الأسطح. يتم فحص المكونات الكيميائية والخصائص الفيزيائية لفلوريد الهيدروجين المعالج وجزيئات الغبار المجمعة باستخدام أدوات تحليلية مثل المسح الضوئي الإلكترون ، مجهر القوة الضوئية والذرية ، مطيافية الطاقة المشتتة ، حيود الأشعة السينية ، مطياف الكتلة المقترنة الاستقرائي ، مطياف الأشعة تحت الحمراء لتحويل فورييه. يتم إجراء تحليل إزالة الغبار على عينات زجاجية من حالات الماء والرطوبة أثناء إدخال الغبار المُجمع والمعالج بفلوريد الهيدروجين على أسطح العينة. يتم إجراء التجارب باستخدام الكاميرا عالية السرعة لتسجيل عملية إزالة الغبار. يتم فحص تأثير فلوريد الهيدروجين على جزيئات الغبار المعالجة لتطبيقات التنظيف الذاتي ؛ توفر معالجة جزيئات الغبار بفلوريد الهيدروجين أحد الحلول الممكنة لعملية إزالة الغبار من الأسطح الزجاجية كما هو موضح بطرق الإمالة الميكانيكية والانهيار الجليدي. هذا .يمكن أن يعزز لاحقًا أداء أجهزة الحصاد الشمسي عند تطبيقها في الظروف الميدانية

CHAPTER 1

INTRODUCTION

Gradual reduction of fossil fuel usage and increase of power demand for keeping the environment pollution free drive many scientists and engineers to search for alternative energy resources. Solar thermal and photovoltaic energy sources offer a bright future for clean energy generation. Countries with monthly average daily radiation between 3-6 KWh/m^2 consider solar radiation as an opportunity to harvest solar energy [1]. The kingdom of Saudi Arabia, with a yearly average solar radiation of 2200 KWh/m^2 stands out as one of the best regions to utilize nature's gift of solar energy for generation of electric power [2]. However, there has been a recent surge in dust storms and dust activities induced by climate change around the globe, particularly in the contemporary Middle East [3]. Environmental dust particles interfere with the optical clarity, operation capacity as well as the aesthetic value of Vehicle windscreen, high rise glass buildings, PV panel protective covers, Electrical and Electronic circuits, etc that are exposed to the atmosphere. Dust activities, its effects, and mitigations have gained global attention both in the industrial and academic environments and therefore provides a wide range of research interests.

1.1 Background on Dust Characteristics and Effects

1.1.1 Global Dust and Its Migration

Studies show that desert environments stand out as the main precursor of dust activities and regions closer to these locations are severely affected [4]. Dust storms are prevalent in arid and semi-arid regions particularly the Middle East and Northern Sahara. North Africa ranks the highest dust activities with around 0.8 x 10^9 tons of dust each year [5]. Dust storms originate from North Africa, move for long-distance into Asia, and the Middle East, Europe, the Caribbean, and the Americas [4-6]. The Arab region is mostly affected by severe dust storms all year round. Sand particles under the influence of huge windy storms are lifted to a great height and make irregular movements [5]. These dust particles begin to travel in suspended form. The regional dusty storms cover extensively a wide area among the nations and they trigger deforestation through topsoil loosening and depositing of sand particles on green plants [7]. The migration of dust and its constituents are tracked by special man-made devices moving through space[8]. These devices popularly known as satellites are used to probe signals from storms, fog, dust particles, and earth surfaces[8]. Studies on dust composition show different physical and chemical characteristics for different regions of the world. Dust occurrences have been grouped by World Meteorological Organization due to its effects on the environment [8].

1.1.2 Composition and Soiling Characteristics of Environmental Dust

Lately, dust storms induced by climatic changes in the Middle East poses a threat not only to energy harvesting devices but to all other devices exposed to the atmosphere. The Arab nations, for the last decade, have seen a rise in dust activities due to excessive dust migration from the north Sahara as well as the gulf sea [9].

Dust is made up of a combination of clay, grains for pollination and sand particles that arise from earth moving vehicles, industries, earthquakes, regional storms, etc. Environmental dust contains some uneven distributed rich elements and compounds of calcium, silicon, and oxygen which also contributes to the shape and complexity of dust particles [6, 10]. Dust particles of size less than 1.2μm are prone to pick charge ionic components when exposed in the atmosphere for a long time, which changes the elemental composition of these particles [10]. Microscopic dust particles vary in sizes from 0.01 microns to 15 microns with an average size of 1.2 microns depending on the regions where they abound [11]. Smaller dust particles are air-borne and suspend at a great height from the earth's surface and are carried by a strong wind from North Africa towards the Middle East targeted particularly at Saudi Arabia. These smaller particles reside longer in the atmosphere and are charged electrostatically and attracted to larger dust particles and attached themselves [12]. Forces that come to play when a dust particle settles on a surface include but not limited to VanderWaal, electrostatic and capillary forces depending on the condition of both the environment and the dust-surface interface. The capillary force arises as a result of water coming in contact with the particle and surface [11], while the electrostatic force which is environment-dependent exist in charged surfaces or particles in contact with each other [10]. The Vander Waal force forms the adhesion force between the surface and the particles, and it is reduced by an increase in the rough texture of the surface [13].

One popular research area of interest among scholars is the consequences of environmental dust accumulation on solar harvesting devices. Dust deposition on the surfaces of the solar concentrator and solar photovoltaic devices affect the operational efficiency of these devices [14]. This negative phenomenon aggravates more in a humid environment where dust compounds dissolves in condensed water vapor, forms a salty solution depending on the rate of condensation, flows through the dust cavities under gravity and settles between the dust and the surfaces of devices forming a crystalline mud layer [15]. Degradation and damages to solar glass surfaces may arise as a result of chemical attacks arising from the resulting alkaline dust solution. Also, as weather condition changes, water molecules evaporate from mud surfaces under the influence of solar radiant heating and dried mud sticks to the PV glass surface. Therefore, solar collectors and solar panel surfaces become difficult to clean due to strong adhesive forces between particles of mud and the surface [15]. Besides dust/mud attacks on the solar harvesting device surface, dirt from dust could prevent effective spectral transmittance [16]; induce an excessive increase in heat and electric resistance of the device module and invariably affect the energy derived from these devices even after undergoing several cleaning cycles. Therefore, dust removal via surface cleaning techniques becomes paramount for these exposed devices.

1.1.3 Dust Control Techniques

Various approaches termed as dust removal techniques, have been proposed and developed to improve the operating capacity of dust-ridden solar harvesting devices. Dust removal and control techniques for renewable energy applications can be classified into two main groups [17]; the passive and the active techniques as shown in figure (1.1). Natural (water, wind) dust cleaning and surface coatings comprise the passive types while the active techniques include both electrostatic and mechanical means of dust removal.

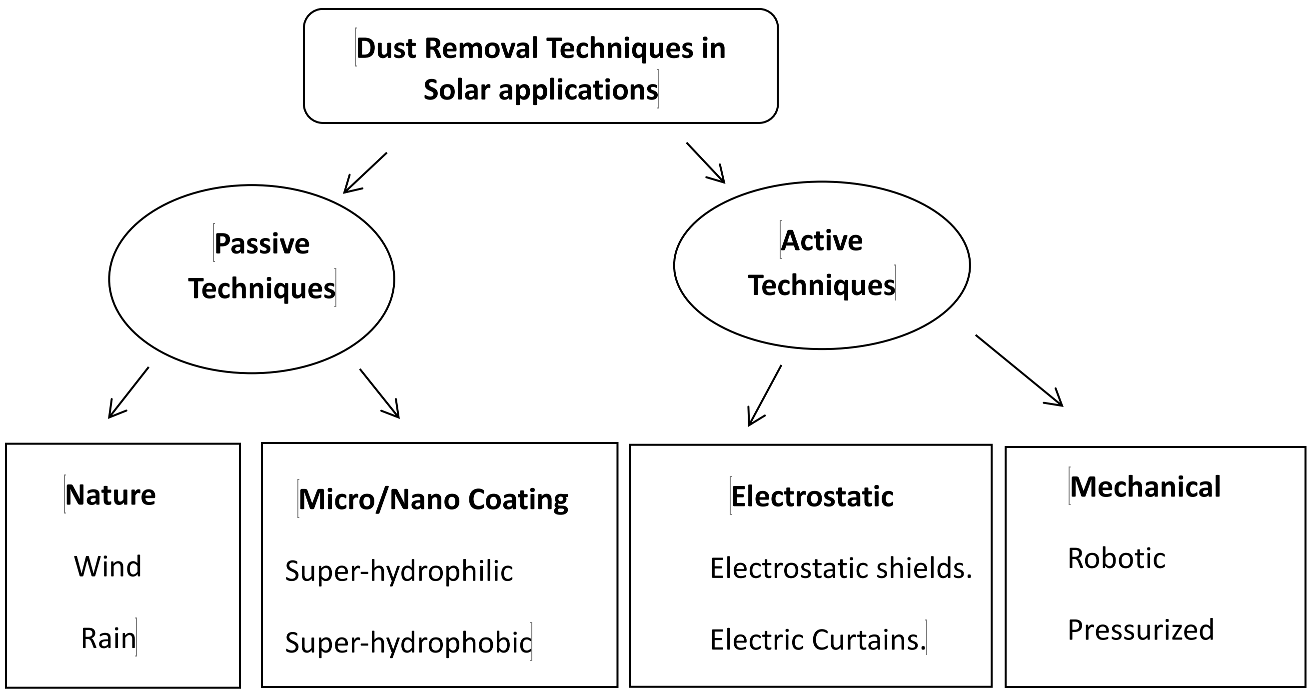

Figure 1.1 Dust Control Techniques for Solar harvesting devices

The natural dust cleaning technique uses the combined effect of either rainfall or wind and the orientation of solar harvesting devices without external effort [18]. The intermittent nature of wind and rainfall availability limits the effective and efficient use of this technique for dust cleaning.

The mechanical and electrostatic techniques depend on a power source to generate the needed motion to rid the surfaces of devices from settled dust particles. The electrostatic methods achieve this through the generation of electrostatic pulses from electrodes of electrostatic shields, electric curtains, etc. to repel and subsequently remove these dust particles [17]. In the case of mechanical dust removal, robotic devices incorporated with wiper and spray guns are used to apply water, air and brush-like movement on the surfaces of solar harvesting devices. The major drawbacks of the active techniques include the capital-intensive nature associated with device procurement and maintenance, and limited resource availability such as water, especially in the arid and semi-arid regions of the Middle East.

Super-hydrophobic and super-hydrophilic coatings are among the passive group of dust removal techniques because no external power source is required to remove dust from surfaces. The super-hydrophobic coatings generate low surface energy phenomena between the dust-surface interface and due to this anti-adhesion effect dust particles could easily be removed either by moving air or water droplets (lotus effect). In contrast to super-hydrophobic, the super-hydrophilic coating generates a high surface energy interaction between surface and dust particles; through film spreading and photo-catalysis, dust particles are easily removed from the surface. The coating techniques are encumbered with durability issues after prolonged use and the limitation of a light source for photo-catalytic conditions needed for the super-hydrophilic dust removal process.

On the other hand, one area that could enhance effective dust removal and maintain better optical properties of the surface is the direct treatment of the dust particles by a suitable chemical agent; followed by manual/mechanical tilting of solar harvesting devices for self-cleaning applications. Consequently, environmental dust deposited on optical surfaces can be considered for treatment by a chemical agent such as hydrogen fluoride in line with dust removal from surfaces.

1.2 Theoretical Background on Interfacial Surface Free Energy and Adhesion Work

The surface energy, as well as other properties such as surface texture, area, etc., determines to a great extent the behavior of a solid or liquid. The surface energy of a material is defined as the work done per unit area to create a new surface in the material, while the surface free energy per unit area (or in some case surface tension) of a liquid or solid is defined as half of the change in the free energy of the solid/liquid due to cohesion in a vacuum [19].

The fundamental formulation involving the surface energy per unit area (or surface tension) of a surface is given by the Young's expression for the equilibrium shape of a droplet on smooth surfaces [20], as shown in figure 1.2.

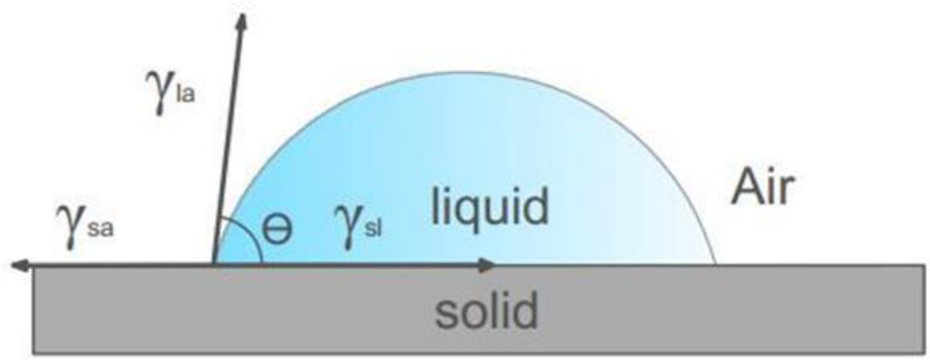

Figure 1.2 Schematic of Interfacial Surface Energy per unit area at Three-phase Interfaces

$$\gamma_{la} \cos \theta = \gamma_{sa} - \gamma_{sl} \qquad (1\text{-}1)$$

Where Θ depicts the equilibrium contact angle, and γ_{la} represent the interfacial surface free energy per unit area between liquid and air, γ_{sa} represents the interfacial surface free energy per unit area between solid and air ,γ_{sl} represents the interfacial surface free energy per unit area between the solid and liquid.

Over the years, many theories and models have been developed to define and quantify the surface free energy of solids/liquids. Zismans [19] defined the surface energy of a solid as the equivalent of the highest value of surface tension attributed to the liquid that completely wet the surface of the solid at a contact angle of zero. He also developed the famous Zisman chart to characterize the surface energy of solids, although his model does not account for polar interactions because it is based on only one-parameter (the surface tension)[21].

van Oss et al further presented the surface energy model of liquids and solids which captures both polar and non-polar interactions between surfaces in contact[22].

$$\gamma = \gamma^{LW} + \gamma^{AB} \qquad (1\text{-}2)$$

Where γ^{LW} represents the Lifshitz-Vanderwalls component and contributes to the non-polar molecular interactions and γ^{AB} is the lewis acid-base component and contributes to the polar (electron acceptor/donor) of the surface free energy.

From the geometric mean expression [22] for the acid-base (polar) component given thus;

$$\gamma^{AB} = 2\sqrt{\gamma^{+}\gamma^{-}} \qquad (1\text{-}3)$$

Where γ^{+} depicts the electron acceptor and γ^{-} depicts the electron donor of the polar component of the liquid and solid free surface energy.

Combining the modified young's equation [23, 24] , for the surface free energy of a solid and the expression for the interfacial free energy for a solid-liquid system [19, 22, 23] gives Adhesion work (W_A) [25],

$$W_A = \gamma_l(1 + \cos\Theta) = 2\sqrt{\gamma_s^{LW}\gamma_l^{LW}} + 2\sqrt{\gamma_s^{+}\gamma_l^{-}} + 2\sqrt{\gamma_s^{-}\gamma_l^{+}} \qquad (1\text{-}4)$$

The surface free energy (γ_s^{LW}, γ_s^+, γ_s^-) of solid material (metal or dust pellets) could be evaluated using equation (4) from the measurement of contact angle of two polar liquids and one nonpolar [23].

Aside from the three-component model developed by Van Oss, Owens, and Wendt [26] developed a model for calculating the surface free energy of a solid made using two liquid components; the dispersive (d) component which accounts for Vander Waal interaction and the polar (p) component which accounts for dipole-dipole and hydrogen bonding interactions. Owen and Wendt mathematically combined the Goods equation [24] and Youngs model [20] to obtain the Owen-Wendt model [26] given thus,

$$1 + \cos\Theta = 2\sqrt{\gamma_s^d}\sqrt{\frac{\gamma_l^d}{\gamma_l}} + 2\sqrt{\gamma_s^p}\sqrt{\frac{\gamma_l^p}{\gamma_l}} \qquad (1\text{-}5)$$

$$\gamma_l(1 + \cos\Theta) = 2\left(\sqrt{\gamma_l^d\gamma_s^d} + \sqrt{\gamma_l^p\gamma_s^p}\right) \qquad (1\text{-}6)$$

By re-arranging the equation 5 into 6 and using measured contact angles (Θ) and standard surface free energy values (γ_l^p, γ_l^d) for polar (e.g water) and non-polar liquid (e.g ethylene glycol), the surface free energy of a solid (dust pellets) in contact with this probe liquids can be estimated.

1.3 Statement of Problem

The efficiency of solar harvesting devices is affected by factors that can either be altered or unaltered, therefore dust accumulation can be categorized under the unalterable environmental factors that are location dependent [27].

In the Middle East regions, particularly areas of high relative humidity and erratic changes in weather conditions, water vapor may precipitate and condense on the surfaces of dust-laden equipment, particularly solar harvesting devices. Mud formed as a result of dust-water vapor interaction interferes and severely damages the surfaces of these installations affecting their optical transmittance [10]. The result is reduced thermal efficiency and electric power output of exposed structures and devices. Dust accumulation on surfaces has three consequences. First, the scattering and blocking of the incident solar radiation by various sizes of dust particles foster weak and diffuse spectral transmittance and thereby reduce the efficient operation of solar devices. The thermal effect is another factor that arises as a result of excessive temperature developed by dust cover panel surface which leads to the malfunction of temperature-sensitive components such as some PV modules that cannot withstand adverse temperature conditions [28]. Also, chemical attacks by acidic or alkali formed mud alter the surface of the PV panel, interfere with incident light intensity and negatively impact on Solar PV photoelectric effect resulting in reduced power output [13]. Consequently, dust removal from protective surfaces becomes essential to sustain the operation capacity of solar harvesting devices. In addition, It is observed that dust sticks to protective covers due to humidity which thus requires severe but meticulous cleaning action to restore solar energy harvesting devices to their initial power outputs [7]. Recently, Methods proposed to remedy the problem caused by dust accumulation include Water/steam cleaning, pressurized air jet, mechanical mopping/ brushing using robotic devices, sonic and electro-mechanical excitation and self-cleaning via water droplet motion on super-hydrophobic surfaces [17]. But the high energy/power required to execute these methods; the complexity/clumsiness of operating the cleaning equipment ; the scarcity of some resources such as water especially in the Middle East, as well as durability issues with coated surfaces prompts a new approach that can maximize scarce resources and minimize energy usage Therefore, one of the cost-effective methods for dust removal is to directly modify the surface chemistry of accumulated dust particles by treatment with a chemical agent. On the other hand, instead of modifying optical surface properties (surface energy and roughness) to obtain dust repellant surfaces, a novel approach is to treat the dust itself using hydrogen fluoride (HF). And by introducing a gravitational effect, such as a tilted surface, enables the removal of considerable amount of settled dust from surfaces. Hydrogen fluoride (HF) dust treatment can help to bypass cost, durability and optical issues encountered with coated and textured surfaces. In addition, the good etching and digestive property of hydrogen fluoride for dust modification needs to be investigated. Moreover, earlier works of literature reveal that most fluoride salts of calcium origin show low surface energy and adhesion characteristics; a suitable property that can be explored when dust made up of predominantly calcium compounds is treated with hydrogen fluoride. The synthesized low surface energy-low density Hydrogen fluoride (HF) dust can easily come off tilted glass surface under the influence of gravity as well as exhibit better anti-soiling characteristics compared to as-received dust. Consequently, the investigation of dust treated with hydrogen fluoride can become critical for self-cleaning applications in solar harvesting devices.

1.4 Motivation and Research Objectives

Changes in climatic condition have increased dust storms occurrences around the globe in recent times. Dust particles settle on protective surfaces and affect optical properties as well as lowers the efficiency of energy harvesting devices. The cost and energy required to clean the surfaces from the dust particles possess a critical challenge, particularly for large area surfaces such as solar farms. In addition, the dust particles possess alkaline and alkaline earth metals, which dissolve in humid air ambient. In this case, dust particles meet condensed water droplets in humid air ambient and result in dissolution of some of the components of the dust particles while forming a chemically active fluid on the surface. This enhances the adhesion of the dust particles upon drying. The dried solution also partially damages the surface because of generating pitting sites while lowering the quality of the optical properties of the surface such as optical transmittance and optical reflectance. One of the effective methods of cleaning dusty surfaces involves with the modification of dust chemistry in the surface region of dust particles. This is aimed at altering the dust adhesion due to interfacial resistance between dust particles and protective surfaces. Mainly, environmental dust is considered for treatment using low concentration hydrogen fluoride in self-cleaning applications. This requires modifying the surface energy and adhesion properties of collected dust via solution treatment in hydrogen fluoride. Consequently, treated dust can easily be self-clean from the protective surfaces under applied gravitational force via mechanical surface tilt and the avalanche effect.

Therefore, effective dust removal via chemical treatment to maintain optical clarity and sustain power output of solar harvesting devices needs to be investigated. The specific objectives of this study include:

- Dust Treatment with a chemical agent (Hydrogen fluoride).

- Dust Characterization (size, distribution and chemical composition of treated and untreated) via analytical tools
- Dust Modifications effects by low concentration hydrogen fluoride (HF) treatment.
- Analysis of treated and untreated dust adhesion on surfaces.
- Cleaning of dusty surfaces (hydrophilic and hydrophobic) by
    1. The Mechanical tilt Method
    2. The Avalanche Method.

1.5 Scope of Work and Approach

The structure of the thesis is as follows

Chapter 1 gives a brief introduction about the causes, characteristics and impacts of environmental dust on solar energy systems. Also, several dust mitigation techniques as well as theoretical background on adhesion of property of surfaces are presented and briefly discussed. In addition, the problem statement, motivation and research objectives are illustrated.

Chapter 2 presents a detailed and comprehensive literature review of the study. The literature review is divided into four sections. The first section looks up the effects of environmental dust accumulation and other environmental factors on solar harvesting devices. These environmental factors include relative humidity, temperature, wind velocity and rainfall. Numerical simulation and modeling of dust dynamics around solar harvesting devices is also presented in the first section. The second section gives a review of contemporary dust removal methods in relation to solar energy applications. Different types of dust cleaning strategies are reported in the literature with their prospects and shortcomings. The third section presents the use of various self-cleaning techniques to mitigate the effect of dust soiling on solar devices. Finally, the Mechanisms of dust removal from a surface is presented. In addition, a detailed literature on the hydrogen fluoride as an effective cleaning agent is reported.

Chapter 3 presents the research methodology. The first part of the research entails the collection and treatment of environmental dust particle with low concentration hydrogen fluoride. The second part summarizes the use of various analytical tools for the characterization of dust samples. The thirds parts analyses the changes in surface properties of treated dust via surface energy measurement techniques. Surface contact angle measurements are carried incorporating the sessile droplet method and relevant surface energy equations are applied to quantify the surface energy for dust samples.

This is closely followed by the determination of adhesion force and work required to remove the dust samples from hydrophilic and hydrophobic surfaces. The final section of this study entails the design of a rotating dust cleaning fixture/device and dust removal analysis are to be investigated on sample surfaces of glass while introducing untreated dust and hydrogen fluoride (HF)-treated dust types. Experiments are conducted using the high-speed camera recording the dust removal process. Finally, dust cleaning experiments are to be investigated on tilted surface via the use of gravitational force. In addition, two methods namely the mechanical tilt and the avalanche effect are applied to remove dust from surfaces.

Chapter four presents the result and conclusion. The effect of hydrogen fluoride on the treated dust particles is examined for self-cleaning applications. Dust particles treatment with hydrogen fluoride provides possible solutions for the dust removal process from the PV/thermal surfaces and subsequently enhance the performance of solar harvesting devices.

Finally, in Chapter 5, the main conclusion for the present study are summarized and possible directions for future study are presented.

CHAPTER 2

LITERATURE REVIEW

This chapter gives a broad and detailed literature about the causes and effects of dust soiling and mitigation strategies of environmental dust with emphasis on solar harvesting devices. The first section of this chapter looks up various experimental and numerical work undertaken to understand the effect of dust accumulation on the performance of solar thermal/photovoltaic devices. The second section provides an overview of the strategies and techniques that are applied to mitigate the effect of dust as regards solar harvesting devices. Next, relevant works of literature on the background principles and mechanisms responsible for dust pinning and removal from surfaces are reviewed. The last section focuses on the suitability of hydrogen fluoride as an effective cleaning agent.

2.1 Effects of Environmental Dust Accumulation on Solar Harvesting Devices

The need for improved efficiency of solar thermal collectors and PV panels prone to dust attacks has necessitated researchers to seek robust and affordable PV-dust removal methods. Method of cleaning Solar harvesting devices could be classified as natural, mechanical, self-cleaning nano-film, and electrostatic methods.

The basic research fields on the study of dust accumulation and mitigation focus on [16]

1. Dust/Sand characteristics, morphology, and environmental conditions.
2. The numerical simulation and modeling of dust dynamics around solar collector/PV panels.

3. Laboratory experiments design to comprehend the factors affecting the dust dynamics.

4. Methods developed to proffer ingenious solutions to dust/solar harvesting devices related problems.

Various studies have gone into understanding the phenomenon behind dust/mud deposition and formation on exposed solar collectors and photovoltaic surfaces and how to better deal positively with its impacts. Liu et al [16] reviewed the effect of dust particles accumulation, deposition, and concentration on a photovoltaic panel for both desert and urban scenarios. Their findings showed that both dust and wind are critical factors that affect solar Panels in the desert regions while other factors such as rainfall and suspended particles from emitted construction sites, industries, and vehicles are prominent in urban locations. The authors concluded that the amount and sizes of deposited dust particles, the strength of the wind and the prevailing weather conditions have tremendous effects on spectral transmittance, temperature, and the Physico-chemical interactions on PV panel surfaces. In a similar study, Mohandes et al [28] investigated the influence of humidity, temperature and dust particles on the output of a PV system in the United Arab Emirates. They found out that water vapor precipitates as dew; due to low temperature at night times in arid regions, it traps dust particles easily on PV surface and dries as mud when temperature increases in the daytime. Also, the power output of the solar Panel dropped by 10% in one month and one week due to the combined interaction of humidity, wind, and accumulated dust. Yilbas et al [15] studied the Characteristics and effects of dust/dried mud on a photovoltaic glass surface using analytical tools such as the scanning electron microscope, atomic force microscope, X-ray diffraction, Fourier transform infrared spectroscopy and micro tribometer. The authors observed that optical transmittance is reduced as a result of blockage of incident radiation by mud residue and surface changes of glass caused by hydroxide attack.

They concluded that more adhesive and cohesive work is carried to remove dried mud from the surface compared to the frictional work of the conventional surface. Hachicha et al [29] studied the features and effect of dust on the retrogressive performance of Solar PV panels for both in/outdoor weather conditions in the United Arab Emirates at various tilt angles of 0^{o}, 25^{o} and 45^{o} for five-month. The experimental results showed that the accumulation of dust on the solar PV surfaces substantially affects their electrical performance both for outdoor and indoor cases. For this reason, maximum power decreases steadily by 1.7% for every 1g per m^2 increase of dust. Micheli et al [30] investigated the impact of soiling/dust accumulation for different solar radiation wavelengths. Loss due to soiling was estimated by comparing the measurement from the transmittance of both clean PV glass (control device) and soiled glass as expressed in equation (2-1).

$$\tau_{Soiling}(\lambda) = \frac{\tau_{soil}(\lambda)}{\tau_{ref}(\lambda)} \qquad (2\text{-}1)$$

Where $\tau_{soiling(\lambda)}$, $\tau_{soil(\lambda)}$, and $\tau_{ref(\lambda)}$ represents the transmittance soiling ratio and the transmittance of the soiled and clean surfaces.

The authors found that the wavelength range of 500nm - 600nm gives good predictions for reduction in spectral transmittance as a result of soiling on solar PV devices. One major drawback of this study lies in its limitation to only spectral transmittance as no correlation was obtained directly between soiling losses and PV power output.

Zitouni et al [31] examined the influence on soiling on a 16.56 KW mono-crystalline grid-connected PV system using the energy-performance and soiling ratio-difference parameters for six months for both rainy and dry seasons in morocco. They found that within the duration of the study for the PV system the rainy season records less daily energy loss of 0.07KWh for

0.02% soiling rate compared to the dry season of 2.7KWh energy loss for 0.32% soiling rate per day. Chen et al [32] studied how dust-induced spectral shielding, corrosion and temperature change affects PV operating efficiency. They found out that dust accumulation impacts negatively on PV output performance with a maximum power reduction of 34% for 10g of dust deposited on every square meter of PV surface. The above studies established that dust soiling and accumulation have negative effects on the performance of solar harvesting devices. Ghassan et al [10] investigated experimentally the adhesion and the cohesion bonding effect between dust particles/residues in a dry mud solution using friction and tensile test. The authors showed that the dry mud film formed between the mud solution and the glass surface is responsible for binding work due to cohesion and adhesion. They concluded that the mud formed from the interaction between dust and water molecules adheres to the surfaces of solar harvesting devices and interferes with the device performance.

Yang et al [33] carried out a laboratory study using ion beam induced charge (IBIC) to understand the impacts of very high dust velocities that cause craters on surfaces of PV deployed in space missions. Their findings revealed that crater efficiency degrades by 20 percent when a Hamamatsu diode was exposed to a high-velocity Al dust from a dust accelerating device shown in Figure (2.1).

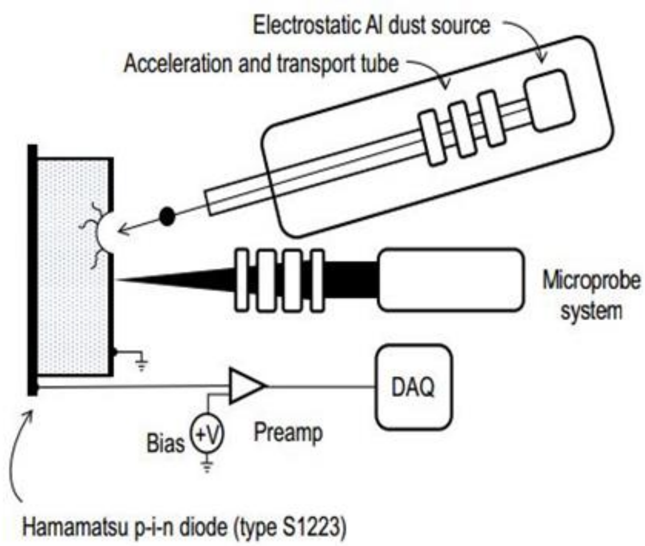

Figure 2.1 Schematic for the Hypervelocity Dust Impacts Experiments [33]

A review about the effect of particulate matter (PM2.5) on the degradation of the transmittance of PV glass was carried out by sun et al [34]. By applying various enhanced experimental and model techniques to investigate the relational effect of PM2.5 deposits and hydrophobic film coatings on a BIPV (building integrated photovoltaic) glass model operating under different conditions. They concluded that PV transmittance could suffer a gross reduction (approximately 42 % to 118 %) if PM2.5 deposition persists for more than one month. Tripathi et al [35] carried out laboratory and field experiments to determine the performance of solar photovoltaic module operating in a dusty environment located in Kamataka state, India. They found out that PV power output reduces by 43.18 percent and 44.75 percent for the field and laboratory studies respectively. A summary of the soiling effect of dust on solar PV power output for different regions is give in table (2.1).

Table 2.1 Degradation of Various PV System for Different Locations

S/N	**Location for study**	**Duration**	**Dust Effects.**
i.	UAE(Mohandes) [28]	One Month, one week	Output power dropped by 10%
ii.	UAE(Hachicha) [29]	Five months	Maximum power decreases by 1.7% for 1g per m^2 increase in dust
iii.	Zitouni(Morroco) [31]	Six Months	2.7Kwh power drop for the dry season and 0.07Kwh power drop for rainy
iv.	Chen (China) [32]	-	Maximum power reduction of 34% for $10g/m^2$ dust deposited.
v.	Tripathi (India) [35]	-	43.18% and 44.75% for laboratory and field test respectively
vi.	Appels (Belgium) [36]	One Month, one week	Power loss between (3% - 4%)

2.1.1 Numerical Studies on Environmental Dust

Lu et al [37] carried out a numerical study on the behavior of dust accumulation under the influence of wind around a PV system installed on top of a building. The study provides insights about the behavior of complicated airflow fields responsible for variations in dust deposition around solar PV panel surfaces. They also found out that the rate of dust accumulation could reach a maximum of 11.45% at an air velocity of 5m/s and predicted a high rate of deposition for medium dust compared to other dust sizes. Also, Nouira and Sammouda [38] performed a numerical study using Comsol Multiphysics software package to determine the effect of dust accumulation, wind velocity and wind direction on the operation of a solar photovoltaic module incorporated with a phase change material (PCM). By using the HDKR model (Hay, Davies, Klutcher, Reindl), a phase change material was introduced to improve heat transfer due to convection, and radiation from an inclined PV-PCM set-up simulated under actual environmental conditions. They found out that a steady increase in the thickness of the phase change material, the dust deposition density, as well as the wind velocity favor the decrease in PV module temperature resulting in an improvement in the device output power and efficiency. Oh [39] investigated the impact of different sizes of accumulated dust particles on the penetration capacity of photovoltaic glass surfaces as well as its performance using the Monte-Carlo simulation approach. He found out that from the lambert-beer-Bouger correlation, the sunlight penetration reduces exponentially with the dust area density and fluctuates more for large dust particles while minute dust particles give rise to a large reduction in the penetration of sunlight according to mass extinction coefficient. The correlation for the Lambert-beer-Bouger law is given in equation (2-2).

$$I = I_0 \exp[-\beta_e x] \qquad (2\text{-}2)$$

Where I_o represents the light intensity incident to a surface, x represents the distance traveled by light through a layer of dust deposited on panel surface and β_e is the extinction coefficient which can be expressed as

$$\beta_e = \rho . K_e \qquad (2\text{-}3)$$

Where K_e represents the mass extinction coefficient and ρ is the density of the dust.

In another work, the impacts of dust particle sizes, the angle of azimuth and installation tilt on flour and high rise-building installed photovoltaic system were investigated by chiteka et al [40] using 3-dimensional CFD modeling approach developed in Ansys fluent V.17.0 software package. They reported that a low azimuth and tilt angle favors more dust deposition when compared to other factors such as dust particles sizes. Also, large dust particles (>100 microns) accumulate more on the surfaces of building installed PV-systems compared to smaller ones (<10 microns). They further explained that more dust deposition is obtained for floor mounted PV system (11.8% more) compared to high rise-mounted PV system as a result of high impact wind velocities (1.8m/s - 3.7m/s). Khandakar et al [41] applied machine learning algorithms to predict the effect of accumulated dust alongside other environmental variables on solar photovoltaic power output. They found out that among the different types of regression models that were trained and tested, the ANN model could accurately predict PV output performance better than other models such as the GPR and linear regression models.

2.2 Dust Cleaning Methods/Techniques in Solar Thermal and Photovoltaic Applications

2.2.1 Natural Dust cleaning

The two major natural dust cleaning mitigations include wind and rainfall. While cleaning due to wind velocity may be unreliable due to the fact that not all of the settled dust particles could be completely removed and dusty wind could even aggravate dust deposition on surfaces in some instances; rainfall serves as a better source of cleaning the photovoltaic surface resulting to increase in the efficient operation of solar harvesting devices. Syed et al [42] reported that lack of rainfall experienced in some arid regions of the world significantly affects the power output of installed solar photovoltaic modules in these locations as shown in table (2.2).

Table 2.2 Observed On-site Module Power Output Degradation for Locations Known to Suffer a Lack of Rainfall in MENA region (Hot and Humid environment) [42].

Locations	Yearly Rainfall	Decrease in power output on site	Period of Exposure
KSA	6 - 10	50%	26 weeks
UAE	80 - 90	10%	5 weeks
Qatar	70 - 75	10%	14 weeks
Palestine	30 - 40	5 – 6 %	1 weeks
Egypt	18 - 50	60 – 70%	26 weeks

Smith et al [43] studied the impacts of rainfall and other factors on the performance of PV panels. They found out that a PV panel cleaned after a moderate downpour restores power to around 1% of that obtained when manually cleaned. In another study, Hammond et al [44] reported that the power output of a rain-cleaned-solar PV module improved to 99.5% to that of its initial operating conditions before dirt settlement. Kalougirou et al [45] carried out a comparative study between natural rainfall and pressurized water cleaning method on the performance improvement of solar photovoltaic subjected to intense dust surface loading and polluted air under Cyprus environmental Conditions. They reported that rainfall could both improve and deteriorate the performance of PV system depending on the prevailing weather conditions. According to them, rainfall during winter period keeps PVs surfaces cleaned, but rainfall after dust storms causes settled dust particles to stick firmly to PV surfaces and need manual cleaning via the use of water and brush. Schill et al [46] conducted an experimental study of solar PV subjected under various environmental and soiling conditions. They observed that light rainfall could partially wash off accumulated dust on the surfaces of solar PV modules which leads to recovery of PV module efficiency. Appels et al [36] reported that among deposited particles, larger particles such as pollen grain (>60microns) could be effectively clean by rainfall from PV module surfaces compared to smaller dust particles (2-10 microns). Apart from natural cleaning by water, wind can also remove deposited dust from the surface of solar harvesting devices, although this depends on environmental conditions and panels orientation [47] as regions associated with strong dusty wind experience more dust accumulations compared to cleaning effect of the wind. Guo et al [48] reported strong wind can cause an induced dust cleaning effect by levitation of deposited dust from solar panel surfaces. They concluded that rainfall remains the most efficient cleaning means provided by nature for Solar panel. In addition, Condensed water droplet may form on PV surfaces for a highly humid environment and effect some cleaning action as the droplet slides on the surfaces of the glass modules [49].

2.2.2 Mechanical and Automated Cleaning Techniques

Aside from natural cleanings like wind and rainfall, mechanical cleaning is the basic form of cleaning PV panel surface and requires human labor, drones and robotic systems. Parrott et al [50] developed a silicone foam and brush-incorporated robot dust/mud cleaning device and compared its performance with the traditional use of mops and water to manually clean the PV surface for three months in thuwal, Saudi Arabia. They found that the automated system is effective and more economical for curbing dust-effects on solar harvesting devices and for improved PV power generation on a large scale compared to manual labor within the period and conditions for carrying out the experimental study. One profound improvement to the robotic cleaning device was the incorporation of silicon foam brush with its; low-cost value, good repellent action towards dirt/mud on the brush, good hydrophobic feature, high cleaning efficiency and non-dent/scratch infliction on the PV panel. The short time for this study, non-inclusion of diverse seasonal conditions and environmental conditions such as rainfall and sandstorms, are among the limitations which could interfere with the results obtained, therefore more research works are needed in this area.

Cai et al [51] used both computational fluid dynamics and orthogonal methods of an experiment to optimize the dimensions of a dust-cleaning PV panel robotic device. They showed that results from the simulation and experiment agree, with little parametric derivations and concluded that the cleaning device could efficiently suck dust at a velocity of 41.8 m/s using the optimal structural dimensions developed for the robotic cleaning device. The limitation to this work is the non-inclusion factor such as humidity which impacts negatively on the sucking ability of the device when dust mixed with condensed water vapor settles on the PV surface, and also the extra cost of component and power that need to be deployed to achieve the cleaning process in real PV applications.

Singh et al [52] investigated and developed a cleaning strategy to curb the effect of dust deposition on an open solar volumetric air receiver-based solar tower from two different experimental setups; a) a heliostat mounted in a wind tunnel and b) a designed porous absorber installed in a solar volumetric air receiver. They found out that sand particles accumulate both on the heliostat and in the porous chamber of the solar volumetric air receiver and that larger dust size causes more blockage compared to smaller ones. Experimental and simulation works incorporating cyclone separators were used by the researchers to effectively remove and collect accumulated dust particles from the solar volumetric air receiver up to a collection efficiency of 96%.

Mondal and Bansal [53] carried out a brief and detailed review of various automated driven solar photovoltaic module systems. The table (2.3) gives a summary of the advantages and shortcomings of various cleaning technologies studied by the authors,

Table 2.3 Different Types of Cleaning Techniques [53]

Cleaning System	Advantage	Shortcomings
EDS for standing wave curtain	1. Highly efficient at high gas pressure. 2. No mechanical movement to scratch the surface.	1.Removal is difficult when gas (atmospheric) pressure is below a certain limit. 2.Dust removal capability depends on size of the particles deposited. 3.Requires high voltage.
EDS for multi-phase electric curtain	1.Efficient and can be used to remove dust from a variety of surfaces. 2.No mechanical movement to scratch the protective surface. 3.Efficient with and without use of external power supply.	1.Requires digital signal controller is costly. 2.Requires switching devices for converters hence more maintenance is required. 3.Requires high voltage.
Heliotex's 'Automatic Solar panel Cleaning System'	1.Water reaches to every part of solar PV module. 2.Helps in cooling of Solar PV modules, which increases the efficiency.	1.Treated Water required. 2.Filter must be changed periodically. 3.Huge wastage of water.
Gekko Solar	1.Self-regulating and flexible uninterrupted cleaning operations.	1.Limitation of inclination up to 45 degrees. 2.Additional stresses on the surface due to gear, belt and vacuum
Gekko Solar farm	1.Self-regulating and flexible uninterrupted cleaning operations.	1.Limitation of inclination up to 30 degrees. 2.Complex gear, belt system.

Cleaning System	**Advantage**	**Shortcoming**
Solar brush	1.Automated robot. 2.Works up to an inclination of 3.5 degrees. 3. Wireless controlled. 4. Rechargeable.	1.Heavy weight. 2.Initial cost is high. 3.Requires human intervention. 4.Performance speed is very slow.
PIC microcontroller and PLC based cleaning	1.Self-regulating and flexible uninterrupted cleaning operations.	1.Complex chain, sprocket-based structure. 2.Single panel-based design.
Hector	1.Comparable, integrated with all supplies. 2.Operational day and night.	1.Performance is slow. 2.Feeding has to be done regularly
Solar panel cleaning robot	1.Washing and wiping both processes are present.	1.Horizontal shifting of the robot over the PV module results in skidding. 2.Stress on the Surface of the panel due to its weights.
Wash panel solar panel cleaning robot	1.Able to clean dust and bird droppings.	1.Human intervention is required to start the operation and while moving from one row to another.
Sunpower-greenbotics GB1	1.Able to clean dust and Bird droppings.	1.Human intervention is required to start the operation and while moving from one row to another.
Tuff Fabs nano clear	1.Long lasting.	2.Cleaning is still required, but with less effort.
Asahi kasei corporation SPV coating	1.High Transmittance.	1.Cleaning is still, but with less effort.

Algamdi et al [54] developed programmable Solar photovoltaic module testbed located on a carport in King Abdullah University, Saudi Arabia, that can be remotely controlled, to investigate and compare the cleaning efficiency of various automated cleaning interventions comprising of electro-mechanical vibrations, pressurized air and water jets, and hybrid cleaning techniques. According to the authors, water cleaning mode provides 27% increase in the power output of the installed PV system when compared with uncleaned mode, while the vibration mode had insignificant impact on the power output for different dust cleaning experiments conducted at different environmental conditions. The work provides insight into the use of hybrid-optimized dust removal techniques applied to solar harvesting systems on a large scale in harsh environments.

Rifai et al [55] researched on the use of an Arduino- driven rotating polycarbonate disk device for possible dust-removal from the surfaces of PV protective cover. The results showed that the centrifugal forces (most dominant among others) generated by the rotary motion of the polycarbonate are effective in dust removal and large particles can be easily removed compared to smaller ones that stick to the surface of the disk due to ionic and Electrostatic charges.

2.2.3 Drone Photovoltaic Cleaning

Drones also serve as an alternative to stationary robotic installations and manual dust removal methods, although the same cleaning components such as brush and micro-fiber-cloth could still be used. The advantage of the drone lies in its flexible, mobile and self-propelling nature while its limited time of flight and energy-dependent nature accounts for its shortcomings.

Al-Housani [56] et al investigated the compatibility and adaptability of various dust removals methods and components (brush, microfiber-cloth wiper, vacuum cleaner) to be fitted into an

Unmanned area vehicle /drone for solar harvesting purposes based on the size, weight, energy requirement of the components. They found that the cloth wiper made from microfiber shows higher effectiveness (7.7% in summer and 3.1% in winter compared to test case) in PV cleaning. On the other hand, brush-cleaning gave better results for drone retrofitting due to its ease of usage, lightweight, and minimal energy requirement. The disadvantage of the robot/drone cleaning system is the high cost of installation, maintenance, and huge water-requirement. Zefri et al [57] inspected various defects such as soiling, crack and hotspots on the surfaces of Solar PV farms installed in Rabat, morocco using cameras attached to drones. The thermal orthomosaics and visual results obtained show the capabilities of using unmanned aerial vehicles for both Visual and thermal imagery of solar installations. Alsafasfeh et al [58] proposed the use of a drone-mounted camera system made of a charge-coupled (CCD) and a thermal imagery device for faults detections in solar PV installation. They found out that the defects could perfectly be detected from the CCD and thermal videos obtained using the camera-drone setup. Grimaccia et al [59] monitored different types of faults and defect developed on the surfaces of PV plants in two different locations in Italy via a camera incorporated UAV system using two different route mapping techniques (vertical and horizontal). After a comprehensive study and comparison of the two routes mapping methods, their experimental findings revealed that the vertical mapping style performs better in terms of effectiveness, economic-advantage, and speed for image data collection and analysis.

2.2.4 Electrostatic Dust Cleaning

The basic principle behind the electrostatic dust shield (EDS) deals primarily with the use of an energetic electric field to repel charged dust particles from a surface via the creation of a varying amount of electrostatic charge [60], the process is expressed in Figure (2.2).

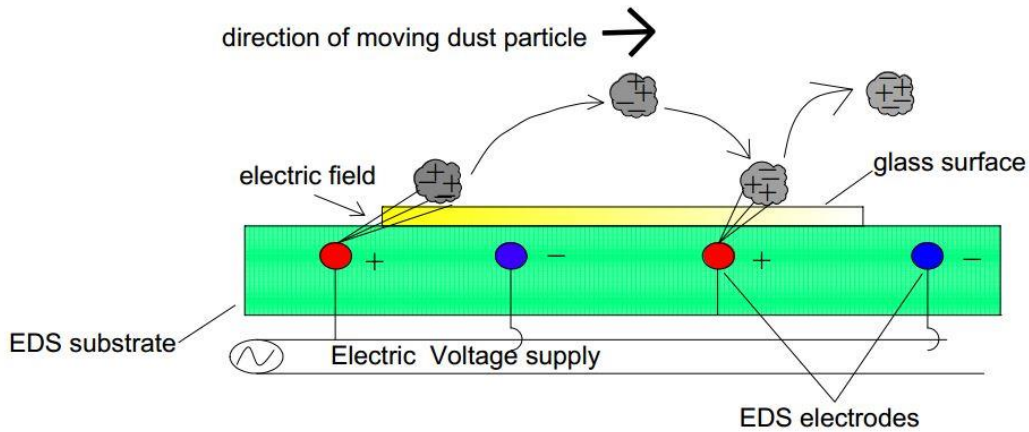

Figure 2.2 Dust Removal Process from an Electrostatically Charged Surface

Assuming the coulombs force exerted by the charged surface on the dust particle makes it drift with a velocity opposed to the viscous drag; the dust particle mobility is expressed in equation (2-4)

$$\mu_{dm} = \acute{\upsilon}/\grave{E} = \frac{q}{6\pi\eta R} \qquad (2\text{-}4)$$

Where μ_{md} represents the particle mobility, $\acute{\upsilon}$ is the dust particle drift velocity, $\grave{E}$ represents the electric field intensity, η is the coefficient of viscosity, R is the radius of the dust particle and q represents the charge on the dust particle.

Guo et al [61] used an OSM (outdoor soiling microscopy) approach, to determine the dust cleaning efficiency of two-phase electrodynamics dust shields (EDS) devices activated under various field conditions. They found out that EDS dust removal efficiency reduces from 45% to 20% within four days of study. The authors concluded that persistent dust residues on surfaces of the EDS causes frequency reduction and suggested that frequent activation of the device could improve the overall dust removal efficiency. In another study, Kawamoto and Guo [62] activated a tilted EDS dust cleaning set up with double-phase rectangular voltage at a frequency of 1Hz. The authors concluded that operating the EDS at the following conditions; i) a high EDS activation voltage combined with high insulation plate strength ii) minimum plate thickness iii) reduced electrode pitch configuration, iv) use of highly insulative anti-dust coating film and v) natural wind, would result in an improved electrostatic cleaning set-up. They also affirmed that smaller dust particles (< 25μm) resist EDS cleaning due to large adhesive forces and larger particles (> 300μm) resist EDS cleaning due to high gravitational forces compared to repelling electrostatic forces.

Guo et al [63] further studied the impact of different dust deposition methods (Aerosol and Sieve) and EDS modes of operation (cyclic and single) on the cleaning efficiency of an electrostatic cleaning system using a detachable die-electric technique. They concluded that dust deposits affect the cleaning efficiencies of EDS devices particularly in cyclic mode of operation and the aerosol deposition showed more severe reduction in dust removal efficiency compared to the sieve type. The authors also explained the concept of how both dead dust and regenerated dust affects the cleaning efficiency of EDS from the gravimetric analysis given in equation (2-5);

$$\eta_{EDS} = \frac{m_{Pre} - m_{Post}}{m_{Pre}} \quad (2\text{-}5)$$

Where η_{Pre} represents the EDS dust cleaning efficiency, while m_{Post} and m_{Pre} represent the measured mass of dust after and before the activation of the electrostatic dust shield set up.

In another study, Guo et al [48] compared the soiling loss obtained when a solar photovoltaic panel is activated with an integrated electrostatic shield (two-phase) at different voltages to when the PV is not activated by the EDS device. The result obtained showed 16% - 33% reduction in soiling loss when the EDS voltage was set to $9KV_{pp}$ and no noticeable reduction in soiling losses was observed when the EDS voltage was set to $6KV_{pp}$. The authors concluded that higher EDS activation voltage could results in high cleaning efficiency and that incorporated EDS as a possible anti-soiling PV technology is feasible. Kawamoto and Shibata [64] studied the use of the combined effect of single - phase rectangular voltage operated EDS device and natural wind for the removal of sand particles from the cover of solar photovoltaic panels as shown in figure (2.3). The maximum dust cleaning efficiency reported by the authors was approximately 80% for the EDS activated at low frequency < 20Hz and threshold voltage range 8.4 – 9.8 KV_{pp}. They concluded that energizing dust particles with an electrostatic force field in the presence of a dynamic wind motion improves dust cleaning action which further improves dusty solar PV power output to 97% when cleaned.

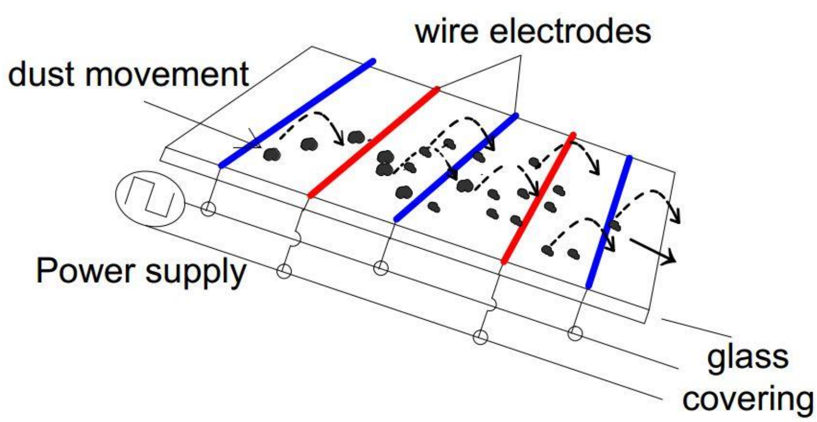

Figure 2.3 Cleaning Process of an Electrostatic Dust Shield [64]

Chesnut et al [65] studied numerically how charged particle sizes and particle-interactions affect the overall performance of an electrostatic dust shield activated by a four-phase traveling wave using the DE (discrete element) simulation method. They found out that continuous operation of EDS at very low voltage settings may improve the cleaning of minute dust particles.

2.2.5 Self-Cleaning Methods for Dust Removal

Over the years the self-cleaning properties of super-hydrophobic/hydrophilic surfaces stand out as excellent soiling-preventive techniques and could be commercialized.

The phenomena of a superhydrophobic surface were first introduced by two groups of scientists Wenzel (1936), and Casie and Baxter (1944).

According to Wenzel [66], a liquid will completely wet a rough surface by covering the contours of its roughness. The Wenzel equation shows the effect of surface roughness on the contact angle as expressed in equation (2-6)

$$\cos\theta_e^W = r\cos\theta_e \qquad (2\text{-}6)$$

The roughness (r>1) in equation (2-6) is given as a ratio between the real surface area and its projection in the horizontal plane. Θ_e represents the equilibrium contact angle on a smooth surface.

However, when a liquid meets the heterogenous surface, the droplet settles on the top composite surface of the flat air gaps in between flat solid and therefore the Casie-Baxter model [67] is more suited to describe the surface phenomenon as expressed in equation (2-7).

$$\cos\theta_e^{CB} = \varphi_s(\cos\theta_e) + (1-\varphi_s)\cos\theta_X \qquad (2\text{-}7)$$

Where, φ_s represent the fractional portion of the protruded top surface, $(1 - \varphi_s)$ represent the air gap fractional part and Θ_e^{CB} and Θ_x represent the Casie-Baxter equilibrium contact angle and contact angle of gas in the air gaps respectively.

The Wenzel and Casie/Baxter model are combined into a general model as given in the equation (2-9) and the three models are illustrated in figure (2.4) [68];

$$\cos\theta_e^{CB} = \varphi_s r(\cos\theta_e) + \varphi_s - 1 \tag{2.8}$$

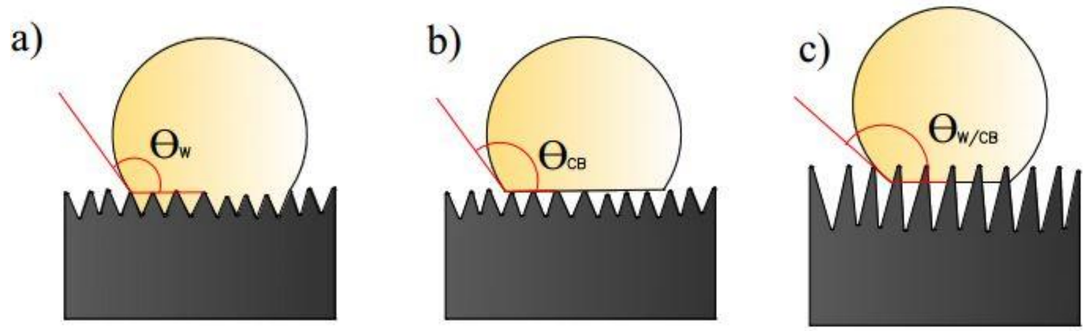

Figure 2.4 Wetting States (a) Wenzel, (b) Cassie-Baxter and (c) Combined Models

Nature provides deep insight into the understanding of principles, structures, and functions of biological plant/animal components that exhibit the phenomenon of self-cleaning [69]. By mimicking this biological component such as lotus leaves, rice husk, etc. scientists have developed highly effective and multifunctional self -cleaning surfaces for application in various industrial sectors. Areas of research could include films coating in the polycarbonate/glass industry, water repellent solutions in the paint and cement industry, self-healing drugs in the medical field, and solar photovoltaic cells [70].

A comprehensive review of Bio-inspired surfaces was done by Nishimoto and Bushan [71]. According to the researchers, three types of surfaces abound in nature that exhibit self-cleaning characteristics and Table (2.4) gives a summary of their findings.

Table 2.4 Overview of Bio-inspired Self-Cleaning Surfaces [71]

Surface Types	**Biological species**	**Properties**
Super-hydrophobic surface	Lotus Leaf	Super hydrophobicity, Low adhesion, Low drag
	Rice Leaf	Super-hydrophobicity, Anisotropic wetting, Low drag
	Cicada Wing	Super-hydrophobicity, Anti-reflection
	Butterfly Wing	Super-hydrophobicity, Directional adhesion, Low Drag
Hydrophilic and Oleophobic (in water) surface	Snail Shell	Superoleophobicity
	Fish Scale	Superoleophobicity
	Shark Skin	Oleophobicity, Low drag, Anti-fouling
Super-hydrophilic surface	Pitcher Plant	Low Drag(slippery)
	Photosynthesis	Photocatalysis, Photo-induced superhydrophilicity, Self-sterilizing, Anti-fogging

The hydrophilicity and hydrophobicity of a surface determine to a large extent its self-cleaning behavior [71]. The two phenomena depend on the surface texture and surface free energy of various materials and could be determined by water droplet contact angle measurements. For a hydrophobic surface, with associated low free surface energy and high contact angle (> 150^o), water droplet in contact with the surface creates a lotus effect which facilitates self-cleaning by picking up dirt and dust particles along its path. In contrast, the high surface free energy and low contact angle (< 90^o) of a hydrophilic surface may also facilitate cleaning by coming in between dirt and surface as it slides in between the surface and dirt enabling it to take the dirt away. Both processes are illustrated in figure (2.5)

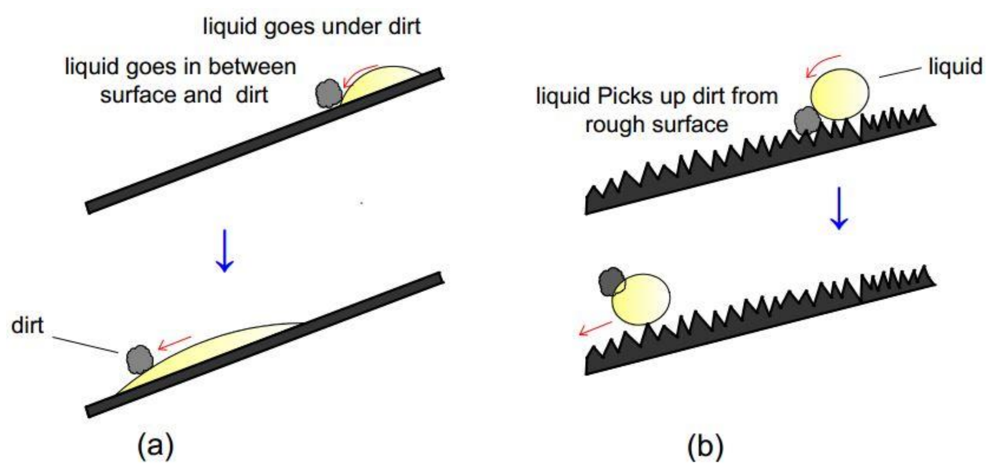

Figure 2.5 Schematic illustrations of Self-cleaning processes on a) Super-hydrophilic Surface, b) Super-hydrophobic Surface

Dust-repellent materials such as TiO_2 and SiO_2 nanoparticles are widely used for making self-cleaning coatings. While SiO_2 film stands out for its hydrophobic coating character [72], TiO_2

serves as the most popular hydrophilic film exhibiting both photocatalytic and hydrophilic behavior when in contact with UV rays [73]. A good PV coating material should possess the following properties (i) Excellent spectral transmittivity; (ii) Surface Durability (iii) self-cleaning and iv) minimum light reflectivity. The process of making the film/coating should be affordable, realistic and able to be mass-produced. Pan et al [72] applied different self-cleaning hydrophobic and super-hydrophobic coatings on glass by combining low surface energy materials such as silica gel and ethanol with SiO_2 microscopic nano-particles to curb the deposition of dust on the surface of PV cells in order to improve spectral transmission and efficiency of the PV devices. They found out that among four sample coatings investigated for a dust accumulation time of one hour and at 30^o tilt angle; the silica sol./SO_2 coated glass present best performance in terms of reduced dust deposition density of 36.8% compared with normal glass, improved spectral transmittance and lowest PV efficiency degradation compared with other samples. Soklic et al [73] studied the morphological and photocatalytic properties of TiO_2 - SiO_2 thin film coatings for self-cleaning application within a two-month duration using the dip coating and spray deposition methods on a PV glass surface exposed to the environment. They discovered that dip-coated glass sample showed high light-penetration, uniform and non-crack characteristics compared with conventional glass; while no significant dirt-removal ability was observed within the short time duration of the experiment for all test samples. Coatings on solar devices surfaces other than glass materials have also been worked on. Yilbas et al [13] studied the hydrophobic, morphological, optical and tribological characteristics of crystallized polycarbonate surfaces with and without dried mud. They observed that micro/nano size fibrils and spherulites make up the hierarchical texture of the crystallized surface, which results in increased hydrophobic state and high-water droplet contact angle. According to the authors, the optical transmittance of the polycarbonate surface reduces with crystallization and more reduction is observed for the mud removed crystalized surface due to the interference of incident radiation by both the mud residue on coated surfaces.

Recently, the need to make a surface both self-cleaning via coating and at the same time maintain the optical transmittance has been the most researched area among scientists. Polizos et al [74] investigated the relationship that exists between the morphology and size of two different surface coatings (silica structured and bimodal-sized unstructured nanoparticles) with dust-removal and spectral transmittance on a concentrating solar power collector surface. By comparing the coated surfaces with the uncoated surfaces of the collector, they concluded that the anti-soiling coatings were effective in the dust removal rate and maintained the mirrors spectral properties with a 17-39% decrease in the rate of soiling for coated mirror compared with uncoated. Nevertheless, the researchers affirmed that the unstructured bimodal coating gives better performance than silica structured coating with a 2-3% increase in transmittance. Li et al [75] used super hydrophobic and anti-reflective coatings made from spin-coated nano silica particles, and tetraethyl orthosilicate and hexadecyl methoxy silane solution to modify the surface of dye sensitive solar cells for self-cleaning and improve spectral transmittance. They found that glass modified through silica particle deposition showed (i) a large transmittance of 99 % at 580nm bandwidth (ii) an improved hydrophobic structure that could remove dust mixed with water/oil effectively and iii) an increased efficient performance of device over 10 percent. One set back of this study is that only the direct transmittance (and not the total transmittance as usually recommended) was taken into consideration during the experiment. Huang et al [76] replicated biological leaf surface topological features of Indian origin on exposed silicon wafers using an easy duplicable transfer method to achieve hydrophobic and antireflective coatings. They discovered that among four photopolymer replicas (of Bamboo, Indian shot, lotus, grape master leaves) on silicon and normal silicon surfaces tested using a solar simulator; lotus photopolymer replica showed the highest transmittance and lowest reflectance while normal silicon exhibited the opposite character. Apart from the positive PV performance (15% improved spectral performance and 11% increased power obtained) demonstrated by lotus leaf replica, it also showed good superhydrophobic characteristics without additional surface treatment resources like a solvent and nanoparticles making it stand out for its endowed self-cleaning ability.

The creation of superhydrophobic and hydrophobic surfaces is not only limited the use of chemical treatment; but other methods such as Laser texturing, PDMS replication and mechanical grinding can also produce a self-cleaning surface. Dey and Naughton [77] reviewed different techniques of modifying the surface of glass and a summary of their finding is given in the figure (2.6).

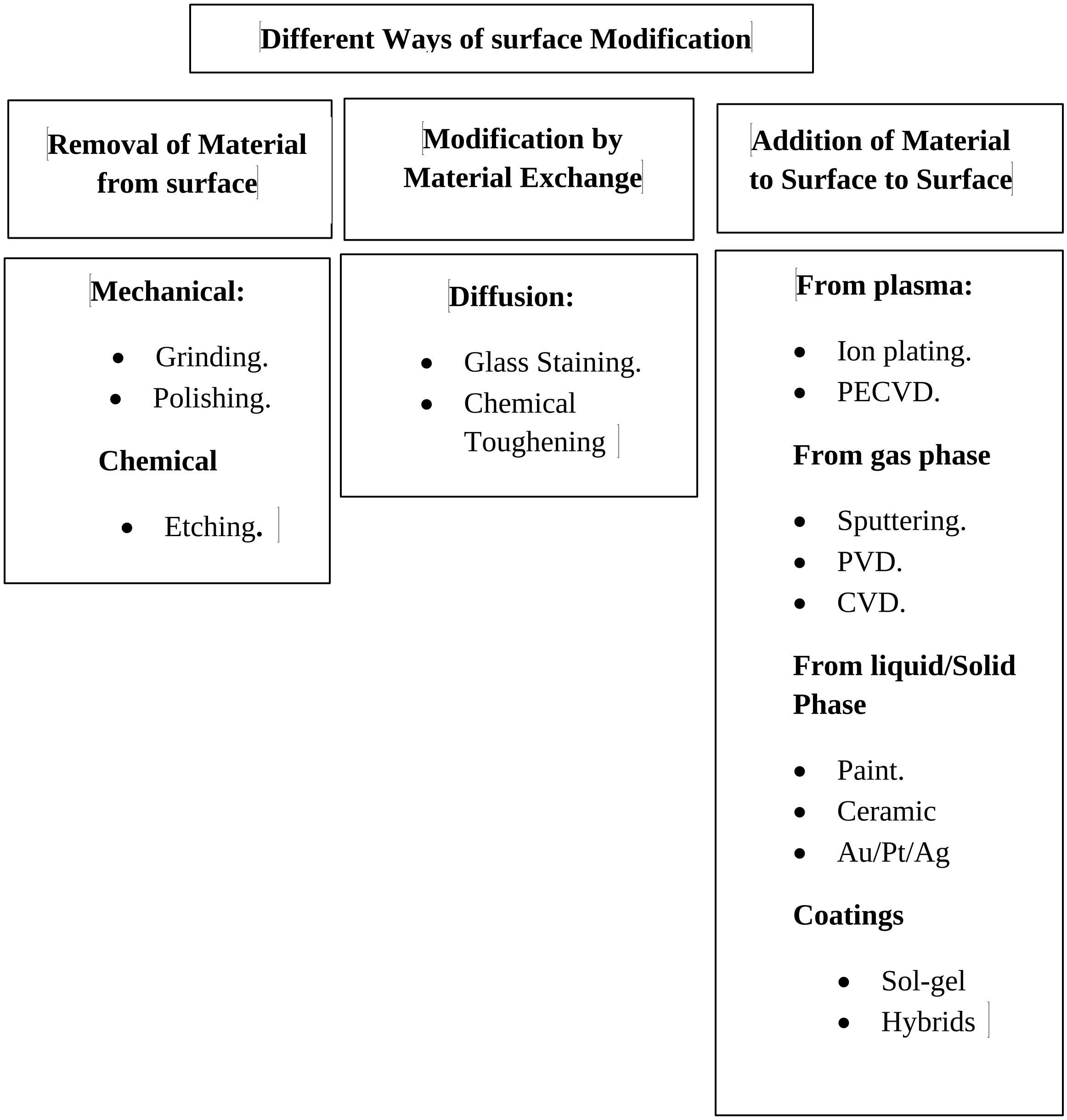

Figure 2.6 Ways of Glass Surface Modification [77]

Zhan et al [78] investigated the use of clear silica-coated superhydrophobic borosilicate glass surface to bounce condensed water vapor droplets for effective dust particle removal. Results showed improvement in hydrophobic features, improved light penetration, and better mechanical stability. They also observed that during condensation, smaller dust particles were easily removed via self-jumping of vapor droplets condensate compared to larger ones. They found out that self-bouncing of droplets condensate could effectively clean tiny dust particles that resist cleaning through mechanical vibration, windspeed, and gravity enhanced surface tilting.

Water droplet motion has also been used to effectively clean dust particles from super-hydrophobic surfaces. Yilbas et al [79] applied a droplet motion of water for the removal of dust from an inclined hydrophobic polycarbonate surface. The authors established that dust particles are removed by moving water droplets via the process of water cloaking of dust. Also, they found out water-cleaned polycarbonate surface showed improved optical transmittivity characteristics compared to the dusty polycarbonate surface, but the transmittance for both surfaces was lower than the as-received polycarbonate. Hassan et al [80] investigated the effects of changing droplets acceleration to enhance dust particles removal from an inclined hydrophobic surface. They varied the inclination angle of the hydrophobic surface for different droplet sizes for effective removal of dust particles. They demonstrated that increasing the inclination angle, increases the droplet acceleration, reduces wobbling and enhances dust picking by the hydrophobic surface. Finally, they demonstrated that Droplet with smaller diameter rolling on a large inclined hydrophobic surface is effective for cleaning of dusty hydrophobic surface.

Another self-cleaning technique for optical surfaces that does not require water and energy resources but at its early stage of development is generating an avalanche effect to induce the removal of large mass of dust particles. Several studies have been conducted to study the flow of particles on surfaces under the influence of avalanche, but studies have been focused on natural occurrences such as fall rocks and snow on mountains and hills surfaces [81-84]. To initiate the avalanche effect [23]; density differences between dust particles are generated so that large particles initiate sliding or rolling motion on the surface and light particles that move down a tilted surface are carried alongside heavier counterparts under the influence of gravitational potential energy. Yilbas et al [23] carried out a novel study where high density particles such as Zirconium oxide and Inconel 625 powders where used to remove large dust particles from the surface of an inclined optical surface via generating the avalanche effect.

2.3 Mechanism of Dust Removal from a Surface

Dust particles role and slide under the influence of an applied external force. The movement of dust particles on an inclined glass surface is mainly influenced by the interaction of gravitational force with shear and pinning forces. The drag force forms the shear force while the pinning force comprises of the adhesion, Vander Waal and interfacial forces. The figure (2.7) shows relevant forces that act on a dust-glass surface interface.

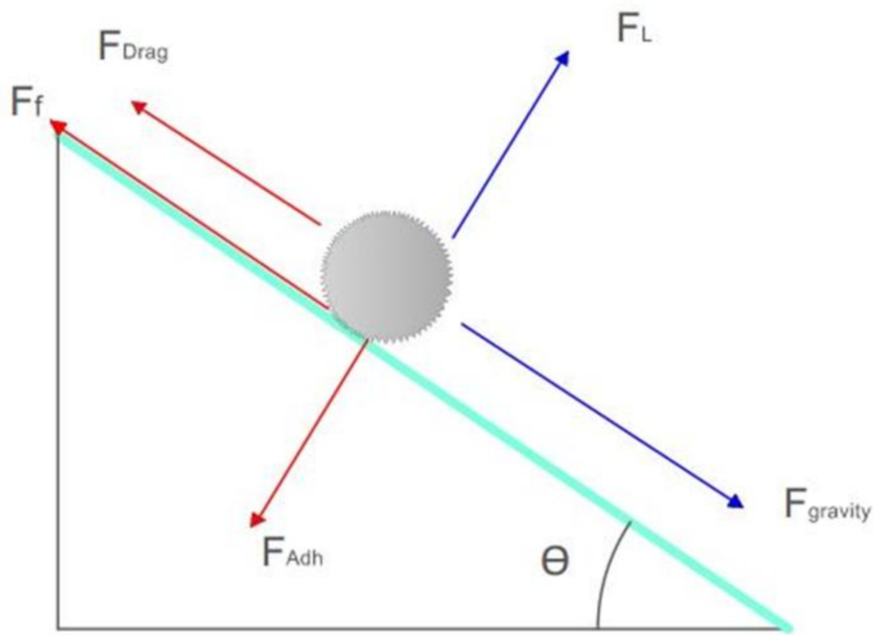

Figure 2.7 External Force Direction of Dust Particle on a Tilted Surface

Where Where $F_{gravity}$, F_L, F_f, F_{Adh}, and F_{Drag} represents the Gravity, Lift, Friction, Adhesion and Drag force respectively.

Dust particles are attached firmly on surface of an inclined plane due to generated forces of adhesion and friction that act in a normal direction along the plane as expressed in figure (2.7).

2.3.1 Models formulated for Adhesion of Dust Particle on a Plane

Vander Waal force dominates among the adhesion force between a particle and a surface in dry and charge free environment [85].

Johnson et al [86] developed the adhesion force relationship for a smooth and spherical particle in contact with surface using the Vander Waals force postulates.

The formulated adhesion force by Johnson et al [86] for a big and fluffy body with high surface energy is given as

$$F_{Adh} = {}^{3}/_{2}\,\pi R_p \gamma_i \tag{2.9}$$

Where; R_p represents the particle's radius, and γ represents surface energy between the surfaces in contact.

Derjaguin et al [87] further modified the constant value of the above equation and adopted it for stony and little particles having low surface energy and smooth surfaces into the adhesion equation given below,

$$F_{Adh} = 2\pi R_p \gamma_i \tag{2.10}$$

To incorporate the particle - surface contact spacing or distance, another model was introduced by Hamaker [88] which can estimate the force of adhesion correctly for a particle in contact with a surface within a specific of particle – surface spacing range.

$$F_{Adh} = A_o R_R / 12 {Z_o}^2 \tag{2.11}$$

Where; Z_o represents the spacing of the particle and A is the Hamakers constant.

Rabinovich et al [89] further modified the Hamakers equation above by incorporating introducing a parameter of the same degree with the root mean square of the rough surface texture, which is called the rough surface parameter.

$$F_{Adh} = A_o R_R / 12 {Z_o}^2 \left\{ \left[{}^{1}\!/\!\left(1 + {}^{R_P}\!/_{1.48 r_s}\right) \right] + \left[{}^{1}\!/\!\left(1 + {}^{1.48 r_s}\!/_{Z_o}\right)^2 \right] \right\} \quad (2.12)$$

Where r_s represents the roughness parameter.

Due to the rough texture of both the modified glass and dust particles under consideration, the above model could be suitably applied to determine the force of adhesion in this case.

The drag force (F_d) for particles moving slowly in shear flow as formulated by Goldman et al and O'Neill et al [90] and can be applied to a dust particle moving on a surface is given thus as;

$$F_D = C_D \pi \mu_f R_p u_F \quad (2.13)$$

Where C_D represent the drag coefficient, μ_f represents the fluid viscosity and u_F is the particle influenced flow velocity. This equation was formulated with the assumption that the velocity due to shell is of the same degree as the velocity of the particle.

According to Rifai et al [55], the gravitational force for a spherical particle is given as,

$$F_g = m.g \ = \ {}^{4}\!/_{3}\, \pi R^3 \rho g \quad (2.14)$$

Furthermore, from the works of Lee et al [91], the particle lift force normal to a surface and opposite to the adhesion

$$F_L = C_L \pi/8 \, \rho_f \left(du_f/dy\right)^2 L^2 (2R)^2 \qquad (2.15)$$

Where; C_L represents the coefficient of lift, du_f/dy represents the shear in the fluid and L represents the distance of the particle center normal to the contact surface.

The friction force F_f generated between the particles of dust on a glass surface during dust movement is given as

$$F_f = \mu_d mg \qquad (2.16)$$

Where μ_d represents the kinetic friction determined from some suitable instruments.

Singh et al [52] formulated the minimum estimated velocity (threshold) required to lift a stationary dust particle as

$$u_O = \left[\frac{\left[\left({}^{8}/_{3\sqrt{3}}\right)\pi\rho_P g r^3 + \frac{Ar}{6Z^2}\right]}{(\rho_a C_d A')}\right]^{\frac{1}{2}} \qquad (2.17)$$

Where, u, A and r are the threshold velocity, Hamakers constant and radius of particle respectively, while Z and C_d are the dust-surface separation distance, and ρ_a and ρ_p represent air and particle density.

Yilbas et al [23] derived the acceleration (a_i) of the dust particle by modifying equation 1 to give,

$$a_i = g sin\delta - g\mu_{fd} - 1/m_p \left[(F_{Adh} sin\delta - F_L) + F_D\right] \qquad (2.18)$$

Where δ is the inclination angel, m_p is the mass of the dust particle,

And they later integrated the acceleration to obtain an expression for the velocity of moving dust particles on the inclined surface.

$$u_i = \int_0^{t_f} gsin\delta\, dt - \int_o^{t_f} \left[g\mu_{fd} - 1/m_p \,(F_{Adh} sin\delta - F_L + F_D) \right] dt \qquad (2.19)$$

Where u_i represents the velocity of dust particle, μ_{fr} is the friction coefficient and F_L, F_{Adh}, F_D are the lift, Adhesion and Drag force respectively.

2.4 Hydrogen Fluoride; as an Efficient Cleaning Additive

Many chemicals and reagents such as tetraethyl orthosilicate, hexadecyl methoxy silane have been used in various studies to either coat glass/polycarbonate surfaces[13],[79]; Perfluorooctyl (PFOTS) and tetraethoxysilane (TEOS) to functionalize the dust particles for self-cleaning applications[80],[92]. But none of these studies have centered on the use of hydrogen fluoride to functionalize the dust particles for solar harvesting purposes. Hydrofluoric acid is an indispensable chemical in all scientific and technological industry, being a basic agent to produce various chemical compounds and other substances. Scheele was the first scientist to mass-produce hydrogen fluoride in 1771[93].

The main raw material for hydrogen fluoride production is fluorspar (CaF_2), although cryolite and Fluorapatite could also serve the same purpose. The chemical is produced in large quantities at a concentration of 70 percent and table (2.5) gives a summary of properties associated with Hydrogen flouride [94].

Table 2.5 Thermophysical Properties of Hydrogen Fluoride are given below [94]

S/N	Property	Value	unit
1	Specific heat capacity	0.675	J/g^oC
2	Vapour pressure at 25^oC	20	KPa
3	Viscosity at 25^oC	0.61	mPas
4	Freezing point	-69	^oC
5	Density at 0^oC	1.256	g/mL
6	Boiling Point at 101.3 KPa	66.4	^oC

Hydrogen fluoride is a weak acid as it ionizes partially in solution nevertheless it is highly corrosive. It corrodes glass as it reacts with silica to form simple and complex fluorides [95]. It also reacts with some metal oxides forming metal fluorides and water.

Although a very useful chemical in the industry, hydrogen fluoride comes with detrimental effects especially to humans and the ecosystem if not properly handled. Inhalation of the gas or liquid contact could be harmful to the body, therefore professionals must be properly trained to handle the acid with high level of precaution and protective kit must always be worn [96]. Despite the limited use of hydrogen fluoride due to its corrosive nature, the acid remains a relevant ingredient in most commercial cleaning solutions but has equally been met with strict sanctions and regulations from regulatory bodies and agencies [96].

Hydrogen fluoride is used as a core additive to produce cleaning agents used in the automobile industry to remove dirt, dust, rust, mud and other particles with ease from the surfaces and other internal parts of vehicles[94]. The acid also finds application for glass etching and stainless-steel pickling in the materials and metallurgical industry because of its highly corrosive nature[97]. One distinctive property that makes hydrogen fluoride suitable for cleaning dust, stains and dirt prone surfaces stems from its reactive nature with oxides and other related compounds. Its relatively low cost and large abundance compared to other cleansing agents make it very popular in the industry.

Another feature of hydrogen fluoride that is synonymous with its cleansing action is its digestive nature when in combination with other chemicals. Feng and Barrat [98] used a combination of hydrofluoric and nitric acid to decompose different samples of dust in a microwave oven. They successfully recovered metals such as lead and cadmium. Ely et al [99] studied the digestion of radioactive geological specimens with hydrogen fluoride mixed with other chemicals. The authors found out that hydrogen fluoride was adsorbed with the platinum group forming flour complexes that were stable. Jonas and Machemer [100] also used hydrogen fluoride to liquefy silica and iron-containing oxides in high-pressure steam boilers during pre-commissioning. Genuino et al [94] carried out a compressive review of the application of hydrogen fluoride in the automobile washing industry. They presented the peculiar characteristics of hydrogen fluoride that enable it to dissolve metals, silicates, oxides, and rocks for effective cleaning alongside its health and environmental implications.

2.5 Research Gap for Dust Modification via Hydrogen Fluoride Treatment for Self-cleaning Applications

Dust mitigations remains critical for alternative and clean-energy technologies. Photovoltaic (PV) modules have been widely employed for electric power generation for many years. However, they are not yet competitive with other energy-generation technologies, especially in environments that suffer from dust, airborne particles, humidity and high ambient temperatures. Researches conducted till date indicate that the dust deposition has a considerable effect on PV module performance as it reduces the light transmittance of the PV module surface cover. Reducing the amount of dust accumulation on protective cover surfaces is an important consideration in arid regions such as the middle east and North Africa where dust build up can significantly affect the performance of PV modules. Environmental dust particles settle on surfaces and reduce both the optical transmittance and power output of these devices [10] - [40]. Many methods are been used to remove dust/mud from the protective surfaces of solar harvesting devices. Research works have concentrated more on modification of the structure, shape of the panel, use of an external agent and surface treatment for effective cleaning [42] - [80] and not much effort has been applied into modifying the dust itself for solar harvesting purposes. The literatures published on this subject indicates the lack of studies on the development of a cost effective and novel approach for cleaning the protective surfaces of this devices. While some of the techniques developed show good prospect for dust mitigation, coatings/film interference of spectral transmittance and residue left on the cleaned surface still poses some challenges for solar harvesting devices. One area that could eliminate dust accumulation on the surface is to directly treat the dust particles with a suitable chemical agent and gently alter the orientation of the solar harvesting devices for self-cleaning without interfering with the panel surface and geometry.

Hence, introducing low concentration acid, such as low concentration hydrofluoric acid, on dust surfaces generates chemical reactions and modifies dust chemistry in the surface region. In the present study, the physical and chemical characteristics of the dust particles before and after low concentration hydrofluoric acid treatment (solution treatment) will be investigated. The adhesion work resulted during the removal of untreated and solution treated dust particles from the hydrophilic and hydrophobic surfaces would be evaluated. In addition, mitigation of untreated and solution treated dust from the hydrophilic and hydrophobic surfaces under the gravitational influence would be carried out for various surface inclination angles. Laboratory tests would also be conducted assessing the surface area at which dust removed from glass surfaces under the gravitational influence.

CHAPTER 3

EXPERIMENTAL WORK

This chapter deals with the experimental work carried out for the thesis as illustrated in Figure (3.1). The first part of this chapter communicates the experimental approach used for the treatment of dust particles by hydrogen fluoride. Next, the details of the characterization techniques used were also sequentially discussed. This was followed by the design and fabrication of a dust-removal device to facilitate the dust cleaning experiments. The details of the protocol adopted to carry out the dust-removal experiment, incorporating the avalanche method were also discussed. Suitable software packages were used to further process the experimental results afterward.

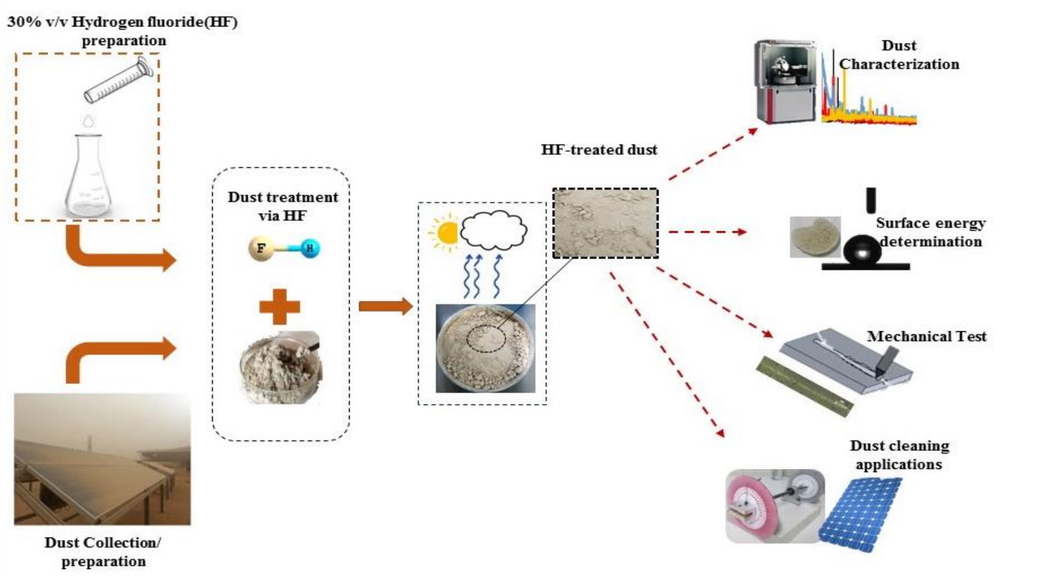

Figure 3.1 Materials and Method

3.1 Collection and Study of Dust Particles in Dharan, Saudi Arabia

Settled dust particles over one year were collected using suitable slides and dishes around the department of Mechanical Engineering at King Fahd University of Minerals and Petroleum, close to Dammam City, Saudi Arabia. Before being analyzed, the collected dust particles were stored in closed miniature containers and were carefully separated from unwanted particles using a fine mesh fabricated specifically for the experiment. Furthermore, assessment and measurement of mass, size, shape, chemical composition and density of conventional dust particles were carried out following the principles and procedure in [79].

3.2 Solvent Preparation of Hydrogen Fluoride

The following procedure was carefully followed to prepare low concentration of 250ml solution of hydrofluoric acid (30% v/v,) for dust treatment. First, the appropriate amount of pure hydrofluoric acid (99.99% v/v) and distilled water required to produce the required concentration of hydrogen fluoride solution was calculated using the dilution equation (3.1) given below.

$$\% \ {}^{v}/_{v} \ of \ HF = \frac{Volume \ of \ HF \ (ml)}{Volume \ of \ H_2o \ Solution} \ x \ 100\% \qquad (3.1)$$

Next, a 250ml plastic volumetric flask was used to prepare the final solution. A plastic measuring cylinder was used to measure and transfer 175ml water to a volumetric flask. The setup was then taken to a fume chamber and 75ml hydrofluoric acid (99.9%, v/v, Sigma Aldrich) was measured into a graduated conical flask and slowly poured into the volumetric flask (containing water) via a plastic funnel. The graduated cylinder containing the acid was rinsed with water and transferred to the 250ml volumetric flask to make up the volume. The final solution containing hydrogen fluoride solution (30%, v/v) was carefully stirred and properly labeled to be used for the next phase of the experiment. Figure (3.2) express the process of preparing the required Hydrogen fluoride concentration

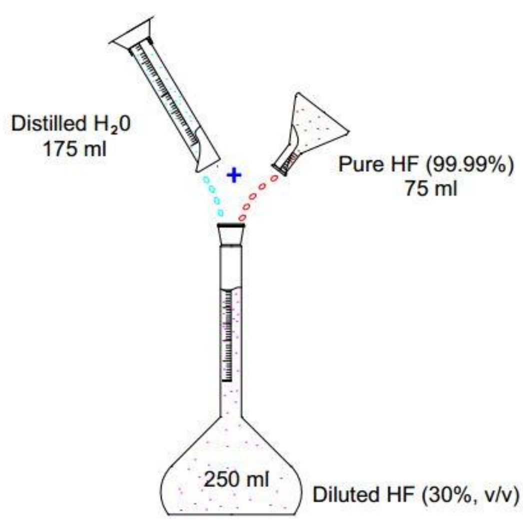

Figure 3.2 Preparation of 30% hydrogen Fluoride Solution

3.3 Dust Treatment using Hydrogen Fluoride

Environmental dust collected was placed in covered small plastics vials and the mass of collected dust was measured using a digital mass weighing scale (Fisher Scientific) before treatment by hydrogen fluoride. Two different samples of collected dust particles were prepared and carefully treated with quantified drops of hydrogen fluoride (HF) using a specific mass ratio. Samples of HF-treated dust were synthesized using the solution immersion method in a fume chamber. In all the studies, the collected dust particles were exposed to the Hydrogen fluoride acid (30%, v/v) in two different mass ratios (1:1 and 1:4) to synthesize HF-treated dust samples as illustrated in figure (3.3). Next, the HF-treated dust was kept in airtight plastics vials for 24 hours and carefully uncovered intermittently within 20 minutes to expose the treated dust particles to atmospheric air for gradual moisture removal.

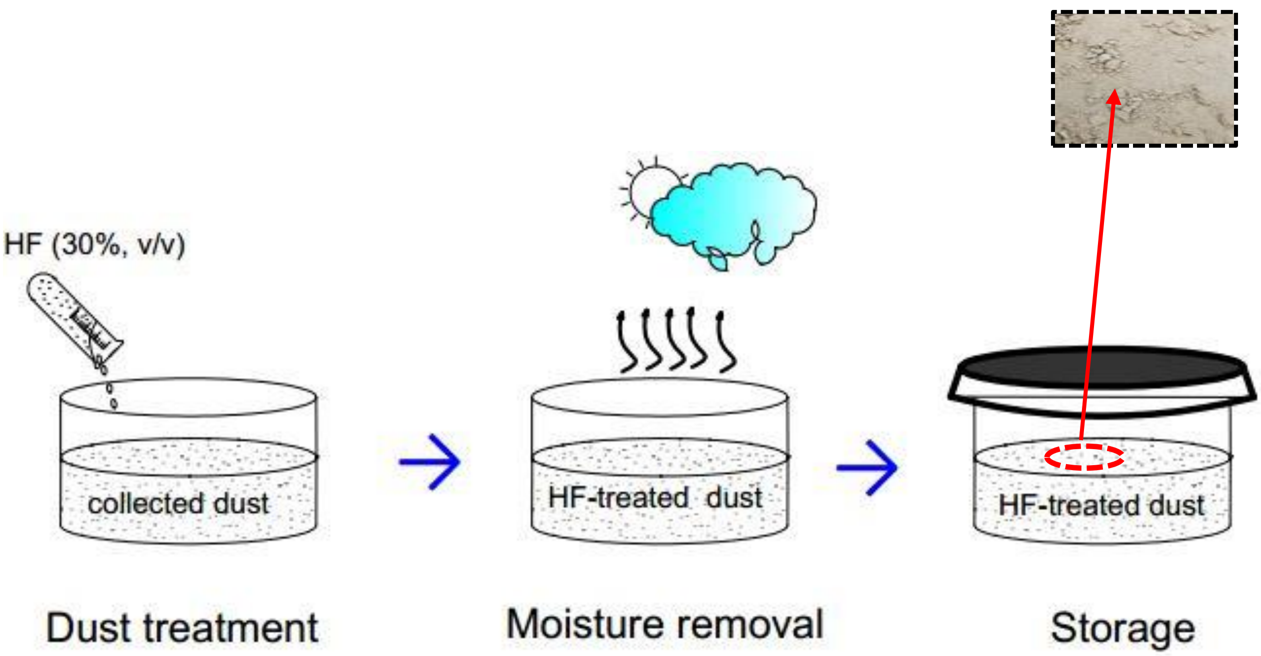

Figure 3.3 Solution Treatment of Dust with Hydrogen Fluoride.

3.4 Characterization of Collected Dust and Hydrogen Fluoride Treated Dust Samples using Analytical Tools

3.4.1 Scanning Electron Microscopy, Energy Dispersive-X-ray spectroscopy and X-ray Diffraction Analysis of Dust Samples

Three different groups of dust samples were prepared from the collected and HF-treated dust and labeled accordingly. The first set named DP-1(for collected dust) and HFDP-1 (for Hydrogen fluoride (HF) treated dust) were sieved using a fine grid and weighed using a fisher scientific digital weighing scale; 0.05 grams each of DP-1 and HFDP-2 was placed on plastic slides. The next two groups of samples were obtained by solution immersion of the two dust types in the water. To prepare the second set of dust samples, 1 gram each from the collected and HF-treated dust was added to 10ml of deionized water and gradually stirred to produce a mud solution. The resulting dust-water mixture was kept for 6 hours for the denser dust particles to settle leaving a clear liquid solution at the top and muddy portion at the bottom. Afterward, the clear liquid portion of the solution was separated from the muddy portion using a filter paper incorporated into a separating funnel. Few drops of the separated clear liquid solution (0.05g) was deposited on plastic slides, exposed to ambient conditions to evaporate and form dried crystallized dust samples, each named as DPC-2 (crystallized dust) and HFDC-2 (crystallized HF-treated dust) as illustrated in figure (3.4). The third set of samples labeled as DPM-3 (dried mud) and HFDM-3 (HF-treated dried mud) were prepared by placing some of the settled mud particles on plastic slides following the same procedure and conditions that were used for the second group of samples. The different groups of dust samples were further modified to be adopted for SEM, EDX and XRD analysis.

Scanning electron microscope-Energy dispersive X-ray spectrometer (SEM-EDX) measurements were carried out using a using a FEI Quanta FEG 250 scanning electron microscope, which consists of an XT microscope console, Microscope controller, Electrical console and the FEG vacuum system. Before the SEM-EDX analysis, the three groups of dust samples made from collected dust (DP-1, DPC-2, DPM-3) and Hydrogen fluoride (HF) treated dust (HFDP-1, HFDC-2, HFDM-3) were attached to a sample holder via carbon tapes and gold coated with a Quorum Q150RS sputter coater for 30 seconds for each piece of samples. The use of carbon tape and gold coating via sputtering technique is to enable better conductivity; prevent electron charging when carrying out the SEM-EDX analysis and thereby obtain better resolution of SEM images. The system settings for gold coating of the samples were given as

- Sputter time = 30 seconds
- Tooling factor = 2.30
- Chamber pressure range = 0.08 - 2.00 mbar

The Gold coated samples were placed in the vacuum chamber of the scanning electron microscope and the SEM-EDX setup was made accordingly to the scan conditions with beam voltage of 15 – 30kW , magnification range of 10x to 10,000 x , chamber pressure of 100Pa and spot type 3.5 for accurate microscopic imagery and elemental dust compositions acquisition

X-ray diffraction analysis was also carried out on another group of collected dust (DP-1, DPC-2, DPM-3) and HF-trested dust (HFDP-1, HFDC-2, HFDM-3) produced following the procedure mentioned earlier. The XRD measurement was performed on a Brucker D8 Advanced Diffractometer with CuKα using the following settings

- Voltage = 40KV

- Current = 30mA
- Scanning angle(2θ) = 20º – 90º

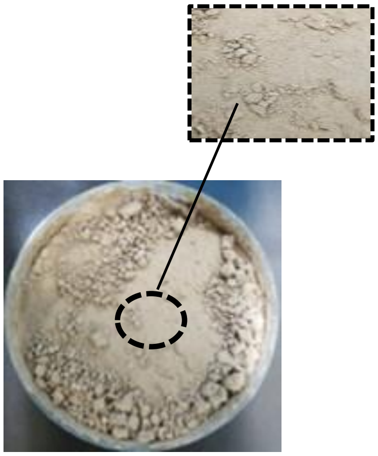

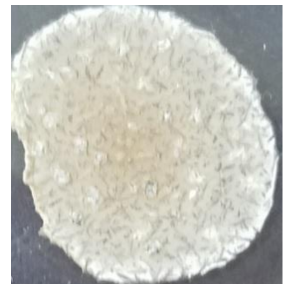

Figure 3.4 a) HF-treated dust **Figure 3.3 b) Dried mud** **Figure 3.3 c) dried crystal**

3.4.2 Inductive Coupled Plasma Spectrometry and PH Measurement of dissolved Dust Sample Solutions

The two types of dust (collected and HF-treated) under investigation were prepared following the same procedure mentioned in the earlier section. Each dust type weighing 2g was placed inside two different plastics vials and 20ml of deionized water was gradually poured into the respective vials and stirred gradually. Concurrently, PH measurement of the dust-water mixture was done with an Acumen AB 15 PH meter (Fisher Scientific) following the standard operating procedure. After calibration, the PH probe was gently inserted into the vial containing the as-received dust solution and readings were taken for three hours while gently stirring the solution. The same procedure was repeated with the HF-treated dust sample. After the PH measurements, the mixture of de-ionized water and dust particles was kept in a fume cupboard for 12 hours, allowed to settle into a clear liquid portion at the top and muddy portion at the bottom as earlier carried out. The clear liquid part of the dust solution was filtered into suitable plastic vials, covered, labeled accordingly and taken for inductively coupled plasma spectrometry (ICP) measurements. ICP measurements were carried out to confirm the presence and solubility characteristics of the constituent elements obtained from EDS and XRD analysis of dust samples.

3.4.3 Dust Characterization via Fourier Transform Infra-Red Spectroscopy (FTIR), and X-ray Photoelectron Spectroscopy (XPS)

Pellets of dust samples needed for XPS and experiments were prepared using a Midvale Heppenstall pressure laboratory press (model: 341-20-6, serial no: 6700-23), keeping the pressure at a load gauge range of 15- 20 tons within 25 seconds. After pressing, each pellet was labeled accordingly as DP (collected dust), HFDP 1:1 (HF-treated dust) and HFDP-1:4 (HF-treated dust), using the same acid to dust mass ratio for the hydrogen fluoride (HF) treated dust samples as done earlier. Figure 3.5 shows optical images for the process of making the dust pellets.

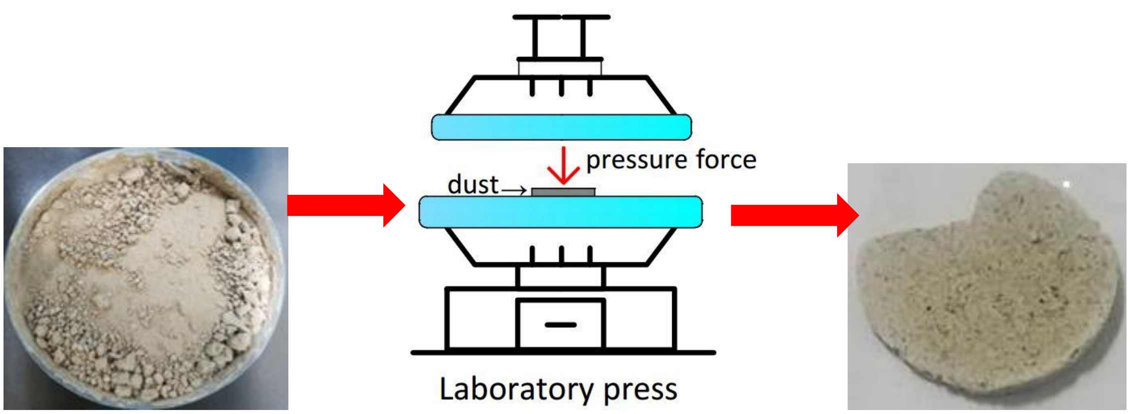

Figure 3.5 a) HF-treated dust **Fig3.3 b) Pressed dust pellets**

A VG ESCALAB 200-X spectrometer was used to perform X-ray photoelectron spectrometer (XPS) measurements on prepared dust pellets. XPS data were recorded while operating a monochromatic ALKα radiation (1,486.6 eV) in the constant analyzer energy mode (CAE = 40eV for high resolution spectra and CAE = 100eV for survey spectra).

Infra-red spectroscopy analysis of the dust samples was performed using a Thermo scientific Nicolet iS10 FT-IR spectrometer incorporated with an OMNIC specta software suite for data collection and molecular analysis. Dust pellets were prepared by a special pellet's maker designed specifically for the IR-spectra device. Prepared pellets were later exposed to the IR beam via clamping on a smart iTX optical base using a pressure anvil to enhance effective spectra measurement.

3.5 Surface Energy Measurement of Dust Samples

To determine the surface free energy of the normal dust and the HF treated dust samples, the contact angle of the dust samples were measured via sessile drop method [25,101,103], incorporating water and ethylene glycol as the experimental liquids. Circular dust pellets of diameter 6 mm and thickness 4mm were prepared using the same procedure described in the earlier section as illustrated by figure (3.6). Afterward, 6μl droplet of the test liquids from a pipette was gently placed on the different dust samples with aid of a manual pressure deposition system, using the high-speed camera for imagery. The above procedure was repeated six times at room temperature for each case of contact angle measurement to ensure measurement consistency and repeatability of results in line with studies done previously [101]. Captured images were then processed and contact angles for each case of dust-liquid interfaces were computed and averaged with the help of open-source Image-j software.

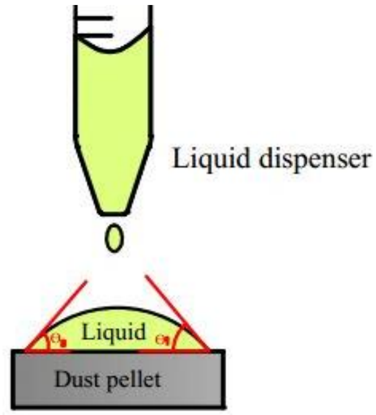

Figure 3.6 Contact Angle Measurement

3.6 Dip Coating of Glass surfaces in Silica Nano Particles

Glass slides were prepared in 75mm × 25mm × 1 mm (width ×length × thickness). Some sample surfaces were hydrophobized via coating by the functionalized nano-size silica particles through adopting the dip coating method as illustrated in figure (3.7). The silica nanoparticles were synthesized in line with the early work [102]. The mixture of tetraethoxysilane (TEOS), octyltriethoxysilane (OTES), ethanol, and ammonium hydroxide solution was utilized in synthesizing cycle. In the process, 14.4 mL of ethanol, 1 mL of distilled water, and 25 mL of ammonium hydroxide were mixed and stirred for 25 minutes. TEOS (1 mL) was first diluted using ethanol (4 ml) and later added to the mixture and mechanically stirred for 25 minutes. Silane was included in the resulting mixture with a molar ratio of 3:4 and the mixture was further stirred for 15 hours at room temperature. The sample surfaces were coated with the resulting mixture via dip coating method. The reactant residuals were removed via centrifuging and the samples were finally washed with ethanol for 5 minutes. The roughness of the resulting coating surface was analyzed using atomic force microscope (NanoSurf, CoreAFM) and the average surface roughness resulted was about 150 nm. The surface free energy of the coating was evaluated incorporating the droplet technique via using water, glycerol, and ethylene glycol as fluids [103]. The surface free energy of the hydrophobized surface is estimated as 35.51 mJ/m^2. A goniometer (Kyowa, model DM 501) was used and droplet contact angle measurements were carried out in accordance with the previous study [104]. The water droplet contact angle of the coating surface is $150^o \pm 2^o$ and contact angle hysteresis is $3^o \pm 2^o$.

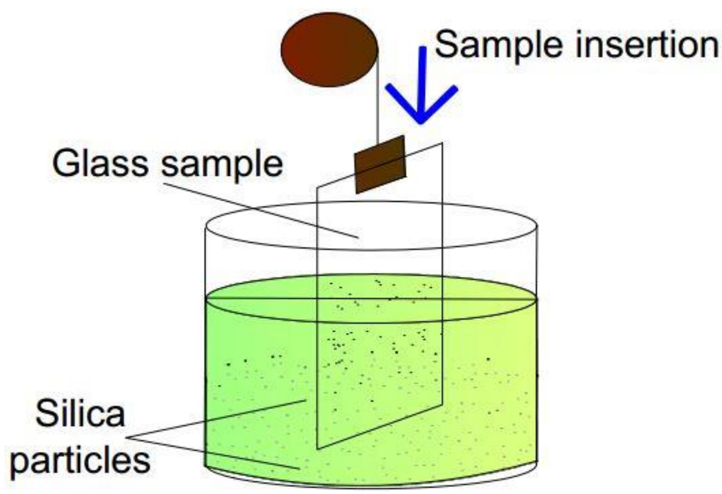

Figure 3.7 Dip Coating of Glass Sample in Nano Silica Particle Suspension

3.7 Design /fabrication of Dust-Removal Device

The design of a dust tilting/cleaning fixture/device was made and drawn via solid works software package (Version 2019) following standard designed principles and relevant design calculations as shown in figure (3.8). Next, a market survey of the various component needed for the dust-removal device was done, the table (3.1) shows various components with corresponding specifications. Afterward, the fixture was fabricated in the KFUPM mechanical workshop and installed in the laser laboratory for the commencement of dust cleaning experiments.

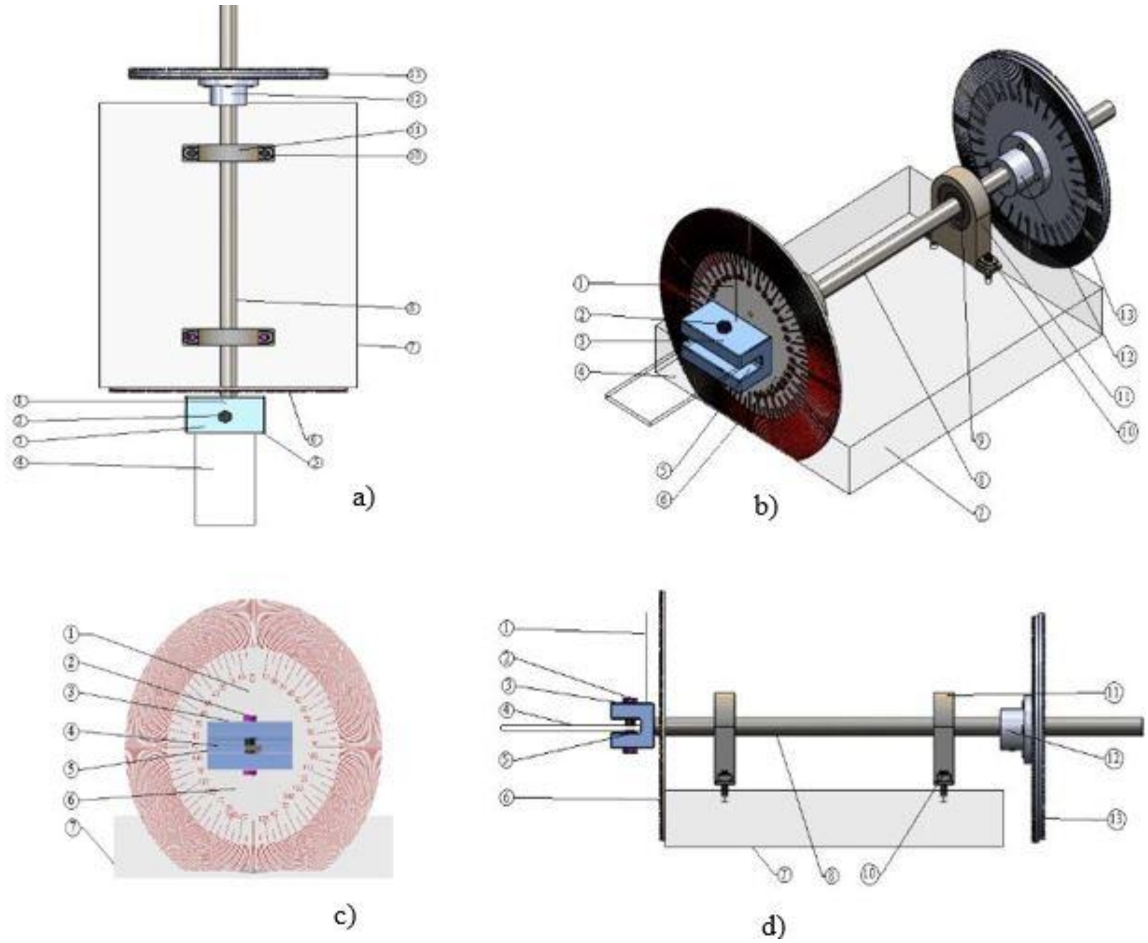

Figure 3.8 Schematic Drawing of Dust Removal Fixture/Device a) Isometric, b) Top view, c) Side View, d) Front View

Table 3.1 Component Specifications/Materials for Dust Cleaning Device

Part No	Component/Materials used	Size/Dimension	Number of pieces
1	0.4 mm Diameter steel pin pointer	46mm	1
2	4mm socket heads adjustable Allen key bolt.	20mm	1
3	Grooved Steel Sample holder	20mm x 20mm x 40mm	1
4	Removable glass slides of 1mm thickness	25mm x 75mm	-
5	Rectangular Groove	6cm x 14mm x 40mm	-
6	120mm Diameter fixed polycarbonate Dial	1.5mm	1
7	25 mm Polycarbonate Base	130 x 170	1
8	8mm diameter steel Rod	250mm	1
9	Steel Radial Ball-Bearing (608EE) with bore Diameter 8mm	6mm x 22mm	2
10	2mm Hex fixed head bolt	10mm	4
11	Steel Bearing guide with hole diameter 22mm	-	2
12	30mm Steel Dial holder	-	1
13	100 mm Diameter Steel Dial	3mm	1

3.8 Optical Experiment using the Dust cleaning Device, High-speed Camera and related Optical Devices

To carry out the dust-removal experiment, a Laboratory set-up was made that comprise the Dust-removal device, high-speed camera (Dantec Dynamic, Specification: Speed Sense 9040, Denmark), iPhone camera (S6, 64GB; Model: A1586, Apple USA) and a digital display system (Dell laptop core i5, connected to the high-speed camera). Figure (3.9) shows optical image of the high-speed camera used to record the dust removal process.

Figure 3.9 A high Speed Recorder

In the experiments, dust samples (collected and HF-treated) were settled uniformly on the glass samples (hydrophilic and hydrophobic) using fine-sized metallic grids (20 µm). A 300µm thickness deposited dust layer of surface area 325mm^2 was maintained throughout the experiment for the four cases (collected dust on hydrophilic glass, collected dust on hydrophobic glass, HF-treated dust on hydrophilic Glass, HF-treated Dust on hydrophobic Glass), while mimicking the actual environmental dust accumulation on exposed solar harvesting devices for a duration one to two weeks [10]. Next, the dust-settled-glass samples were then inserted and gently fastened to the hollow groove of the device sample holder via an adjustable screw. Finally, dust sliding experiments were performed by a gradual tilt of the dust-glass samples attached to the sample holder with a 1^{o} angle step for every 1 second. The sliding of dust particles on glass surfaces was monitored and sliding velocities were measured via the combined high-speed camera and iPhone camera set up. The Cleaning Experiments were repeated four times at ambient temperature conditions (101.32Pa, 311K and 85% relative humidity) for each dust sliding case to ensure that measurements are consistent and repeatable in line with previous studies [23] . Figure (3.10) illustrates the cleaning process via surface tilt.

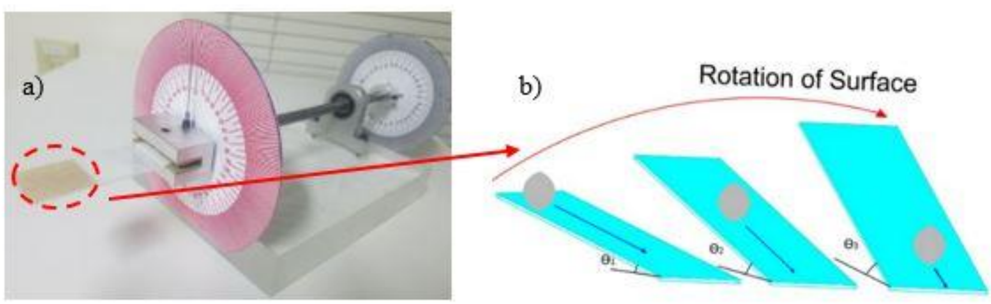

Figure 3.10 a) Dust Cleaning Set-up b) Dust Particle Sliding via Surface Rotation

In another set of experiments, the avalanche effect was used to facilitate effective and efficient dust removal using zirconium oxide (ZrO_2) powder. Zirconium oxide (ρ = 5680 Kg m^{-3}), denser than dust particles were carefully placed at three locations on the top region of the glass samples and dust layer of thickness 300µm were deposited on same glass samples covering an area of $770mm^2$ as shown in Figure (3.11). The settled Zirconium Oxide particles with an average coverage diameter of 3 mm, were evenly separated at 6mm on the surface of the glass sample for each case of the experiment. Avalanche dust-removal experiment was then commenced while following the experimental procedure/set-up mentioned earlier and maintaining the same test conditions as illustrated in figure (3.11).

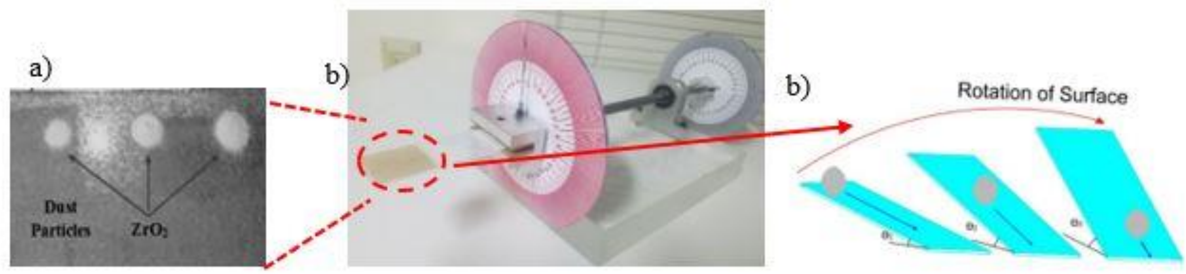

Figure 3.11 a) Zirconium Oxide Particle on Dusty Surface b) Cleaning Device Set-up c) Surface tilt

3.9 Scratch Test and UV transmittance

The Adhesion work needed to remove the collected and HF-treated dust particles from the plain and modified glass surfaces were estimated using the friction coefficient and tangential force data obtained from a linear micro scratch tester (MCTX-S/N: 01-04300). Fine dust particles were settled on the surfaces of the glass mimicking the environmental dust layer accumulation of 200µm - 300µm. The dust-glass test piece was then clamped firmly to the scratch tester for surface profiling and measurements. The instrument was set at a constant load of 0.05N and a scanning speed of 5mm/min with a loading rate of 5N/s. A Rockwell diamond indenter (I-176) of radius 100 µm was used to perform the scratch test over 10mm as illustrated in Figure (3.12).

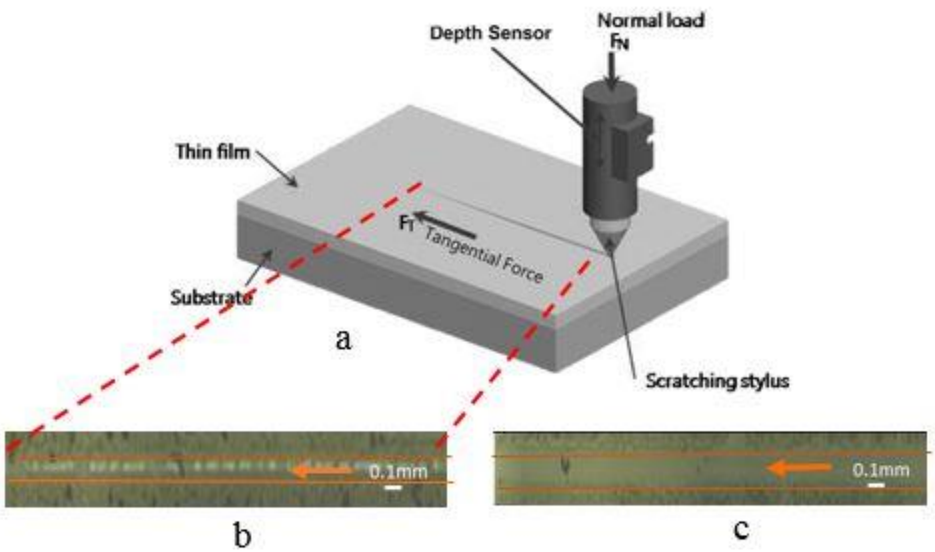

Figure 3.12 a) Scratch Test b) Collected Dust on plain surface c) Treated Dust on Hydrophobic Surface

Further computation of the Adhesion force between the dust particles (HF-treated dust) and glass samples was carried out via a suitable adhesion work-force relation given in the equation. Scratch test values for adhesion work and cleaned area values of both collected and HF-treated dust, and the AFM (Atomic force microscope) value of collected dust obtained from [81] were used alongside equation (3-2) to determine the force of adhesion for the adhesion for HF-treated dust.

$$F_{Ad(HF\ dust)} = \frac{W_{Ad(HF\ dust)}}{W_{Ad(collected\ dust)}} \cdot \frac{Ac_{(collected\ dust)}}{A_{HF\ dust}} \cdot F_{Ad(collected\ dust\ dust)} \tag{3-2}$$

Where F_{Ad} represent the adhesion force, W_{Ad} is the work of adhesion, A_c is the cleaned area.

To compare the optical performance of different dust-glass samples, a UV spectrometer (Jenway 67 Series spectrophometer) was used to measure the UV-visible transmittance of the glass surface before and after conducting the dust-removal experiments.

3.10 Analysis from Tracker, Image j, and Mat-lab Software

Post-processing of results obtained via image and video recordings of dust removal experiments were carried out using open-source video (Tracker) software, open-source image-J software and Mat-lab software (version 2019). The open-source tracker software was used to track the sliding and falling velocities of dust particles. The open-source image j software was used to modify and transform all images taken from dust removal experiments into binary form. Finally, a mat-lab software code was written and used alongside the obtained binary images to calculate the percentage area of cleaned dust surface relative to uncleaned at specific time intervals of the dust removal process. Figure (3.13) illustrated the sequence for analyzing the experimental result.

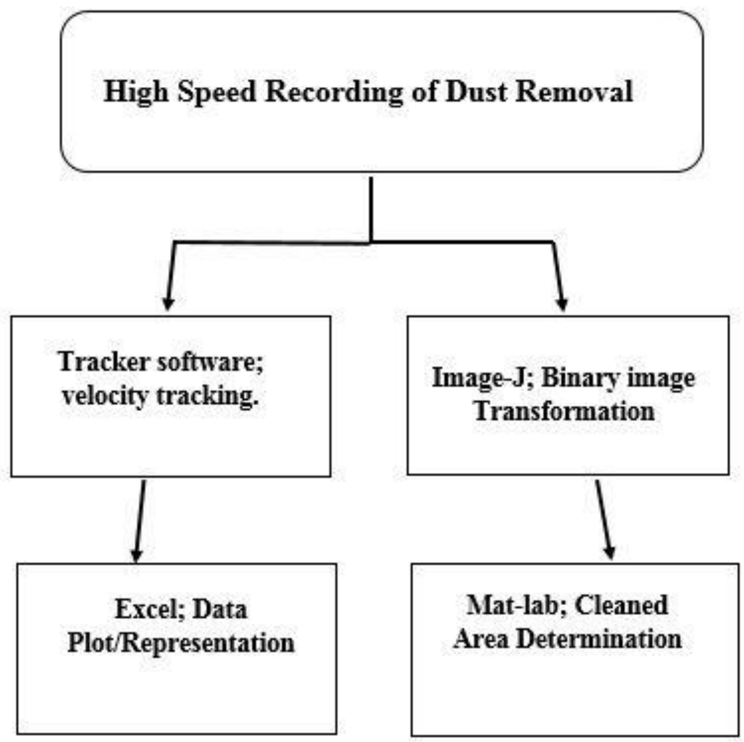

Figure 3.13 Chart Showing the Sequence of Operations for Analysis of Experimental Results

Table 3.2 Operations in Tracker, Image J and Mat-Lab Software

	Settings/operation	**Value/Code**
Tracker Software	Length scale Calibration	25mm (Glass glides width),
	Real time frame rate	29.99frame/s
	Cartesian coordinate	(x, y)
	Point mass Tracking	1.00 Kg
Image-J Software	Length scale Calibration	25mm (Glass glides width),
	Contrast Range	20-254
	Threshold Range	10-255
	Make Binary	White (Cleaned area), Black (Uncleaned Area)
Mat-lab Software	Binary Image Code	`Clc ,` `clear all` `% reading the image file` `BW=imread('modified glass- normal dust-90.jpg');` `percentageWhite = nnz(BW) / numel(BW);` `percentageBlack = nnz(~BW) / numel(BW);`

3.11 Materials

Hydrogen fluoride (30%, v/v) was obtained from Sigma Aldrich, USA. Glass slides were purchased from Fisher Scientific, USA. Polycarbonate materials were also used for the base of the duct cleaning device.

CHAPTER 4

RESULTS AND DISCUSSION

This chapter focuses on the solution treatment of collected dust particles for self-cleaning applications. Analysis of solution-treated dust and untreated dust particles are carried out using analytical tools such as SEM, XPS, AFM, FTIR, 3d-optical microscope, contact angle goniometer, and ICP. Measurement of Adhesion work and area of cleaned work pieces are carried out with respect to dust removal from the surfaces of glass samples.

4.1 Dust particle Description and Characterization

4.1.1 SEM, EDS and XRD analysis of Solution Treated and Untreated Dust Particles

Figure 4.1 (a) and (b), shows SEM images of collected dust (untreated dust) while figure (4.1, c – f) depict SEM images of the solution treated dust. Dust composes of different shapes and sizes figure (4.1, a) and some dust agglomerates forming dust clusters figure (4.1, b). Some dust compounds are formed from alkaline (Na, K) metals with chlorine, which are attributed to the salt compounds in dust. Table (4.1) gives the elemental composition of collected dust. Elemental composition of collected dust slightly changes as the dust particle size reduces (≤ 2 μm), i.e. oxygen content in the dust compounds increases for small dust particles. Nevertheless, dust has various elements including Fe, Si, Ca, K, Na, S, O, and Cl. EDS data Table (4.1) reveals that some compounds do not satisfy the stoichiometric elemental ratios such as Na_xCl_y and K_mCl_n, where $x \neq y$ and $m \neq n$. These compounds can create anionic and/or cationic forces on the dust particles.

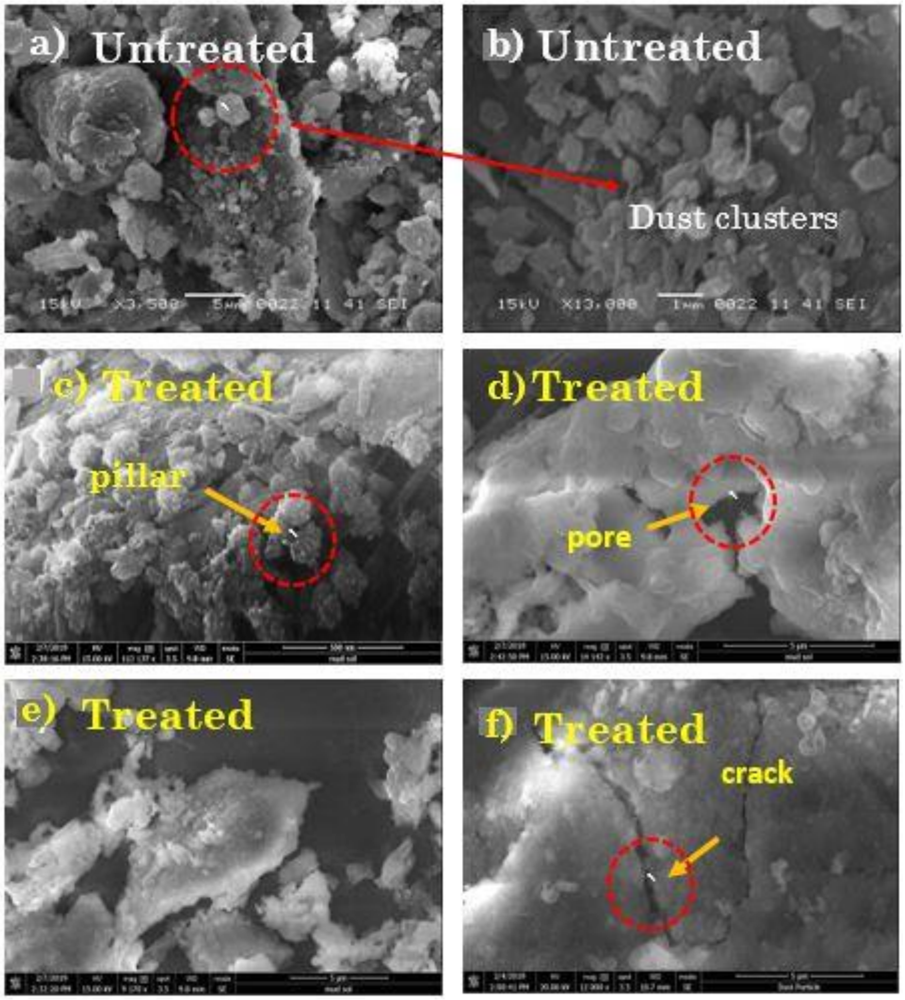

Figure 4.1 SEM Micrographs of a) Collected Dust showing various sizes, b) Collected Dust clusters, c) Solution treated Dust with submicron /nano pores d) Fine size pores in solution treated Dust, e) Mechanically anchored solution treated Dust, and f) Micro-cracks on solution treated Dust surface.

EDS data Table (4.1) reveals that some compounds do not satisfy the stoichiometric elemental ratios such as Na_xCl_y and K_mCl_n, where $x \neq y$ and $m \neq n$. These compounds can create anionic and/or cationic forces on the dust particles.

Table 4.1 Elemental Composition of Dust Particles (wt%) from EDS

	Size	Si	Ca	Na	S	Mg	K	Fe	Cl	F	O
Untreated	≥ 1.2 μm	11.8	8.3	2.2	1.3	2.5	0.8	1.2	0.4	0	**Balance**
Untreated	< 1.2 μm	10.2	7.3	2.7	2.5	1.3	1.2	1.1	1.1	0	**Balance**
Treated	≥ 1.2 μm	8.1	8.2	1.2	1.1	1.8	0.5	0.8	0.2	27	**Balance**
Treated	< 1.2 μm	7.6	7.4	1.3	1.2	0.9	0.7	0.7	0.6	31	**Balance**

Hence, these forces contribute to adhesion of dust particles while forming the dust clusters Figure (4.1, b). In the case of low concentration hydrofluoric acid treated (solution treated) dust Figure (4.1, c to f), the solution treatment initiates spontaneous chemical reactions. The solution treated dust particle surfaces possess pores and submicro/nano pillars like structures Figure (4.1, c) because of dissolution of some dust compounds in the hydrofluoric acid mixture solution during dust treatment. However, as collected dust particles mixed with desalinated water, pH of the mixture increases from 5.8 to 8.6 after five minutes. This shows that alkaline (Na, K) and alkaline earth metal (Ca) compounds of collected dust dissolve in water while forming a chemically basic mixture.

Figure (4.2, a and b) show X-ray diffractogram of collected and solution treated dusts. In the case of collected dust in figure (4.2, a), the sulfur peak occurs because of the calcium in the form of anhydrite or gypsum ($CaSO_4$). The iron peak is due to clay-aggregated hematite (Fe_2O_3). While the XRD in Figure (4.2, b) data reveals HF-treated dust particle contains predominantly fluorine compounds

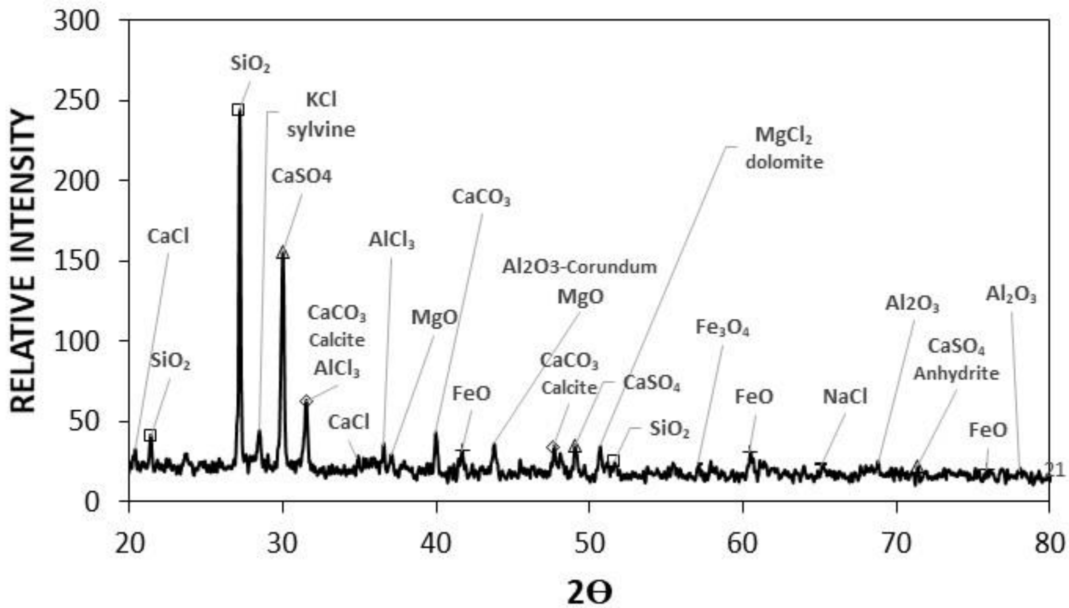

Figure 4.2 a) X-ray Diffractogram of Collected Dust

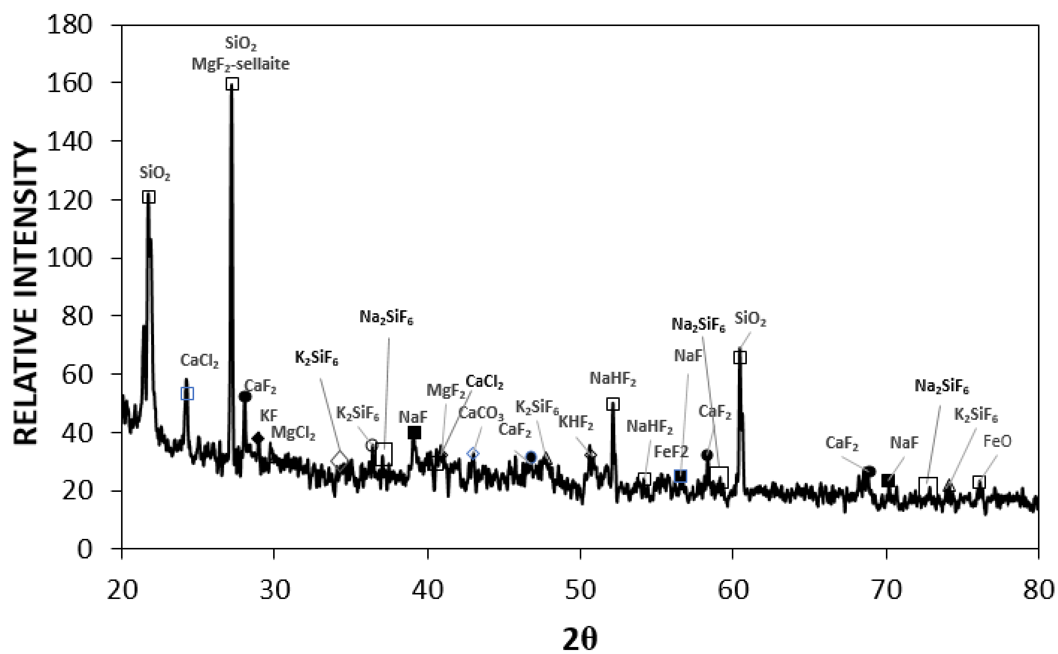

Figure 4.2 b) X-ray Diffractogram of Hydrogen Fluoride Treated Dust

As the dust particles are mixed with the low concentration hydrofluoric acid solution (30% hydrofluoric acid and 70% water), several reactions can take place between hydrofluoric acid solution and dust. Some compounds of the dust particles ($CaCO_3$, NaCl, SiO_2, etc) in the mixture solution undergo reactions with hydrofluoric acid.

4.1.2 Possible Reactions and Dust Compounds Formed During Solution Treatment.

Figure (4.3) shows a reaction scheme for dust treatment by hydrogen fluoride. Some of these reactions can include:

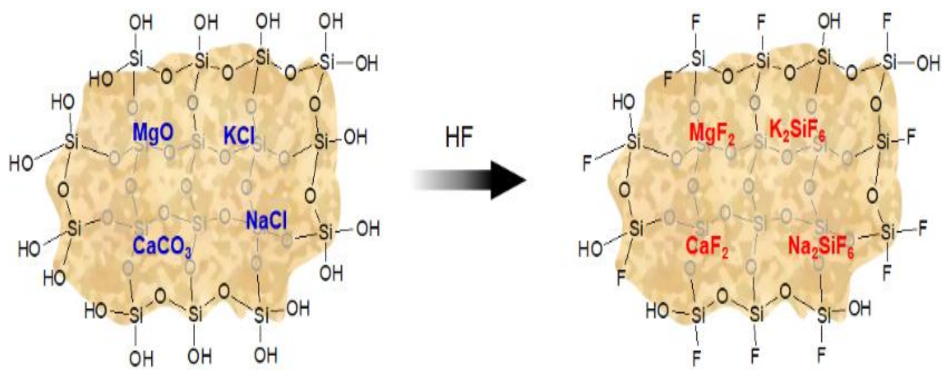

Figure 4.3 Reaction between Dominant Dust Constituents and Hydrogen Fluoride

$$SiO_2 + 6HF \rightarrow H_2\,SiF_6 + 2H_2O \quad (4.1)$$

Hence, hexafluorosilicate ($H_2\,SiF_6$) can be formed. Since, salt compounds (NaCl, KCl) is present in dust, this can undergo reaction with hexafluorosilicate, i.e.:

$$2NaCl + H_2\,SiF_6 \rightarrow Na_2SiF_6 + 2HCl \quad (4.2)$$

Similarly, KCl undergoes a reaction while forming:

$$2KCl + H_2\,SiF_6 \rightarrow K_2SiF_6 + 2HCl \qquad (4.3)$$

Na_2SiF_6 and K_2SiF_6 are the crystalline solids, which can dissolve in a mixture solution and it is denser than water. However, the presence of calcite ($CaCO_3$) in dust can also undergo a reaction with HCl, which is the produced after NaCl reaction with hexafluorosilicate ($H_2\,SiF_6$), i.e:

$$CaCO_3 + 2HCl \rightarrow CaCl_2 + CO_2 + H_2O \qquad (4.4)$$

$CaCl_2$ is highly soluble salt in water and dissolves in the mixture solution. In addition,

$$CaCO_3 + 2HF \rightarrow CaF_2 + CO_2 + H_2O \qquad (4.5)$$

Similarly, magnesium oxide (MgO) in dust can react with the mixture solution, i.e.:

$$MgO + 2HF \rightarrow MgF_2 + H_2O \qquad (4.6)$$

and with HCl:

$$MgO + 2HCl \rightarrow MgCl_2 + H_2O \qquad (4.7)$$

MgF_2 is the fluorescent crystals, which cannot dissolve in water; however, $MgCl_2$ is the magnesium salt, which can dissolve in water. Table (4.1) gives the elemental composition of dust after solution treatment. The elemental composition of treated dust differs from untreated dust Table (4.1). The main differences are associated with the reduction of quantification of some elements and addition of presence of fluorine in Table (4.1). Several new compounds are formed for solution treated dust, which can be observed from the x-ray diffractogram Figure (4.2, b). The peaks of CaF_2, MgF_2, Na_2SiF_6, and K_2SiF_6 demonstrate the solution treated dust possess new fluorine compounds.

4.1.3 XPS, FTIR and ICP Analysis of Solution Treated and Untreated Dust Particles

Further characterization analysis was carried out for the solution treated dust particles and characteristics of solution treated dust were examined by means of X-ray photoelectron spectroscopy (XPS).

Table (4.2) summarizes elemental composition of samples estimated XPS analysis. Solution treated dust shows increased composition of fluorine and calcium, and diminished composition of oxygen and silicon. This demonstrate that the surface of solution treated dust have CaF_2 content as reference to the collected dust.

Table 4.2 XPS Data for Collected and Solution Treated Dust

		O1s	C1s	Si2p	Ca2p	N1s	Al2p	F1s
Prior Etching	**Collected**	52.11	23.19	10.82	5.17	0.27	5.71	1.10
	Solution Treated	30.19	21.93	3.82	10.04	1.41	2.61	29.99
After 20 s Etching	**Collected**	58.26	9.15	12.75	7.14	1.03	7.42	0.00
	Solution Treated	26.86	8.72	7.60	11.99	0.00	3.42	41.32

The details of high-resolution XPS analysis as shown in Figure (4.4) reveal on shifting of Ca2p peak from 347 eV, which is characteristic to $CaCO_3$ to 348 eV characteristic of CaF_2 for the solution treated dust. Moreover,

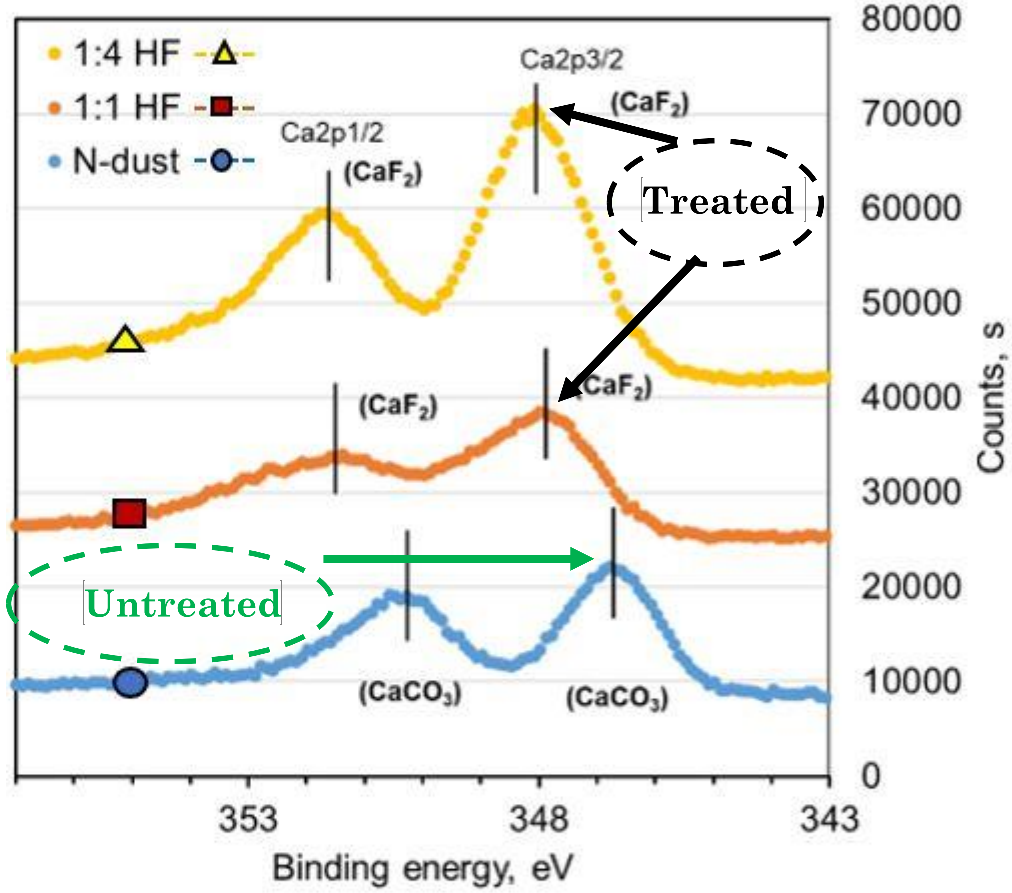

Figure 4.4 XPS Data for Collected and Solution treated dusts. HF represents the ratio of hydrofluoric acid dust at two different mass, 1:4 represent 25% of HF in treated dust, 1:1 represent 50% of HF in treated dust, N represents collected dust.

Figure (4.5) shows Fourier infrared spectroscopy (FTIR) data for solution treated dust. The peak occurring at 1128 cm^{-1} corresponds to Si-O-Si rotational vibration as described in the early work [105]. This demonstrates that polysiloxane compound is formed on Na_2SiF_6 surface [106]. The peak at 477 cm^{-1} is due to stretching vibration of Mg-F [107]. In addition, peak at 3448 cm^{-1} and 1661 cm^{-1} are the characteristic bending vibration of hydroxyl groups (H-O-H) [108]. The peak observed at 775 cm^{-1} is attributed to Ca-F stretching vibration [109]. The chemical reaction occurring with the dust compounds around the dust particles almost eliminates the adhesion of small size dust particles on the dust particle surface, i.e. clustering of the dust particles diminishes as observed for collected dust, i.e. individually oriented dust particles are observed on the surface.

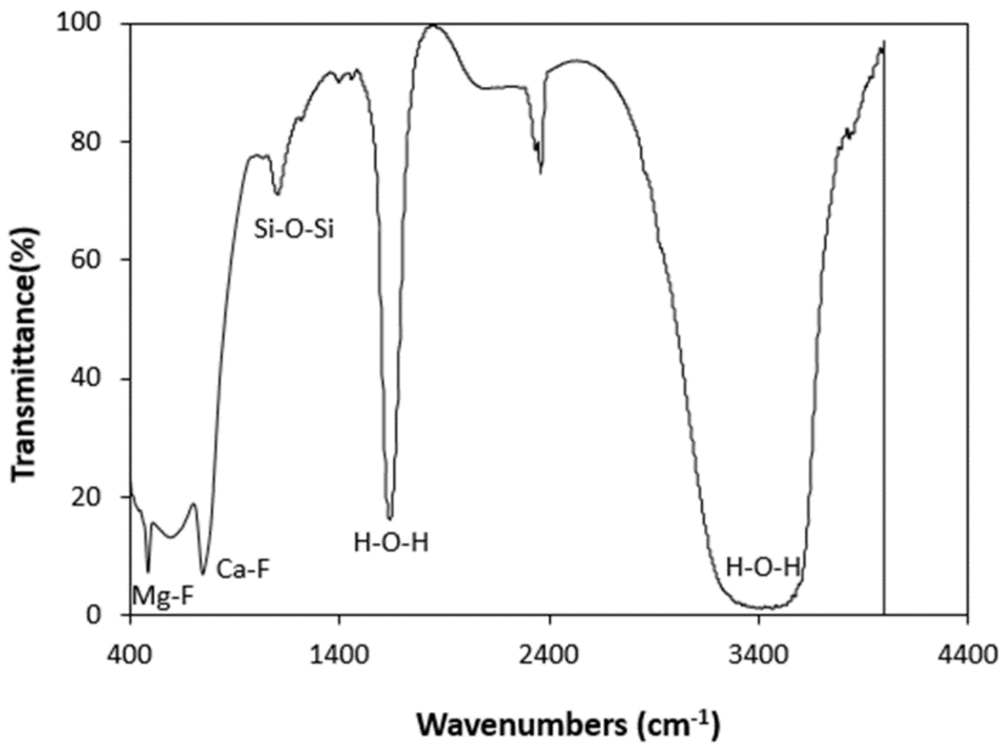

Figure 4.5 FTIR data for solution treated dust

In addition, solution treatment results in some salt products, such as Na_2SiF_6, K_2SiF_6 and $CaCl_2$, and $MgCl_2$, which are the inorganic compounds and they can dissolve in the liquid mixture. The solution treated dust particles are mixed with desalinated water for one hour and, later, the resulting solution is tested by inductively coupled plasma mass spectrometer (ICP) for Ca, Mg, K, and Na. In addition, same ICP tests are also repeated for the collected dust particles. Table (4.3) gives ICP data for collected and solution treated dust particles.

Table 4.3 ICP Data for Collected and Solution Treated Dust

	Ca 317.933	**K 766.490**	**Mg 285.213**	**Na 589.592**
	mg/L	**mg/L**	**mg/L**	**mg/L**
Collected	78.17	8.118	8.581	15.77
Solution Treated	37.58	56.31	144.2	11.79

The amount of dissolved calcium in water reduces for the solution treated dust, which is attributed to formation of CaF_2 and $CaCl_2$, i.e. only $CaCl_2$ is soluble in water is soluble. The amount of dissolved magnesium and potassium attain larger values for solution treated dust as compared to collected dust. The compound of $MgCl_2$ salt is soluble in water, which increases Mg content in the solution. Sodium reduces slightly for the solution treated dust as compared to that of the collected dust. Moreover, the dissolution of the products around the dust particle results in the formation of local porous structures on the dust particle surface (Figure 4.1, d). Since the elemental distribution of alkaline salt compounds within the dust particle is nonuniform, this causes irregular sub-micro/nano pores and pillars like structures around the dust particles. Hence, irregular texture patterns are observed on the treated dust particle surface (Figure 4.1, c). The irregular texture patterns with sub-micro/nano pores and pillars on the dust surface gives rise to interlocking of the dust particles when the particles are mechanically in contact to each other. Hence, mechanical locking of the particles after solution treatment is observed (Fig 4.1, e). As the solution treated particles are located on the smooth surface, the area of contact between the dust particle and the smooth surface becomes less because of the fact that the interfacial gaps, due to submicron/nano pores and pillars, are filled with an air. This lowers the adhesion between the solution treated dust particles and the smooth surface. CaF_2 compound formed around the dust particle is insoluble solid in water and remains in the surface region of the dust particles. The density of CaF_2 (3180 kg/m^3), which is formed locally around the dust particle, differs than the density of dust (2800 kg/m^3). This can cause formation of mechanical strains, due to volume contraction/expansion, and as a result some small local cracks are formed on the dust surface (Figure 4.1, f). However, the size of cracks are small and do not form crack-webs on the dust surface.

4.2 Dust Samples Surface Free Energy Determination

The surface free energy of collected and solution treated dusts is assessed incorporating the contact angle measurement technique [103] . Three liquids namely water, glycerol, and ethylene glycol are used in contact angle measurements. To measure the contact angle, two procedures are adopted. In the first approach, the Washburn technique [110] is employed to measure the liquid contact angle on dust and in the second approach small dust pellets are formed via slight compression of the dust particles and contact angle measurements are carried out using the Goniometer adopting the previous procedure [103, 111]. In the case of the Washburn method, a small diameter (3 mm) glass tube is used and dust particles are put into tube while tube is placed on a small liquid container as shown in figure (4.6).

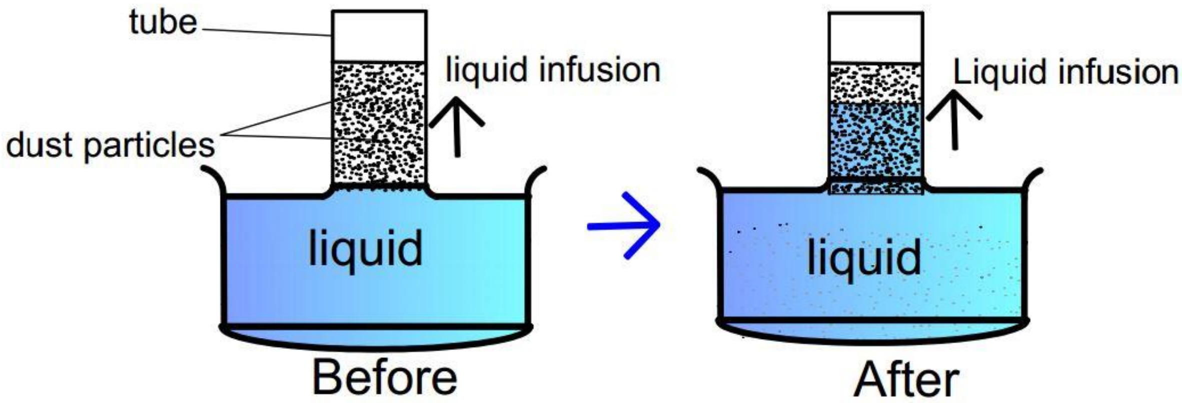

Figure 4.6 Washburn Technique

Hence, the dust particles can draw-up the liquid via liquid infusion. The mass increase in the tube due to liquid infusion is related to the Washburn equation, i.e.: $\frac{(\Delta m)^2}{\Delta t} = \frac{c.\rho^2 \gamma cos\theta}{\mu}$, here Δm represents the mass gain, Δt is the duration for the mass gain (flow-time), c is the capillary constant of dust, ρ corresponds to the liquid density, θ is the contact angle, μ represents the liquid viscosity. The value of c (capillary constant) for dust is evaluated using n-hexane as a liquid, which gives rise to zero contact angle ($\theta = 0$). Hence, the value of c is determined as $6.84 \pm 1.3 \times 10^{-16}$ m^{-5} for collected dust particles and $5.52 \pm 1.2 \times 10^{-16}$ m^{-5} for the solution treated dust particles. The variations of the capillary constant for collected and solution treated dust are related to shape and size of the dust particles, since force balance generated due to capillary and gravity changes on the particle surface as the size and shape of the particle change, which is also reported for powders in the early study [112]. Nevertheless, the estimation for the capillary constant varies within less than 20%. The contact angle measured for the water using the Washburn method is $37.2^{o} \pm 3^{o}$ for collected dust and it is 38.4° ± 3° for solution treated dust. In the case of dust pellets, the contact angle measured, via goniometer, is about 38.2° ± 3° for collected dust and it is 38.7° ± 3° for solution treated dust. Experiments are repeated seven times ensuring the repeatability of the contact angle measurements and the experimental error estimated is within 8%. Nevertheless, the Washburn method incorporated in the contact angle measurement results in similar droplet contact angle to that obtained from the goniometer measurements on pellet surfaces. The surface free energy of dust is evaluated using the formula developed for liquid-solid contact, i.e.: $\gamma_L(\cos\theta + 1) = 2\sqrt{\gamma_S^L.\gamma_L^L} + 2\sqrt{\gamma_S^+.\gamma_L^-} + 2\sqrt{\gamma_S^-.\gamma_L^+}$ [103]. The subscripts L and S are for liquid and solid phases, γ_S is the surface energy for solid, $\gamma_{S\text{-}L}$ represents free energy for solid-liquid interface, γ_L is liquid surface tension, θ corresponds to contact angle, γ^+ and γ^- are parameters for electron acceptor and donor due to acid-base component of free energy for solid and liquid phases. Table (4.4) gives the data for Lifshitz-van der Walls components and electron-donor parameters [22, 103].

Table 4.4 Lifshitz-van der Walls Component and Electron-donor Parameters used in the Simulation [22, 103,113]

	γ_L (mJ/m^2)	γ_L^L (mJ/m^2)	γ_L^+ (mJ/m^2)	γ_L^- (mJ/m^2)
Water	72.8	21.80	25.5	25.5
Glycerol	63.3	33.11	10.74	21.23
Ethylene glycol	48.2	31.09	6.59	11.16

The surface energy estimated from contact angle measurement method for collected dust is around 112.3 ± 7.8 mJ/m^2 while it is about 94.8 ± 6.2 mJ/m^2 for solution treated dust. Since several new compounds are formed in the dust surface region after the treatment, such as CaF_2 and some salt compounds (Na_2SiF_6, K_2SiF_6 , $CaCl_z$, and $MgCl_2$) the surface free energy of collected dust changes after the solution treatment. It should be noted that the interfacial chemical feature of the compounds, particularly fluorite compounds play important role on wetting state of the liquid on the surface [114], e.g. the cleavage plane of CaF_2 (111) results in low surface energy than CaF_2 crystals with different structure, such as (100) and (110) planes. Moreover, the spreading rate of the liquid on dust depends on the spreading coefficient (S). The spreading factor for liquid infusing on a solid surface satisfies the relation: $S = \gamma_s - \gamma_L - \gamma_{s-L}$ [115, 116]. Here, γ_s represents surface free energy of dust, γ_L represents liquid surface tension, and $\gamma_{s\text{-}L}$ is interfacial tension of liquid-dust pair. The interfacial tension can be evaluated via $\gamma_{s-L} = \gamma_s - \frac{\gamma_L}{r}\cos\theta$ [116]. Here, r is the roughness parameter, which represents the ratio of area of pillars in the texture over the projected area of the textured surface, and it takes the values between 1 and 0; here, 1 being the extremely rough surface and 0 being the extremely smooth surface. After close examination of several SEM micro-images of the dust particles, roughness parameter is evaluated as r = 0.52 for collected dust and r = 0.62 for solution treated dust. Since the water contact angle is $37.2^o \pm 3^o$ for normal dust and it is $38.4^o \pm 3^o$ for solution treated dust and substituting surface energies obtained from contact angle methods, the interfacial tension between dust and water is estimated to be $\gamma_{s-L} = 2.1$ mJ/m^2 for collected dust and it becomes $\gamma_{s-L} = 3.74$ mJ/m^2 for solution treated dust. The initial period of liquid spreading over the dust particle is governed by liquid infusion (cloaking), which takes place via forming a thin layer of liquid onto the dust particles in line with the Joos, law [117] and energy dissipated by the liquid during infusion is associated with the Ohnesorge number ($Oh = \mu/\sqrt{\rho a \gamma_L}$), where a is the size of the dust particle [118]. Incorporating the dust particle size in between 20 μm to 0.5 μm, Ohnesorge number takes the values within the range of ~ 0.025 - 0.105; hence, dissipated energy of the liquid during cloaking becomes small, i.e. liquid totally covers the dust particles. This argument is true for solution treated and collected dust particles, which are also observed during the experimental tests.

4.3 Adhesion Work and Force Determination of Dust Glass Sample Surface

The hydrophobic surfaces has texture characteristics consist of hierarchically distributed micro/nano pillars, which reduces the particle pinning due to adhesion on surfaces [119]. The tests are carried out to assess the adhesion of solution treated and collected dust particles individually on the hydrophobic and hydrophilic glass samples using the atomic force microscopy (AFM); at which, the force of AFM probe deflection is associated with the formula $F = k\sigma_d \Delta V$, here k is the probe tip spring constant (N/m), σ_d is the slope of the deflection at friction mode ($\Delta z/\Delta V$, m/V), and ΔV represents the voltage (mV) recorded during AFM probe deflection [120]. The AFM probe used has $k\sigma_d$ = 5.80275×10^{-13} N/mV and the probe voltage recorded for 1.2 µm collected dust particle on hydrophilic glass sample surface is 290 mV, which results in adhesion force of about 1.68×10^{-10} N. However, the probe voltage recorded for same size collected dust particle on hydrophobic glass surface is about 90 mV, which corresponds to the force of adhesion of 0.522 x 10^{-10} N. Hence, hydrophobic surface lowers the dust particle adhesion almost 1/3 of that of the hydrophilic surface. Experiments are repeated for the assessment of adhesion force for the solution treated dust particles on the hydrophilic and hydrophobic glass surfaces. The probe voltage recorded for about 1.2 µm solution treated dust particle on hydrophilic glass sample surface is 210 mV and it results the adhesion force of 1.22×10^{-10} N, which is almost 70% of that of the collected dust. Hence, low concentration of hydrofluoric acid solution treated dust particle results in low adhesion to the hydrophilic glass surface as compared to that of the collected dust particle. This behavior is attributed to the surface texture characteristics of the solution treated dust, i.e. some dust compounds formed during the solution treatment (Na_2SiF_6, K_2SiF_6, $CaCl_2$, and $MgCl_2$) can dissolve in the solution while creating submicron/nano pores textures on the solution dust particle surface (Figure

4.1c). This reduces the area of contact between the solution treated dust particle and the glass surfaces. In the case of similar size of the solution treated dust particle, the AFM probe reading is about 65 mV and it gives rise to the adhesion force of 0.38×10^{-10} N, which is about 75% of that of the collected dust on the hydrophobic surface. This indicates that solution treatment of dust lowers the adhesion force of the dust particle on the hydrophobic surface as compared to that of the collected dust particle. Furthermore, the adhesion tests are conducted determining the average adhesion work required to remove the solution treated and collected dust particles from the hydrophobic and hydrophilic sample surfaces. The solution treated and collected dusts with same quantity are located on the glass sample surfaces and micro-scratch tester (CSM Instruments, Micro Scratch Tester (MST)) was used to record the resistance force and corresponding probe scanning distance along the scanning line on the glass sample surface. In the tests, the hydrophobic and hydrophilic samples are used separately. To assess the correct adhesion work for the solution treated and collected dusts, the resistance force due to friction on the sample surfaces are initially evaluated using micro-scratch tester. To obtain the corrected tangential force (F_{cor}), the tangential force measured along the probe path (L_d, total dust removal length along the scanning direction) is subtracted by the frictional force obtained along the same length. It is worth to mention that the local adhesion work is recorded, which represents the adhesion work over the incremental distance where the probe scans on the surface ($W_{ad-\Delta l} = F_{cor} \times \Delta l$, where Δl is the scratch tester probe minimum incremental length on the dusty sample surface). Figure (4.7) shows the local adhesion work along the probe path (L_d) for collected and solution treated dusts on the hydrophilic and hydrophobic sample surfaces.

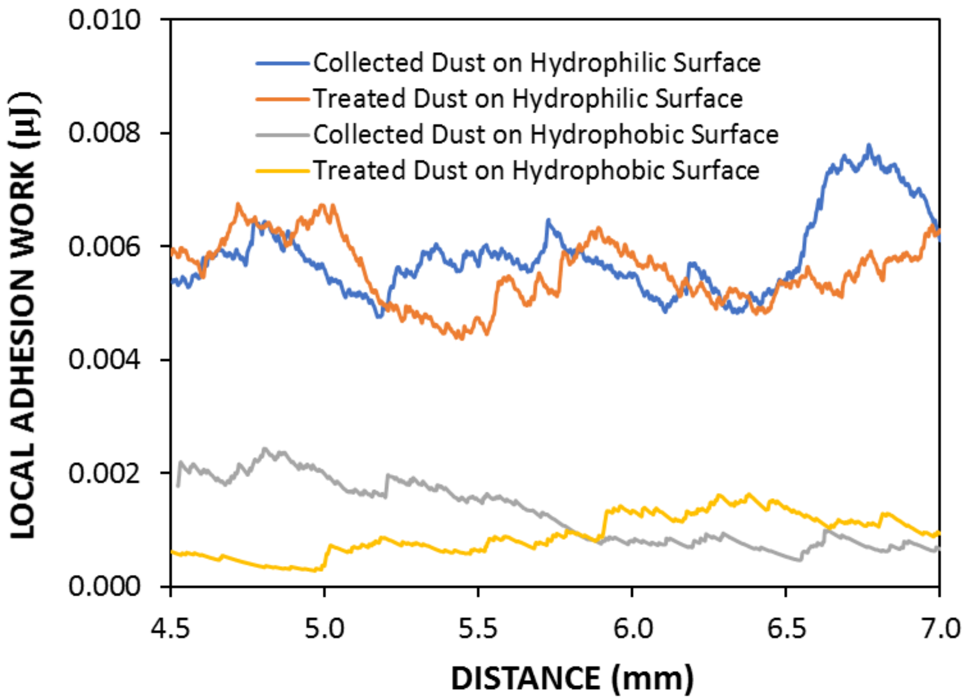

Figure 4.7 Local adhesion work along the scanning distance on dusty sample surfaces. Local adhesion work represents the adhesion work over the incremental distance where the probe scans on the surface $W_{ad-\Delta l} = F_{cor} \times \Delta l$, where Δl is the scratch tester probe minimum incremental length on the dusty sample surface)

The local adhesion work becomes smaller for the solution treated dust than that corresponding to collected dust. This situation is more apparent for the hydrophobic sample surface. Hence, the solution treatment of the dust particles not only lowers the surface energy, but reduces the dust particle adhesion on the surface, despite the fact that submicron/nano textures are formed on the solution treated dust particles, i.e. these textures can act as anchoring sites towards pinning the dust particles on the sample surface. Since, the texture height of the solution treated surface is considerably small, texture influence on pinning becomes negligibly small. On contrary, the surface texture of the solution treated dust reduces the contact area between the dust particle and the sample surface while suppressing the dust pinning force on the sample surface. In addition, hydrophobic texture results in lower tangential force required to remove the dust particles from the surface.

Hence, hydrophobizing the surface through generating nano-size texture with low surface energy coating on the samples reduces the dust pinning force considerably, which becomes more apparent for the solution treated dust. The average work of adhesion (W_{ad}) is determined through numerical integration of local adhesion work ($W_{ad-\Delta L}$) over the total length of probe scan (L_d, which is also the length of dust removed by the probe on the sample surface during scanning) i.e. $W_{ad} = \frac{1}{L_d}\int_0^{L_d} W_{ad-\Delta L}dl$, here dl is the length scale variable. Hence, the average work of adhesion is about 4.9758 µJ for collected dust while it is 0.9361 µJ on the hydrophilic glass surface. The average adhesion work (W_{ad}) for solution treated dust on the hydrophilic glass surface it is 4.0912 µJ while it is 0.6027 µJ on the hydrophobic sample surface. Hence, solution treatment of dust lowers the average adhesion work on the sample surfaces, which is more pronounced for the hydrophobic surfaces.

4.4 Treated and Untreated Dust Removal from Glass Surfaces Via Mechanical Tilt

Outdoor tests are carried out to assess the adhesion of the collected and solution treated dust on the inclined hydrophobic and hydrophilic glass surfaces. The fixture (Figure 3.7a) is designed to incline the samples at 1^{o} increments along the horizontal axis and the gravitational pull allows the dust particles to slide over the sample surfaces. The tests are repeated separately for solution treated and collected dust located on the hydrophilic and hydrophobic glass surfaces. Figure (4.8) shows optical images of dusty surfaces of hydrophobic and hydrophilic samples after the rotation for solution treated and collected dust. It should be noted that the rotational angle for complete collected and solution treated dust removal changes for the hydrophilic and hydrophobic surfaces.

In this case, the inclination angle for total dust removal from the surface becomes smaller for solution treated dust on the hydrophobic surface as compared to those of i) solution treated dust on the hydrophilic surface, ii) collected dust on hydrophobic surface, and iii) collected dust on hydrophilic surface. Hence, solution treated dust has low adhesion on the sample surface than the collected dust, which is particularly true for the hydrophobic surface. However, some dust residues are observed on the sample surfaces.

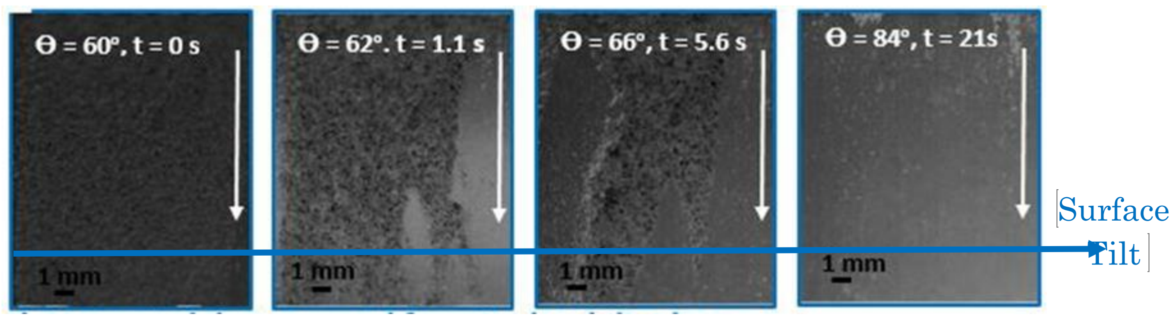

Figure 4.8 a) Untreated Dust Removal from Hydrophilic Glass

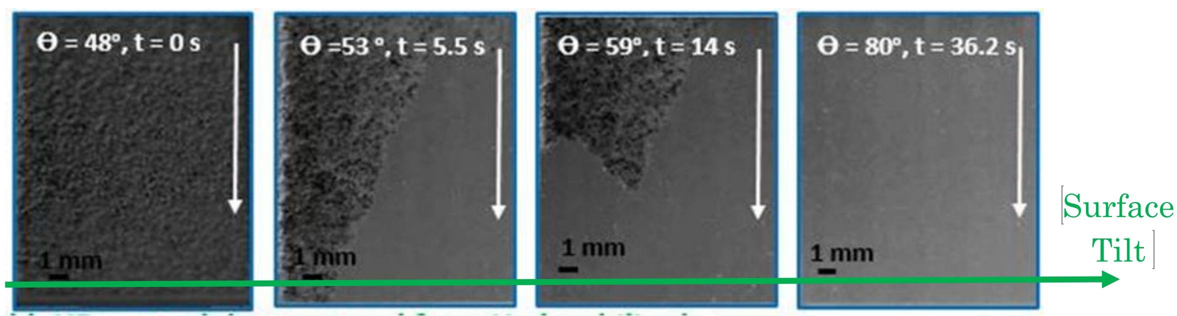

Figure 4.8 (b) HF-treated Dust Removal from Hydrophilic Glass

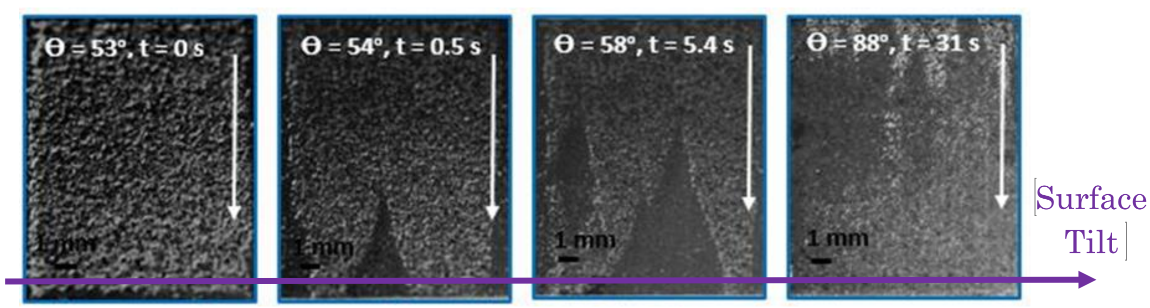

Figure 4.8 (c) Untreated Dust Removal from Hydrophobic Glass

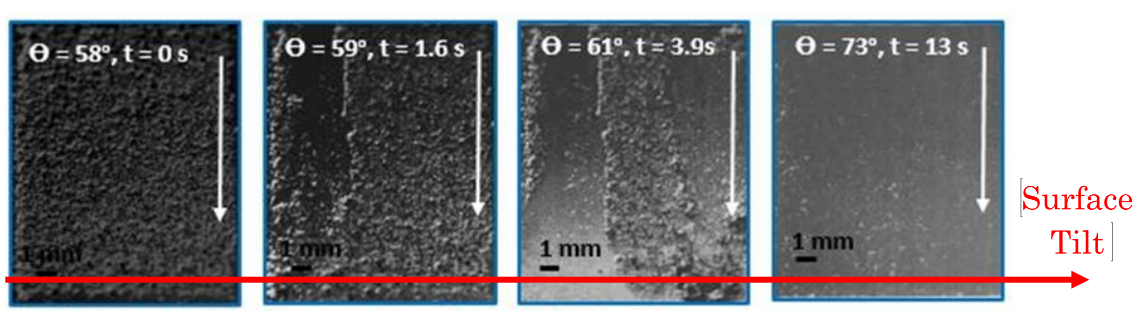

Figure 4.8 (d) HF-treated Dust Removal Hydrophobic Glass

In order to assess, the percentage of area cleaned by the rotation of the dusty samples, the ratio of the area (η_A) that the dust is removed over the total area of the dusty surface prior rotation is estimated, i.e. $\eta_A = \frac{Surface\ Area\ Remaining}{Total\ Surface\ Area}$. Figure (4.9) shows the ratio (η_A) of area that remain on the sample surface with the inclination angle of the sample surface for the cases: i) solution treated dust on hydrophobic surface, ii) solution treated dust on hydrophilic surface, iii) collected dust on hydrophobic surface, and iv) collected dust on hydrophilic surface.

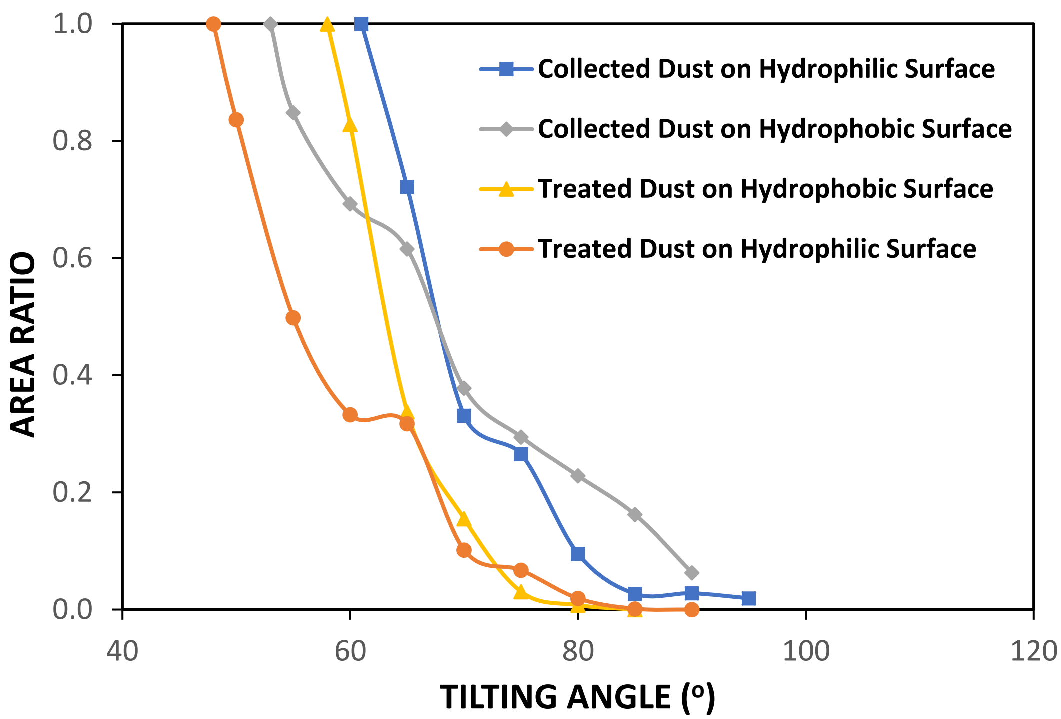

Figure 4.9 Area ratio with Tilting angle of Sample Surface. Area ratio (η_A) represents area of Dust that remain over Total Area of the Dusty Surface prior Rotation .

The inclination angle of the surface for 98% of the area ratio remains the minimum for the solution treated dust on the hydrophobic surface, then follows collected dust on hydrophobic surface, solution treated dust on hydrophilic surface, and finally collected dust on hydrophilic surface.

Consequently, solution treatment of dust particles can be removed from the hydrophobic surface at a low inclination angle of the surface, which reduces the mechanical work required to rotate the surface.

To evaluate the dust residues' shape and size, microscopic analysis is carried out. Figure (4.10) depicts SEM micrographs of typical solution treated and collected dust particles on hydrophobic and hydrophilic surfaces. Dust residues are small with various shapes. Small size dust residues are mainly because of the anchoring of small dust particles on the sample surfaces, which is particularly true for hydrophobic sample surfaces. Nevertheless, they are only a few on the sample surfaces.

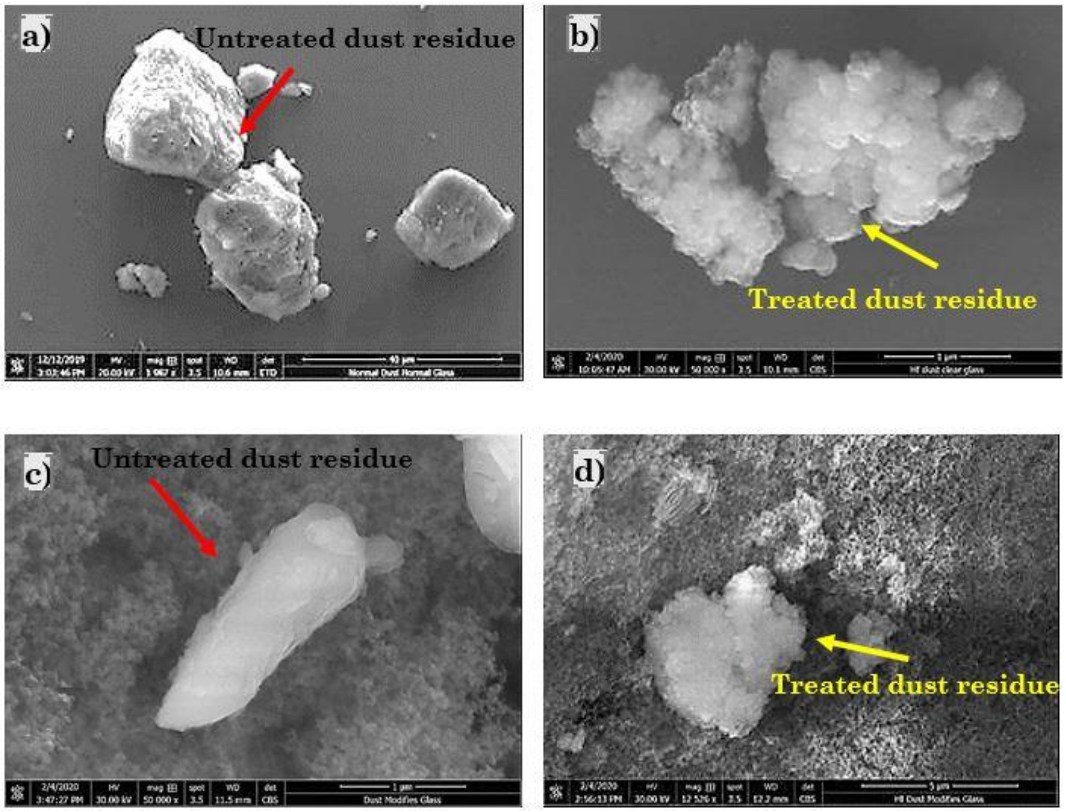

Figure 4.10 SEM micrographs of dust residues on glass surface: a) untreated dust on hydrophilic surface, b) solution treated dust on hydrophilic surface, c) untreated dust on hydrophobic surface, and d) solution treated dust on hydrophobic surface.

4.5 UV Visible Transmittance of Cleaned Hydrophobic and Hydrophilic Surfaces

The dust particle particle-removed surfaces for the different cases were examined optically by measuring the UV-visible transmittance of the cleaned and as-received surfaces. Figure (4.11) shows the UV-visible transmittance of as-received hydrophilic surface, collected dust-removed hydrophilic surface, HF-treated dust-removed hydrophilic surface, as-received hydrophobic surface, collected dust-removed hydrophobic surface, and HF-treated dust-removed hydrophobic surface. The optical transmittance for the as-received hydrophobic surface reduces significantly because of the deep coating of the surfaces with silica-nano sized particles. The silica nano-sized particle reduces the optical transmittance of the as-received hydrophobic surfaces; however, a significant reduction in transmittance is obtained for both collected and HF-treated dust-removed hydrophobic surfaces. Although the optical transmittance of the collected dust-removed surfaces remains slightly lower than that of the HF-treated dust-removed surfaces. This reduction in optical transmittance of the dust-removed surfaces is due to the small dust residues that anchor and remains at sample surfaces, which intensifies for collected dust residue on hydrophobic surface.

Therefore, in choosing a surface, a compromise is made between choosing a hydrophobic surface that cleans dust better but is accompanied by a drastic reduction in its UV-transmissivity and a hydrophilic surface that cleans moderately but also have an improved transmittance capacity even after self-cleaning.

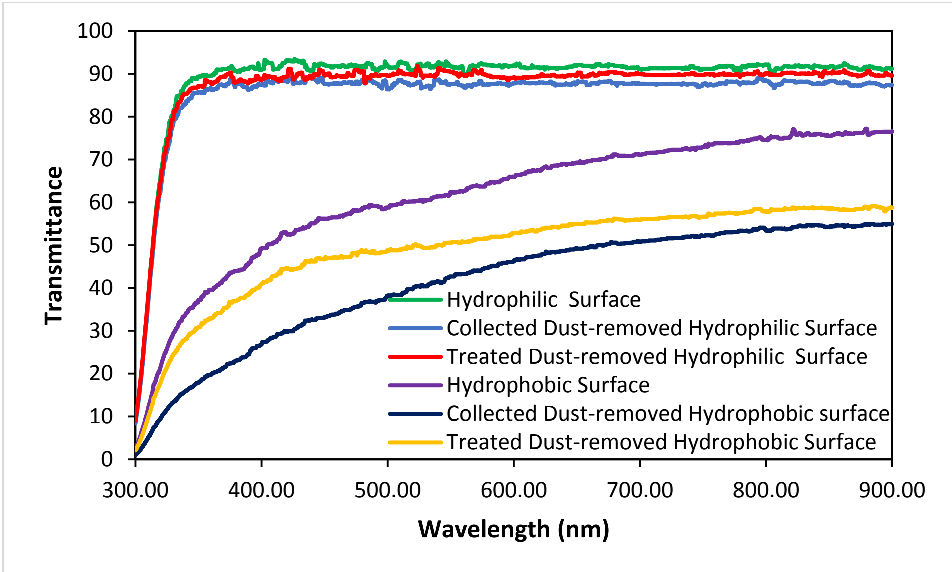

Figure 4.11 UV Visible Transmittance of Cleaned Surfaces for Untreated and HF-treated Dust Samples.

4.6 Avalanche Effect for Dust Removal from tilted Glass Surfaces.

In order to increase dust particle removal rate of dust from glass surfaces, the avalanche effect is introduced. This involves the use of high-density Zirconium oxide (ZrO_2, $\rho = 5680$ Kg m^{-3}) powders heavier than the dust particles ($\rho = 2800$ Kg m^{-3}) to initiates rolling and sliding of dust particles under the influence of gravity. The glass samples are tilted for each set of experiments using the fixture in figure (3.3b) to observe the motion of both ZrO_2 and dust particles via a high-speed recording system as earlier explained in chapter three.

Figure (4.12) shows the optical images of zirconium oxide and dust-covered surfaces of hydrophilic and hydrophobic samples after tilting for both collected and HF-treated dust. The change in the tilt angle for all cases, causes the dust particles in the region of the heavy ZrO_2 powder to move faster under the influence of gravitational potential energy compared to other dust particles that a further from the vicinity of the heavy oxide. This is because the high-density ZrO_2 particles experience a higher gravitational force due to their higher density, which makes the dust particles to move earlier at a lower angle of rotation compared to the case where only dust particles are placed on the surfaces. Therefore, the ZrO_2 particle movement creates an avalanche effect on the tilted surface and the surface area cleaned remains larger for the path taken by the high-density particle (ZrO_2) which is true for the motion of dust on the hydrophobic surface. Moreover, the inclination time and angle remain larger for the untreated dust removal from the hydrophilic surface compared to those of (i) HF-treated dust on hydrophilic glass surface, (ii) collected dust on hydrophilic surface and iii) HF-treated dust on the Hydrophobic surface. Nevertheless, most dust residues are observed on sample surfaces. Some residue remains on the dusty surface indicating that the gravitational potential initiating the dust particle removal from these surfaces is not high enough to overcome all the pinning forces, irrespective of the high-density particles used to generate the avalanche effect. This becomes much pronounced for the untreated dust on the hydrophilic surface.

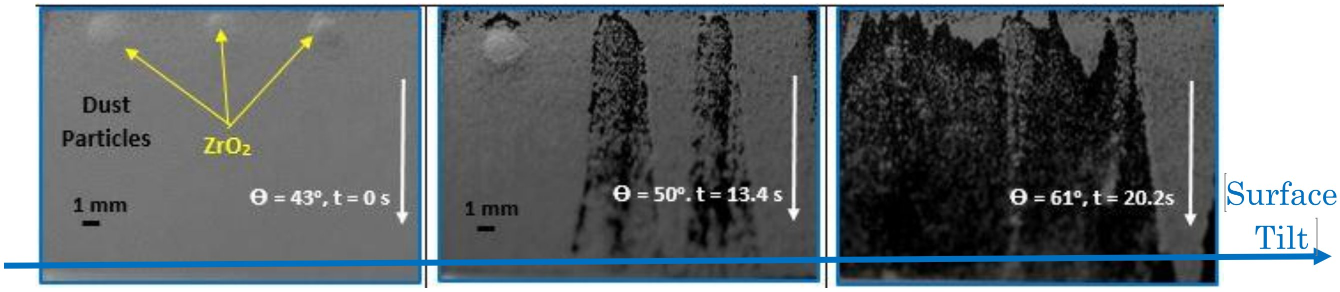

Figure 4.12 (a) Avalanche effect for Untreated Dust Removal from Hydrophilic Surface

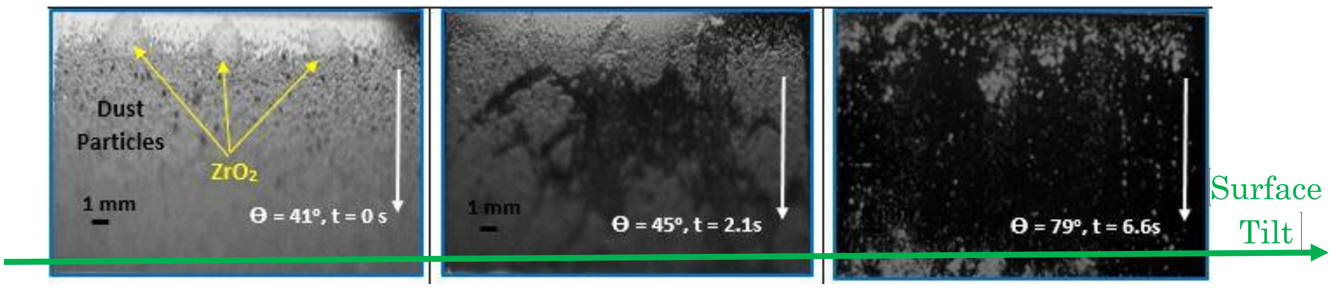

Figure 4.12 (b) Avalanche effect for Treated Dust Removal from Hydrophilic Surface

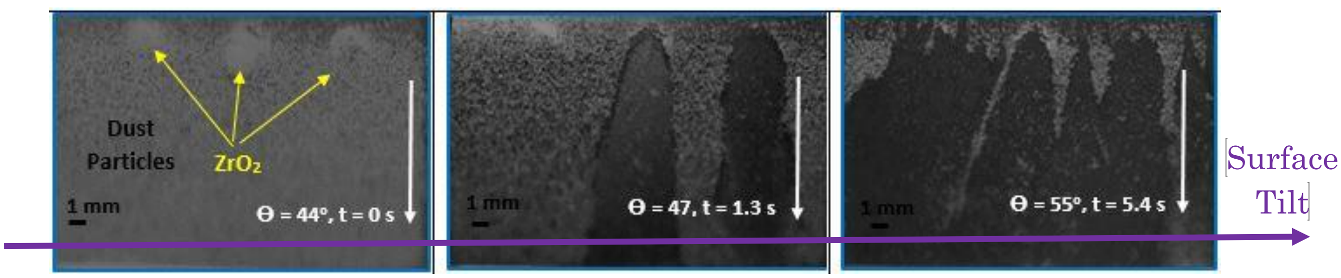

Figure 4.12 (c) Avalanche effect for Untreated Dust Removal from Hydrophobic Surface

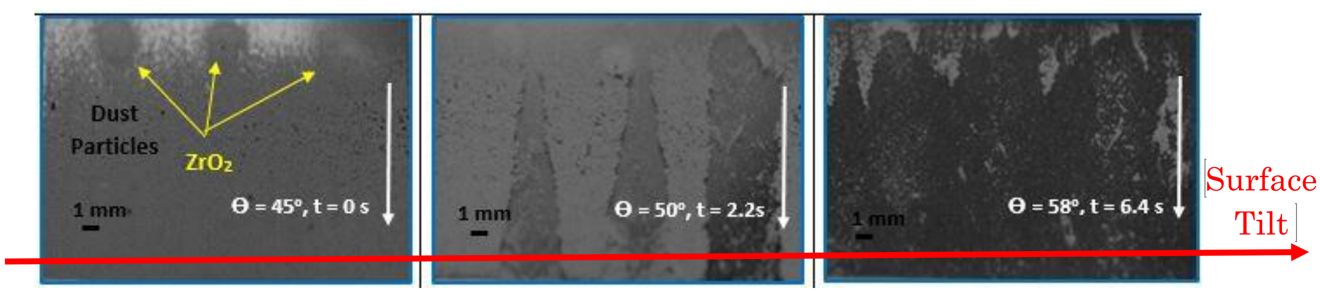

Figure 4.12 (d) Avalanche effect for Treated Dust Removal from Hydrophobic Surface

To compare the performance dusty glass samples for the avalanche effect, the cleaned surface area at various time interval is estimated. Figure (4.13) shows the area cleaned by tilting of the dusty surface under avalanche influence for 5 seconds for the i) collected dust on hydrophilic surface ii) collected dust on hydrophobic surface iii) Treated dust on hydrophobic surface iv) Treated dust on hydrophobic surface.

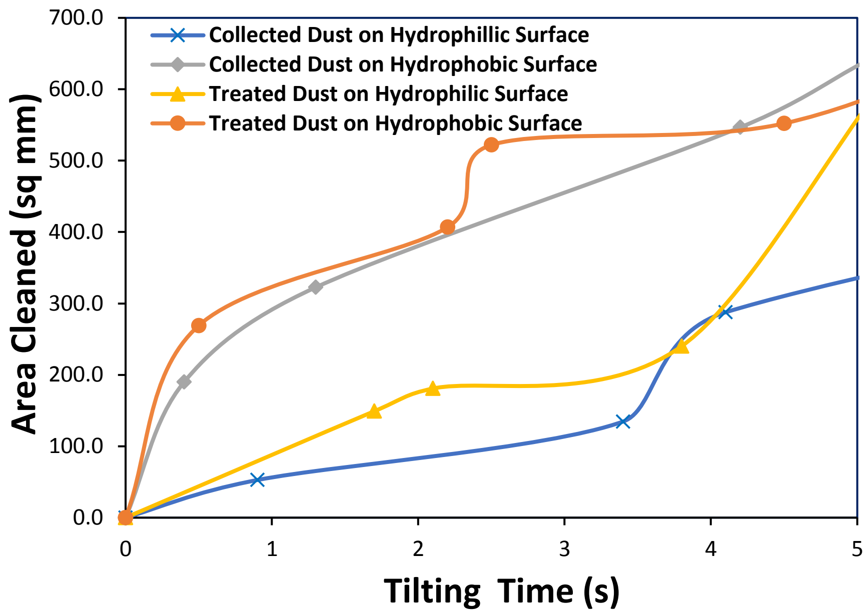

Figure 4.13 Area Cleaned for 5 Seconds of Surface Tilting for the Avalanche effect.

The cleaned area for the untreated dust on hydrophilic surface increases slightly with the tilting time due to resistance to dust particle motion on the surface. The high surface energy that exist between the collected dust and the hydrophilic surface creates high surface adhesion of dust particle to the sample surface which is responsible for minimum dust removal when the surface is tilted. However, the clean surface area rises sharply with time at the onset of dust removal for both dust types on the hydrophobic surface compared to other cases. Dust removal enhances more for the hydrophobic surface due to reduced pinning forces, which becomes more evident for the HF-treated dust due to its low surface energy character.

Figure (4.14) shows the velocity variation at different times due to the movement of high-density particles along the tilted surfaces for the four cases. The velocity rise of treated dust on the hydrophobic surface is rapid for the first second of tilting the surface, remains steady for the next 2 seconds, and rises gently again. Modifying the surface properties of dust and sample surfaces results in the early motion of the particles from the tilted surface under the influence of gravitational potential energy. Some delay occurs as the treated dust move in bulk from the surface as a result of being mechanically interlocked with each other, while the collected dust particles which are not interlocked shows gentle but continuous rise in velocity. The maximum velocity attains more than $0.14 m\ s^{-1}$ for the treated dust on the hydrophobic surface at a tilting time of 4 seconds, followed by the collected dust on hydrophobic surface, then the collected dust on hydrophilic surface and treated dust on hydrophobic surface.

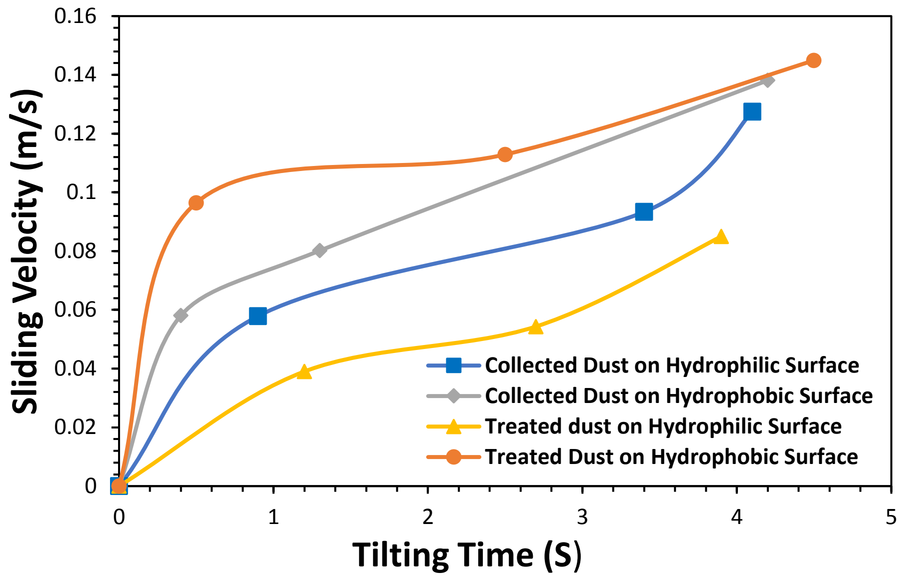

Figure 4.14 Velocity for Dust Particles for 5 Seconds of Surface Tilting for the Avalanche effect

4.7 Performance of Simple Mechanical Tilt Method Versus Avalanche effect for Dust Removal

In order to access the performance of the two methods used in this study to clean the dusty surface dust velocity ratio and clean area ratio for the different case are estimated according to equation (4-1) and equation (4-2)

$$V_n = \frac{V_t}{V_{Max}} = \frac{V_t}{g sin\theta_t} \quad (4.1)$$

Where V_n represents the normalized velocity ratio, V_t is the measured velocity from the experiment, V_{Max} is the maximum velocity of a dust particle moving under the influence of gravitational force without any other external forces acting on it, g is the acceleration due to gravity and Θ_t represents the tilt angle.

$$A_r = \frac{Surface\ Area\ Cleaned}{Total\ Surface\ Area} \quad (4.2)$$

Where A_r represents the Area ratio.

Fig. (4.15) shows the cleaned surface area of treated and collected dust on hydrophobic and hydrophilic surface with and without the avalanche effect. The removal of the treated dust from the hydrophobic surface for the avalanche effect results in higher surface area cleaned per sq mm for a short period compared to that without the avalanche effect.

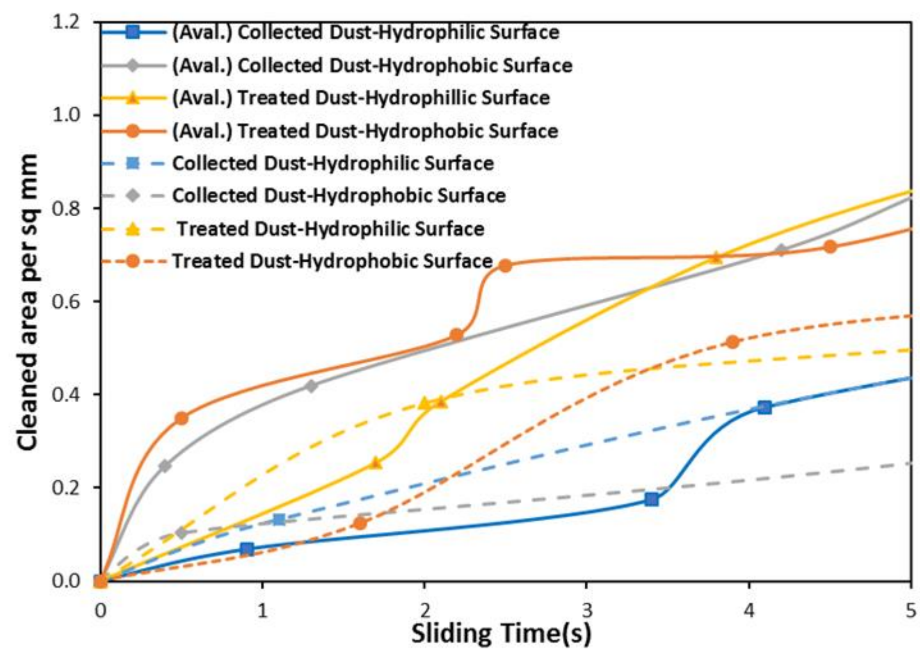

Figure 4.15 Cleaned Area Ratio for Simple Mechanical Tilt and Avalanche method

Fig. (4.16) shows the normalized velocity ratio for the different cases of dusty sample surfaces for both the avalanche effect and simple mechanical tilt. The dust removal velocity ratio for the avalanche sharply increases for both dust types on the hydrophobic due to reduced particle retention by the surface particularly for the HF-treated dust on both the hydrophobic and hydrophilic surfaces.

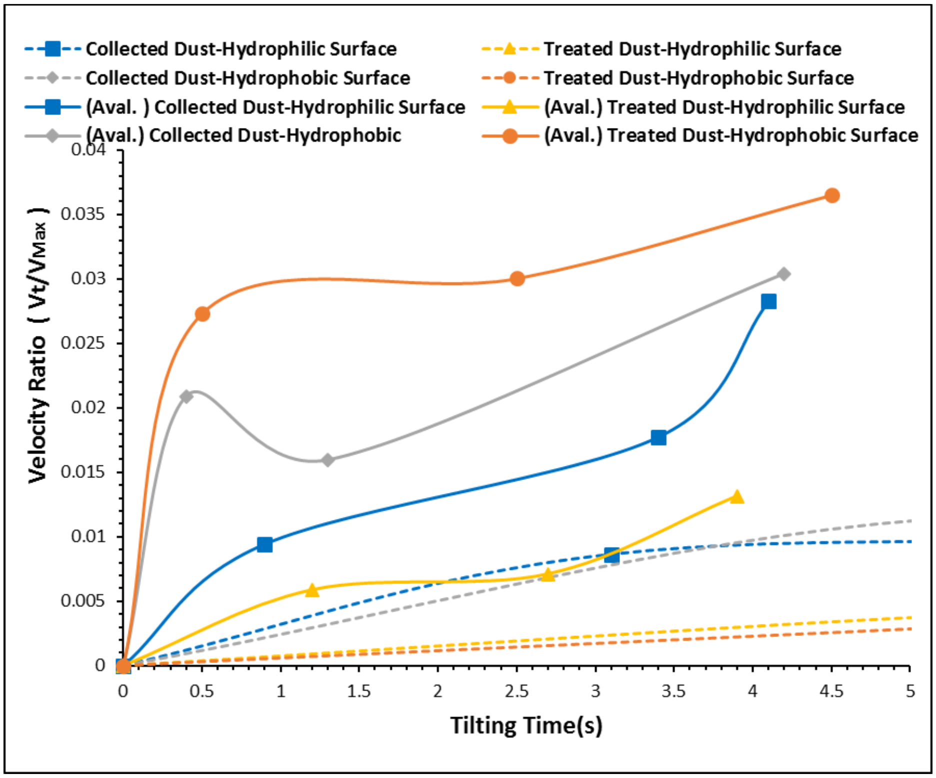

Figure 4.16 Velocity Ratio for Simple Mechanical Tilt and Avalanche method.

Therefore, it could be concluded that the avalanche effect enhances efficient and time saving cleaning process when compared to dust removal without using the avalanche effect.

CHAPTER 5

CONCLUSION

5.1 Dust Treatment and Characterization

Environmental dust modifications towards their removal from surfaces is considered. The solution modified and collected dust particles adhesion on hydrophilic and hydrophobic glass surfaces are examined. The dust particles are collected from Dammam area of Saudi Arabia and low concentration hydrofluoric acid solution (30% HF and 70% water mixture) is used to treat the dust particles. The collected and solution treated dust particles are chemically analyzed and dissolution of the components of the dust particles in water-hydrofluoric acid mixture is evaluated. The findings demonstrate that environmental dust possess various elements and compounds and some of these compounds do not satisfy the stoichiometric elemental ratio while causing cationic/anionic forces on the dust surface. This gives rise to attachment of some small size dust particles forming the dust clusters. The low concentration hydrofluoric acid solution treatment of collected dust particles minimizes this effect and the dust clustering ceases. Some new complex salt compounds are formed in the dust particles during the solution treatment, which cause micro/sub micro size cracks on the dust particle surfaces. Some compounds of solution treated dust can dissolve in the solution while creating sub-micron/nano pores and pillars on the surface of the dust particles.

5.2 Dust Samples Surface Free Energy Determination

The surface free energies of collected and modified dust are estimated using the droplet method.

Three liquids namely water, glycerol, and ethylene glycol are used in contact angle measurements. To measure the contact angle, two procedures are adopted. In the first approach, the Washburn technique is employed to measure the liquid contact angle on dust and in the second approach small dust pellets are formed via slight compression of the dust particles and contact angle measurements are carried out using the Goniometer adopting the previous procedure. The estimated surface free energy for collected dust is relatively higher at around 112.3 ± 7.8 mJ/m^2 ,while it is about 94.8 ± 6.2 mJ/m^2 for hydrogen fluoride treated dust. This change in the surface free energy is because several new compounds such as CaF_2 and some salt compounds (Na_2SiF_6, K_2SiF_6 , $CaCl_z$, and $MgCl_2$ are formed in the dust surface region after treatment with hydrogen fluoride. The formation of fluorite compounds results in low surface free energy of the treated dust.

5.3 Determination of Dust Particles Adhesion on Glass Sample Surface

Adhesion of the dust particles on hydrophilic and hydrophobic glass surfaces is assessed using atomic force microscopy (AFM) and scratch testing methods. For the collected dust particle on hydrophilic glass sample, the adhesion force recorded using AFM measurement is 1.68×10^{-10} N, while that obtained for the same dust type and size on a hydrophobic glass is 0.522×10^{-10} N. However, the adhesion force recorded for the hydrogen fluoride (HF) treated dust on hydrophilic glass sample is 1.22×10^{-10} N while the value recorded for the HF-treated dust on hydrophobic glass sample is 0.38×10^{-10} N. Therefore, the adhesion force obtained from AFM analysis for solution treated dust on the hydrophilic and hydrophobic glass surfaces remains almost 1/3 of that of the collected dust. In addition, the average adhesion work determined is about 4.9758 µJ for collected dust on the hydrophilic glass surface while it is 0.9361 µJ on the hydrophobic surface. However, the average adhesion work for HF-treated dust on the hydrophilic glass surface is 4.0912 µJ while it is 0.6027 μJ on the hydrophobic glass surface. Consequently, the solution treatment reduces dust adhesion force and work respectively on both hydrophobic and hydrophobic surfaces, which can be attributed to: i) solution treated dust has lower surface free energy than that corresponding to collected dust while reducing interfacial molecular forces between the dust particles and the glass surface, and ii) surface texture generated on the dust particles after solution treatment lowers the mechanical contact area between the dust particles and the glass surface.

5.4 Mechanical Removal of Solution Treated and Untreated Dust

Experiments are extended to include dust removal from inclined hydrophilic and hydrophobic glass surfaces under the gravitational influence and the resulting area of dust removed and dust residues are examined incorporating the digital imaging system. The dust removal tests via mechanical tilt revealed that inclination angle of the glass surface becomes less for the solution treated dust removal from the glass surface as compared to collected environmental dust; hence, the gravitational influence cleans the glass surface from dust at low tilt angle as the dust is treated by low concentration hydrofluoric acid. In addition, 98% of the cleaned area ratio remains maximum at the end of surface inclination for the hydrogen fluoride (HF) treated dust on hydrophobic surface, then follows collected dust on hydrophobic surface, HF-treated dust on hydrophilic surface and collected dust on hydrophilic surface. For dust removal via the avalanche effect, the area of HF-treated dust cleaned on the hydrophobic surface for the first 3 seconds attains 70% of the total covered surface before inclination, while the area cleaned for that of the collected dust on the hydrophilic surface attains the minimum value of 14% of the dusty surface before inclination. Finally, for the avalanche effect for dust removal, the maximum velocity attains more than $0.14 ms^{-1}$ for the treated dust on the hydrophobic surface for the first 4 seconds of tilting the surface, this value agrees with that obtain in previous study [23].

5.5 Future Works

This thesis work presents a novel approach of mitigating dust effects on solar harvesting through the solution treatment of dust particles for self-cleaning of devices surfaces. The following research areas are being considered as a consolidation to the present work and its findings.

- Detail optimization work should be carried out on the parametric amount of Hydrogen Fluoride used for dust treatment to obtain specific quantity of solution needed for large scale removal of accumulated dust on the surfaces of solar thermal/photovoltaic panels.
- Application of other mitigations strategies aside mechanical dust removal of solution treated dust can be further investigated. Consequently, Investigation into the Mechanism for the water droplet cleaning for comparison of the solution treated and the untreated dust particles would expand knowledge about the literature.
- Further investigation into the use of electrodynamic dust shield (EDS) to repel treated dust and untreated dust particles from the surfaces of solar harvesting devices. An experiment using an activated electrostatic force field should be performed to compare the cleaning efficient of treated and untreated dust particles by varying the voltage and frequency of activation.
- Possible use of an alternative chemical agent such as Ammonium Difluoride in place of Hydrogen fluoride could be further researched upon.

References

[1] Hepbasli, A., and Alsuhaibani, Z., 2011, "A Key Review on Present Status and Future Directions of Solar Energy Studies and Applications in Saudi Arabia," Renew. Sustain. Energy Rev., 15(9), pp. 5021–5050.

[2] Alawaji, S. H., 2001, "Evaluation of Solar Energy Research and Its Applications in Saudi Arabia — 20 Years of Experience," 5, pp. 59–77.

[3] Kalderon-Asael, B., Erel, Y., Sandler, A., and Dayan, U., 2009, "Mineralogical and Chemical Characterization of Suspended Atmospheric Particles over the East Mediterranean Based on Synoptic-Scale Circulation Patterns," Atmos. Environ., 43(25), pp. 3963–3970.

[4] Guan, Q., Luo, H., Pan, N., Zhao, R., Yang, L., Yang, Y., and Tian, J., 2019, "Contribution of Dust in Northern China to PM10 Concentrations over the Hexi Corridor," Sci. Total Environ., 660, pp. 947–958.

[5] Querol, X., Perez, N., Reche, C., Ealo, M., Ripoll, A., Tur, J., Pandolfi, M., Pey, J., Salvador, P., Moreno, T., and others, 2019, "African Dust and Air Quality over Spain: Is It Only Dust That Matters?," Sci. Total Environ., 686, pp. 737–752.

[6] Oduber, F., Calvo, A. I., Blanco-Alegre, C., Castro, A., Nunes, T., Alves, C., Sorribas, M., Fernández-González, D., Vega-Maray, A. M., Valencia-Barrera, R. M., and others, 2019, "Unusual Winter Saharan Dust Intrusions at Northwest Spain: Air Quality, Radiative and Health Impacts," Sci. Total Environ., 669, pp. 213–228.

[7] Su, J., Huang, G., Cao, L., and Bai, L., 2019, "Evaluation and Analysis of Cascading Spread Caused by Multisource Dust Migration in a Pollution-Related Ecosystem," Sci. Total Environ., 686, pp. 10–25.

[8] Shao, Y., and Dong, C. H., 2006, "A Review on East Asian Dust Storm Climate, Modelling and Monitoring," Glob. Planet. Change, 52(1–4), pp. 1–22.

[9] Notaro, M., Alkolibi, F., Fadda, E., and Bakhrjy, F., 2013, "Trajectory Analysis of Saudi Arabian Dust Storms," J. Geophys. Res. Atmos., 118(12), pp. 6028–6043.

[10] Hassan, G., Yilbas, B. S., Said, S. A. M., Al-Aqeeli, N., and Matin, A., 2016, "Chemo-Mechanical Characteristics of Mud Formed from Environmental Dust Particles in Humid Ambient Air," Sci. Rep., 6(1), pp. 1–14.

[11] Yilbas, B. S., Hassan, G., Al-Sharafi, A., Ali, H., Al-Aqeeli, N., and Al-Sarkhi, A., 2018, "Water Droplet Dynamics on a Hydrophobic Surface in Relation to the Self-Cleaning of Environmental Dust," Sci. Rep., 8(1), pp. 1–19.

[12] Hassan, G., Yilbas, B. S., Al-Sharafi, A., and Al-Qahtani, H., 2019, "Self-Cleaning of a Hydrophobic Surface by a Rolling Water Droplet," Sci. Rep., 9(1), pp. 1–14.

[13] Yilbas, B. S., Ali, H., Al-Aqeeli, N., Abu-Dheir, N., and Khaled, M., 2016, "Influence of Mud Residues on Solvent Induced Crystalized Polycarbonate Surface Used as PV Protective Cover," Sol. Energy, 125, pp. 282–293.

[14] Chen, W., Yang, M., Zhang, S., Andrews-Speed, P., and Li, W., 2019, "What Accounts for the China-US Difference in Solar PV Electricity Output? An LMDI Analysis," J. Clean. Prod., 231, pp. 161–170.

[15] Yilbas, B. S., Ali, H., Khaled, M. M., Al-Aqeeli, N., Abu-Dheir, N., and Varanasi, K. K., 2015, “Influence of Dust and Mud on the Optical, Chemical and Mechanical Properties of a Pv Protective Glass,” Sci. Rep., 5(1), pp. 1–12.

[16] Liu, S., Yue, Q., Zhou, K., and Sun, K., 2019, “Effects of Particle Concentration, Deposition and Accumulation on Photovoltaic Device Surface,” Energy Procedia, 158, pp. 553–558.

[17] Syafiq, A., Pandey, A. K., Adzman, N. N., and Rahim, N. A., 2018, “Advances in Approaches and Methods for Self-Cleaning of Solar Photovoltaic Panels,” Sol. Energy, 162(November 2017), pp. 597–619.

[18] Fathi, M., Abderrezek, M., and Friedrich, M., 2017, “Reducing Dust Effects on Photovoltaic Panels by Hydrophobic Coating,” Clean Technol. Environ. Policy, 19(2), pp. 577–585.

[19] Van Oss, C. J., Chaudhury, M. K., and Good, R. J., 1988, “Interfacial Lifshitz-van Der Waals and Polar Interactions in Macroscopic Systems,” Chem. Rev., 88(6), pp. 927–941.

[20] Young, T., 1832, “An Essay on the Cohesion of Fluids,” Abstracts of the Papers Printed in the Philosophical Transactions of the Royal Society of London, pp. 171–172.

[21] Zisman, W. A., 1964, “Relation of the Equilibrium Contact Angle to Liquid and Solid Constitution,” ACS Publications.

[22] Oss, C. J. van, Good, R. J., and Busscher, R. J., 1990, “Estimation of the Polar Surface Tension Parameters of Glycerol and Formamide, for Use in Contact Angle Measurements on Polar Solids,” J. Dispers. Sci. andTechnology, 11(1), pp. 75–81.

[23] Yilbas, B. S., Al-Sharafi, A., Ali, H., Al-Aqeeli, N., Al-Qahtani, H., Al-Sulaiman, F., Abu-Dheir, N., Abdelmagid, G., and Elkhazraji, A., 2018, “Environmental Dust Removal from

Inclined Hydrophobic Glass Surface: Avalanche Influence on Dynamics of Dust Particles," RSC Adv., 8(59), pp. 33775–33785.

[24] Good, R. J., and Girifalco, L. A., 1960, "A Theory for Estimation of Surface and Interfacial Energies. III. Estimation of Surface Energies of Solids from Contact Angle Data," J. Phys. Chem., 64(5), pp. 561–565.

[25] Rymuszka, D., Terpiłowski, K., and Hołysz, L., 2014, "Influence of Volume Drop on Surface Free Energy of Glass," Ann. UMCS, Chem., 68(1–2), pp. 121–132.

[26] Owens, D. K., and Wendt, R. C., 1969, "Estimation of the Surface Free Energy of Polymers," J. Appl. Polym. Sci., 13(8), pp. 1741–1747.

[27] Zaihidee, F. M., Mekhilef, S., Seyedmahmoudian, M., and Horan, B., 2016, "Dust as an Unalterable Deteriorative Factor Affecting PV Panel's Efficiency: Why and How," Renew. Sustain. Energy Rev., **65**, pp. 1267–1278.

[28] Mohandes, B. M. A., El-Chaar, L., and Lamont, L. A., 2009, "Application Study of 500 W Photovoltaic (PV) System in the UAE," Appl. Sol. energy, 45(4), pp. 242–247.

[30] [29] Hachicha, A. A., Al-Sawafta, I., and Said, Z., 2019, "Impact of Dust on the Performance of Solar Photovoltaic (PV) Systems under United Arab Emirates Weather Conditions," Renew. Energy, **141**, pp. 287–297.

[30] Micheli, L., Caballero, J. A., Fernandez, E. F., Smestad, G. P., Nofuentes, G., Mallick, T. K., and Almonacid, F., 2019, "Correlating Photovoltaic Soiling Losses to Waveband and Single-Value Transmittance Measurements," Energy, **180**, pp. 376–386.

[31] Zitouni, H., Merrouni, A. A., Regragui, M., Bouaichi, A., Hajjaj, C., Ghennioui, A., and

Ikken, B., 2019, “Experimental Investigation of the Soiling Effect on the Performance of Monocrystalline Photovoltaic Systems,” Energy Procedia, **157**(2018), pp. 1011–1021.

[32] Chen, Y., Liu, Y., Tian, Z., Dong, Y., Zhou, Y., Wang, X., and Wang, D., 2019, “Experimental Study on the Effect of Dust Deposition on Photovoltaic Panels,” Energy Procedia, **158**, pp. 483–489

[33] Yang, C., Wu, Y., Lv, G., Rubanov, S., and Jamieson, D. N., 2015, “Hypervelocity Dust Impact Craters on Photovoltaic Devices Imaged by Ion Beam Induced Charge,” Nucl. Instruments Methods Phys. Res. Sect. B Beam Interact. with Mater. Atoms, **348**, pp. 251–254.

[34] Sun, K., Lu, L., Jiang, Y., Wang, Y., Zhou, K., and He, Z., 2018, “Integrated Effects of PM2. 5 Deposition, Module Surface Conditions and Nanocoatings on Solar PV Surface Glass Transmittance,” Renew. Sustain. Energy Rev., **82**, pp. 4107–4120.

[35] Tripathi, A. K., Aruna, M., and Msurthy, S. N., 2017, “Performance Evaluation of PV Panel Under Dusty Condition,” Int. J. Renew. Energy Dev., **6**(3), p. 225.

[36] Appels, R., Lefevre, B., Herteleer, B., Goverde, H., Beerten, A., Paesen, R., De Medts, K., Driesen, J., and Poortmans, J., 2013, “Effect of Soiling on Photovoltaic Modules,” Sol. energy, **96**, pp. 283–291.

[37] Lu, H., Lu, L., Zhang, L. Z., and Pan, A., 2019, “Numerical Study on Polydispersed Dust Pollution Process on Solar Photovoltaic Panels Mounted on a Building Roof,” Energy Procedia, **158**, pp. 879–884.

[38] Nouira, M., and Sammouda, H., 2018, "Numerical Study of an Inclined Photovoltaic System Coupled with Phase Change Material under Various Operating Conditions," Appl. Therm. Eng., **141**, pp. 958–975.

[39] Oh, S., 2019, "Analytic and Monte-Carlo Studies of the Effect of Dust Accumulation on Photovoltaics," Sol. Energy, **188**, pp. 1243–1247.

[40] Chiteka, K., Sridhara, S. N., and Arora, R., 2019, "Numerical Investigation of Installation and Environmental Parameters on Soiling of Roof-Mounted Solar Photovoltaic Array," Cogent Eng., **6**(1), p. 1649007.

[41] Khandakar, A., EH Chowdhury, M., Khoda Kazi, M., Benhmed, K., Touati, F., Al-Hitmi, M., Gonzales, J. S. P., and others, 2019, "Machine Learning Based Photovoltaics (PV) Power Prediction Using Different Environmental Parameters of Qatar," Energies, **12**(14), p. 2782.

[42] Said, S. A. M., Hassan, G., Walwil, H. M., and Al-Aqeeli, N., 2018, "The Effect of Environmental Factors and Dust Accumulation on Photovoltaic Modules and Dust-Accumulation Mitigation Strategies," Renew. Sustain. Energy Rev., **82**, pp. 743–760.

[43] Smith, M. K., Wamser, C. C., James, K. E., Moody, S., Sailor, D. J., and Rosenstiel, T. N., 2013, "Effects of Natural and Manual Cleaning on Photovoltaic Output," J. Sol. energy Eng., **135**(3).

[44] Hammond, R., Srinivasan, D., Harris, A., Whitfield, K., and Wohlgemuth, J., 1997, "Effects of Soiling on PV Module and Radiometer Performance," *Conference Record of the Twenty Sixth IEEE Photovoltaic Specialists Conference-1997*, pp. 1121–1124.

[45] Kalogirou, S. A., Agathokleous, R., and Panayiotou, G., 2013, "On-Site PV Characterization

and the Effect of Soiling on Their Performance," Energy, **51**, pp. 439–446.

[46] Schill, C., Brachmann, S., Heck, M., Weiss, K.-A., and Koehl, M., 2011, "Impact of Heavy Soiling on the Power Output of PV Modules," *Reliability of Photovoltaic Cells, Modules, Components, and Systems IV*, p. 811207.

[47] Jamil, W. J., Rahman, H. A., Shaari, S., and Salam, Z., 2017, "Performance Degradation of Photovoltaic Power System: Review on Mitigation Methods," Renew. Sustain. Energy Rev., **67**, pp. 876–891.

[48] Guo, B., Javed, W., Khoo, Y. S., and Figgis, B., 2019, "Solar PV Soiling Mitigation by Electrodynamic Dust Shield in Field Conditions," Sol. Energy, **188**, pp. 271–277.

[49] Javed, W., Guo, B., and Figgis, B., 2017, "Modeling of Photovoltaic Soiling Loss as a Function of Environmental Variables," Sol. Energy, **157**, pp. 397–407.

[50] Parrott, B., Zanini, P. C., Shehri, A., Kotsovos, K., and Gereige, I., 2018, "Automated, Robotic Dry-Cleaning of Solar Panels in Thuwal, Saudi Arabia Using a Silicone Rubber Brush," Sol. Energy, **171**, pp. 526–533.

[51] Cai, S., Bao, G., Ma, X., Wu, W., Bian, G.-B., Rodrigues, J. J. P. C., and de Albuquerque, V. H. C., 2019, "Parameters Optimization of the Dust Absorbing Structure for Photovoltaic Panel Cleaning Robot Based on Orthogonal Experiment Method," J. Clean. Prod., **217**, pp. 724–731.

[52] Singh, G., Saini, D., Yadav, N., Sarma, R., Chandra, L., and Shekhar, R., 2015, "Dust Deposition Mechanism and Cleaning Strategy for Open Volumetric Air Receiver Based Solar Tower Sub-Systems," Energy Procedia, **69**, pp. 2081–2089.

[53] Mondal, A. K., and Bansal, K., 2015, “A Brief History and Future Aspects in Automatic Cleaning Systems for Solar Photovoltaic Panels,” Adv. Robot., **29**(8), pp. 515–524.

[54] Alghamdi, A. S., Bahaj, A. S., Blunden, L. S., and Wu, Y., 2019, “Dust Removal from Solar PV Modules by Automated Cleaning Systems,” Energies, **12**(15), p. 2923.

[55] Rifai, A., Dheir, N. A., Yilbas, B. S., and Khaled, M., 2016, “Mechanics of Dust Removal from Rotating Disk in Relation to Self-Cleaning Applications of PV Protective Cover,” Sol. Energy, **130**, pp. 193–206.

[56] Al-Housani, M., Bicer, Y., and Koç, M., 2019, “Experimental Investigations on PV Cleaning of Large-Scale Solar Power Plants in Desert Climates: Comparison of Cleaning Techniques for Drone Retrofitting,” Energy Convers. Manag., **185**, pp. 800–815.

[57] Zefri, Y., ElKettani, A., Sebari, I., and Ait Lamallam, S., 2018, “Thermal Infrared and Visual Inspection of Photovoltaic Installations by UAV Photogrammetry—Application Case: Morocco,” Drones, **2**(4), p. 41.

[58] Alsafasfeh, M., Abdel-Qader, I., Bazuin, B., Alsafasfeh, Q., and Su, W., 2018, “Unsupervised Fault Detection and Analysis for Large Photovoltaic Systems Using Drones and Machine Vision,” Energies, **11**(9), p. 2252.

[59] Grimaccia, F., Aghaei, M., Mussetta, M., Leva, S., and Quater, P. B., 2015, “Planning for PV Plant Performance Monitoring by Means of Unmanned Aerial Systems (UAS),” Int. J. Energy Environ. Eng., **6**(1), pp. 47–54.

[60] Calle, C. I., Immer, C. D., Clements, J. S., Chen, A., Buhler, C. R., Lundeen, P., Mantovani, J. G., Starnes, J. W., Michalenko, M., and Mazumder, M. K., 2006, “Electrodynamic Dust

Shield for Suacrfe Exploration Activities on the Moon and Mars."

[61] Guo, B., Figgis, B., and Javed, W., 2019, "Measurement of Electrodynamic Dust Shield Efficiency in Field Conditions," J. Electrostat., **97**, pp. 26–30.

[62] Kawamoto, H., and Guo, B., 2018, "Improvement of an Electrostatic Cleaning System for Removal of Dust from Solar Panels," J. Electrostat., **91**, pp. 28–33.

[63] Guo, B., Javed, W., Pett, C., Wu, C.-Y., and Scheffe, J. R., 2018, "Electrodynamic Dust Shield Performance under Simulated Operating Conditions for Solar Energy Applications," Sol. Energy Mater. Sol. Cells, **185**, pp. 80–85.

[64] Kawamoto, H., and Shibata, T., 2015, "Electrostatic Cleaning System for Removal of Sand from Solar Panels," J. Electrostat., **73**, pp. 65–70.

[65] Chesnutt, J. K. W., Guo, B., and Wu, C.-Y., 2019, "Numerical Analysis of the Effects of Particle-Particle Interactions and Particle Size on the Performance of an Electrodynamic Dust Shield," J. Electrostat., **98**, pp. 58–68.

[66] Wenzel, R. N., 1936, "Resistance of Solid Surfaces to Wetting by Water," Ind. Eng. Chem., **28**(8), pp. 988–994.

[67] Cassie, A. B. D., and Baxter, S., 1944, "Wettability of Porous Surfaces," Trans. Faraday Soc., **40**, pp. 546–551.

[68] Roach, P., Shirtcliffe, N. J., and Newton, M. I., 2008, "Progess in Superhydrophobic Surface Development," Soft Matter, **4**(2), pp. 224–240.

[69] Bhushan, B., 2009, "Biomimetics: Lessons from Nature--an Overview."

[70] Ragesh, P., Ganesh, V. A., Nair, S. V, and Nair, A. S., 2014, "A Review on 'Self-Cleaning and Multifunctional Materials,'" J. Mater. Chem. A, **2**(36), pp. 14773–14797.

[71] Nishimoto, S., and Bhushan, B., 2013, "Bioinspired Self-Cleaning Surfaces with Superhydrophobicity, Superoleophobicity, and Superhydrophilicity," Rsc Adv., **3**(3), pp. 671–690.

[72] Pan, A., Lu, H., and Zhang, L.-Z., 2019, "Experimental Investigation of Dust Deposition Reduction on Solar Cell Covering Glass by Different Self-Cleaning Coatings," Energy, **181**, pp. 645–653.

[73] Soklič, A., Tasbihi, M., Kete, M., and Štangar, U. L., 2015, "Deposition and Possible Influence of a Self-Cleaning Thin TiO2/SiO2 Film on a Photovoltaic Module Efficiency," Catal. Today, **252**, pp. 54–60.

[74] Polizos, G., Sharma, J. K., Smith, D. B., Tuncer, E., Park, J., Voylov, D., Sokolov, A. P., Meyer III, H. M., and Aman, M., 2018, "Anti-Soiling and Highly Transparent Coatings with Multi-Scale Features," Sol. Energy Mater. Sol. Cells, **188**, pp. 255–262.

[75] Li, W., Tan, X., Zhu, J., Xiang, P., Xiao, T., Tian, L., Yang, A., Wang, M., and Chen, X., 2019, "Broadband Antireflective and Superhydrophobic Coatings for Solar Cells," Mater. Today Energy, **12**, pp. 348–355.

[76] Huang, Z., Cai, C., Kuai, L., Li, T., Huttula, M., and Cao, W., 2018, "Leaf-Structure Patterning for Antireflective and Self-Cleaning Surfaces on Si-Based Solar Cells," Sol. Energy, **159**, pp. 733–741.

[77] Dey, T., and Naughton, D., 2016, "Cleaning and Anti-Reflective (AR) Hydrophobic Coating

of Glass Surface: A Review from Materials Science Perspective," J. Sol-Gel Sci. Technol., **77**(1), pp. 1–27.

[78] Zhan, W., Wang, W., Xiao, Z., Yu, X., and Zhang, Y., 2018, "Water-Free Dedusting on Antireflective Glass with Durable Superhydrophobicity," Surf. Coatings Technol., **356**, pp. 123–131.

[79] Yilbas, B. S., Hassan, G., Al-Sharafi, A., Ali, H., Al-Aqeeli, N., and Al-Sarkhi, A., 2018, "Water Droplet Dynamics on a Hydrophobic Surface in Relation to the Self-Cleaning of Environmental Dust," Sci. Rep., **8**(1), pp. 1–19.

[80] Hassan, G., Yilbas, B. S., Al-Sharafi, A., and Al-Qahtani, H., 2019, "Self-Cleaning of a Hydrophobic Surface by a Rolling Water Droplet," Sci. Rep., **9**(1), pp. 1–14.

[81] Baranowski, S., and Liebersbach, J., 1977, "The Intensity of Different Kinds of Rime on the Upper Tree Line in the Sudety Mountains," J. Glaciol., **19**(81), pp. 489–497.

[82] Socco, L. V., Jongmans, D., Boiero, D., Stocco, S., Maraschini, M., Tokeshi, K., and Hantz, D., 2010, "Geophysical Investigation of the Sandalp Rock Avalanche Deposits," J. Appl. Geophys., **70**(4), pp. 277–291.

[83] Wang, Y. F., Dong, J. J., and Cheng, Q. G., 2017, "Velocity-Dependent Frictional Weakening of Large Rock Avalanche Basal Facies: Implications for Rock Avalanche Hypermobility?," J. Geophys. Res. Solid Earth, **122**(3), pp. 1648–1676.

[84] Zhang, M., and McSaveney, M. J., 2017, "Rock Avalanche Deposits Store Quantitative Evidence on Internal Shear during Runout," Geophys. Res. Lett., **44**(17), pp. 8814–8821.

[85] Li, Q., Rudolph, V., and Peukert, W., 2006, "London-van Der Waals Adhesiveness of Rough

Particles," Powder Technol., **161**(3), pp. 248–255.

[86] Johnson, K. L., Kendall, K., and Roberts, aAD, 1971, "Surface Energy and the Contact of Elastic Solids," Proc. R. Soc. London. A. Math. Phys. Sci., **324**(1558), pp. 301–313.

[87] Derjaguin, B. V, Muller, V. M., and Toporov, Y. P., 1975, "Effect of Contact Deformations on the Adhesion of Particles," J. Colloid Interface Sci., **53**(2), pp. 314–326.

[88] Hamaker, H. C., 1937, "The London—van Der Waals Attraction between Spherical Particles," physica, **4**(10), pp. 1058–1072.

[89] Rabinovich, Y. I., Adler, J. J., Ata, A., Singh, R. K., and Moudgil, B. M., 2000, "Adhesion between Nanoscale Rough Surface. I. Role of Asperity Geometry," J. Colloid Interface Sci, **232**(10).

[90] Goldman, A. J., Cox, R. G., and Brenner, H., 1967, "Slow Viscous Motion of a Sphere Parallel to a Plane Wall—II Couette Flow," Chem. Eng. Sci., **22**(4), pp. 653–660.

[91] Lee, H., and Balachandar, S., 2010, "Drag and Lift Forces on a Spherical Particle Moving on a Wall in a Shear Flow at Finite Re," J. Fluid Mech., **657**, pp. 89–125.

[92] Watanabe, S., Iimori, M., Chan, D. V., Hara, E., Kitao, H., and Maehara, Y., 2018, "MDC1 Methylation Mediated by Lysine Methyltransferases EHMT1 and EHMT2 Regulates Active ATM Accumulation Flanking DNA Damage Sites," Sci. Rep., **8**(1), pp. 1–10.

[93] Hunter, L., 2015, "Fluorine Chemistry," Aust. J. Chem., **68**(1), p. 3.

[94] Genuino, H. C., Opembe, N. N., Njagi, E. C., McClain, S., and Suib, S. L., 2012, "A Review of Hydrofluoric Acid and Its Use in the Car Wash Industry," J. Ind. Eng. Chem., **18**(5), pp. 1529–

1539.

[95] Spierings, G. A. C. M., 1993, "Wet Chemical Etching of Silicate Glasses in Hydrofluoric Acid Based Solutions," J. Mater. Sci., **28**(23), pp. 6261–6273.

[96] Amended, C., "Hydrogen Final Fluoride Study Report," Assets.Documentcloud.Org, **112**(6).

[97] Hance, C. D., Solomon, P. A., Salmon, L. G., Fall, T., and Cass, G. R., 1997, "Hydrofluoric Acid in the Southern California Atmosphere," Environ. Sci. Technol., **31**(4), pp. 956–959.

[98] Feng, Y., and Barratt, R. S., 1994, "Digestion of Dust Samples in a Microwave Oven," Sci. Total Environ., **143**(2–3), pp. 157–161.

[99] Ely, J. C., Neal, C. R., O'Neill Jr, J. A., and Jain, J. C., 1999, "Quantifying the Platinum Group Elements (PGEs) and Gold in Geological Samples Using Cation Exchange Pretreatment and Ultrasonic Nebulization Inductively Coupled Plasma-Mass Spectrometry (USN-ICP-MS)," Chem. Geol., **157**(3–4), pp. 219–234.

[100] Jonas, O., and Machemer, L., 2014, "Tight Control of Cycle Chemistry Key to Succesful Commisioning," pp. 1–7.

[101] Terpiłowski, K., Hołysz, L., Rymuszka, D., and Banach, R., 2016, "Comparison of Contact Angle Measurement Methods of Liquids on Metal Alloys," Ann. UMCS, Chem., **71**(1).

[102] Yong, W. Y. D., Zhang, Z., Cristobal, G., and Chin, W. S., 2014, "One-Pot Synthesis of Surface Functionalized Spherical Silica Particles," Colloids Surfaces A Physicochem. Eng. Asp., **460**, pp. 151–157.

[103] Van Oss, C. J., Good, R. J., and Chaudhury, M. K., 1987, "Mechanism of DNA (Southern)

and Protein (Western) Blotting on Cellulose Nitrate and Other Membranes," J. Chromatogr. A, **391**, pp. 53–65.

[104] Heib, F., and Schmitt, M., 2016, "Statistical Contact Angle Analyses with the High-Precision Drop Shape Analysis (HPDSA) Approach: Basic Principles and Applications," Coatings , **6**(4).

[105] Ishida, H., and Koenig, J. L., 1978, "Fourier Transform Infrared Spectroscopic Study of the Silane Coupling Agent/Porous Silica Interface," J. Colloid Interface Sci., **64**(3), pp. 555–564.

[106] Nakabo, S., Torii, Y., Itota, T., Yoshiyama, M., Ishikawa, K., and Suzuki, K., 2002, "Regulation of Fluoride Ion Release from Na2SiF6 Contained in Resin Based on Hydrophobic Siloxane Layer Coating," J. Oral Rehabil., **29**(7), pp. 675–681.

[107] Nakamoto, K., 2006, "Infrared and R Aman Spectra of Inorganic and Coordination Compounds," Handb. Vib. Spectrosc.

[108] Zhou, L., Chen, D., Luo, W., Wang, Y., Yu, Y., and Liu, F., 2007, "Transparent Glass Ceramic Containing Er3+: CaF2 Nano-Crystals Prepared by Sol--Gel Method," Mater. Lett., **61**(18), pp. 3988–3990.

[109] Khunur, M. M., Risdianto, A., Mutrofin, S., and Prananto, Y. P., 2012, "Synthesis of Fluorite (CaF2) Crystal from Gypsum Waste of Phosphoric Acid Factory in Silica Gel," Bull. Chem. React. Eng. Catal., **7**(1), pp. 71–77.

[110] Washburn, E. W., 1921, "The Dynamics of Capillary Flow," Phys. Rev., **17**(3), p. 273.

[111] Heib, F., and Schmitt, M., 2016, "Statistical Contact Angle Analyses with the High-Precision

Drop Shape Analysis (HPDSA) Approach: Basic Principles and Applications," Coatings, **6**(4), p. 57.

[112] Galet, L., Patry, S., and Dodds, J., 2010, "Determination of the Wettability of Powders by the Washburn Capillary Rise Method with Bed Preparation by a Centrifugal Packing Technique," J. Colloid Interface Sci., **346**(2), pp. 470–475.

[113] Jańczuk, B., Wójcik, W., and Zdziennicka, A., 1993, "Determination of the Components of the Surface Tension of Some Liquids from Interfacial Liquid-Liquid Tension Measurements," J. Colloid Interface Sci., **157**(2), pp. 384–393.

[114] Zhang, X., Wang, X., and Miller, J. D., 2015, "Wetting of Selected Fluorite Surfaces by Water," Surf. Innov., **3**(1), pp. 39–48.

[115] Kim, D., Pugno, N. M., and Ryu, S., 2016, "Wetting Theory for Small Droplets on Textured Solid Surfaces," Sci. Rep., **6**, p. 37813.

[116] Anand, S., Rykaczewski, K., Subramanyam, S. B., Beysens, D., and Varanasi, K. K., 2015, "How Droplets Nucleate and Grow on Liquids and Liquid Impregnated Surfaces," Soft Matter, **11**(1), pp. 69–80.

[117] Bergeron, V., and Langevin, D., 1996, "Monolayer Spreading of Polydimethylsiloxane Oil on Surfactant Solutions," Phys. Rev. Lett., **76**(17), p. 3152.

[118] Carlson, A., Kim, P., Amberg, G., and Stone, H. A., 2013, "Short and Long Time Drop Dynamics on Lubricated Substrates," EPL (Europhysics Lett., **104**(3), p. 34008.

[119] Yilbas, B. S., Al-Qahtani, H., Al-Sharafi, A., Bahattab, S., Hassan, G., Al-Aqeeli, N., and Kassas, M., 2019, "Environmental Dust Particles Repelling from A Hydrophobic Surface

under Electrostatic Influence," Sci. Rep., **9**(1), pp. 1–18.

[120] Butt, H.-J., Cappella, B., and Kappl, M., 2005, "Force Measurements with the Atomic Force Microscope: Technique, Interpretation and Applications," Surf. Sci. Rep., **59**(1–6), pp. 1–152.

Vitae

Name	: Adukwu Johnny Ebaika
Nationality	: Nigerian
Date of Birth	: 7/30/1988
Email	: Johnnyadukwu4@gmail.com
Address	: #04, Badagry Str., Makurdi, Benue, Nigeria, Zip code: 972211.
Academic Background	: **MS Mechanical Engineering** April 2020 King Fahd University of Petroleum and Minerals Dharan, Saudi Arabia **BS Mechanical Engineering** August 2014 University of Nigeria Nsukka, Enugu State, Nigeria.
Publication	: Stretchable Hydrophobic Surfaces and Self-Cleaning Applications (Published 11 October 2019 by Nature Scientific Reports) Ref no: SREP 19-21047, Co-authored.